Alma Mater Studiorum · Università di Bologna

FACOLTÀ DI INGEGNERIA
Corso di Laurea Magistrale in Ingegneria Meccanica
Dipartimento di Ingegneria Industriale

Micro-FEM models based on micro-CT reconstructions for the in vitro characterization of the elastic properties of trabecular bone tissue.

Sviluppo di modelli micro-FEM derivati da ricostruzioni micro-CT per la caratterizzazione in vitro delle proprietà elastiche del tessuto osseo trabecolare.

Tesi di Laurea in Laboratorio Di Meccanica Dei Tessuti Biologici M

Candidato:
Gianluca Iori

Relatore:
Chiar.mo Prof.
Luca Cristofolini
Correlatore:
Ing. Martino Pani

Anno Accademico 2011/12
Sessione III

Summary

This master's thesis describes the research done at the *Medical Technology Laboratory* (LTM) of the Rizzoli Orthopedic Institute (IOR, Bologna, Italy), which focused on the characterization of the elastic properties of the trabecular bone tissue, starting from october 2012 to present.
The approach uses *computed microtomography* to characterize the architecture of trabecular bone specimens. With the information obtained from the scanner, *specimen-specific* models of trabecular bone are generated for the solution with the *Finite Element Method* (FEM). Along with the FEM modelling, mechanical tests are performed over the same reconstructed bone portions. From the linear-elastic stage of mechanical tests presented by experimental results, it is possible to estimate the mechanical properties of the trabecular bone tissue.
After a brief introduction on the biomechanics of the trabecular bone (chapter 1) and on the characterization of the mechanics of its tissue using FEM models (chapter 2), the reliability analysis of an experimental procedure is explained (chapter 3), based on the high-scalable numerical solver ParFE. In chapter 4, the sensitivity analyses on two different parameters for micro-FEM model's reconstruction are presented.
Once the reliability of the modeling strategy has been shown, a recent layout for experimental test, developed in LTM, is presented (chapter 5). Moreover, the results of the application of the new layout are discussed, with a stress on the difficulties connected to it and observed during the tests. Finally, a prototype experimental layout for the measure of deformations in trabecular bone specimens is presented (chapter 6). This procedure is based on the Digital Image Correlation method and is currently sunder development in LTM.

Sommario

La presente tesi magistrale descrive l'attività di ricerca svolta presso il Laboratorio di Tecnologia Medica (LTM) dell'Istituto Ortopedico Rizzoli (IOR, Bologna, Italia) dall'ottobre 2012 ad oggi, nell'ambito della caratterizzazione delle proprietà elastiche del tessuto osseo trabecolare.
L'approccio utilizzato è quello della modellazione, con il Metodo degli Elementi Finiti (FEM), di porzioni di osso trabecolare la cui architettura viene ricostruita grazie ad una scansione con microtomografia computerizzata. Alla modellazione FEM è abbinata l'esecuzione di test meccanici sulle stesse porzioni di osso ricostruite. In virtù del comportamento elastico lineare del campione che si evidenzia nella prima fase di caricamento meccanico, è possibile ricavare una stima delle proprietà elastiche del tessuto osseo trabecolare, altrimenti difficilmente analizzabili per vie sperimentali.
Dopo una breve introduzione sulla biomeccanica dell'osso trabecolare (capitolo 1), e sulla caratterizzazione delle sue proprietà meccaniche di tessuto per mezzo di modelli FEM (capitolo 2), nel capitolo 3 si affronta l'analisi sulla affidabilità di una procedura sperimentale basata sull'utilizzo del solutore numerico ad alta scalabilità ParFE. Sempre nell'ottica di una conferma della accuratezza delle stime di modulo di tessuto ottenute grazie alla strategia in questione, il capitolo 4 presenta due differenti studi di sensitività su parametri chiave della ricostruzione di modelli micro-FEM di osso trabecolare.
Una volta attestata l'affidabilità di suddetto approccio modellistico, viene descritto, nel capitolo 5, un layout per test sperimentali sviluppato di recente presso l'LTM. In questa sezione, si affrontano sia i risultati della applicazione del nuovo layout che le criticità ad esso connesse e venute alla luce con la conduzione dei primi test.
In conclusione, nel capitolo 6 viene illustrata una strategia per la misura delle

deformazioni in provini di osso trabecolare fondata sull'utilizzo di un sistema di correlazione di immagini digitali. Tale sistema si trova, alla data odierna, in fase prototipale presso l'LTM dello IOR.

Contents

List of Figures

List of Tables

"Todo hacer es conocer y
todo conocer es hacer"

"Todo lo dicho es dicho por alguien".

Humberto Maturana R.
Francisco Varela G.

Chapter 1

Principles of Bone Biomechanics

Bone is a self-repairing and self-remodeling material.
The skeletal system provides support and protection for soft tissues of the body.
It supplies the framework for the bone marrow and allows transmission of forces originated by muscular contraction during the movement. Finally, with its mineral content, bone serves as a reservoir of calcium ions.
Bones, which constitute the skeleton, present various sizes and shapes. Despite their functional and morphological remarkable differences, all bones are composed by the same elemental structure. Bone tissue, a mineral-base matrix characterized by high rigidity and hardness, is the main constituent of the skeletal system.
A sheet of fibrous connective tissue called Periostium covers most of the external surface of the bone. Similarly, Endostium, another fibrous connective layer, covers the surface of internal bone cavities.
Cavities are filled with bone marrow, an hematopoietic tissue witch can be distinguished between red and yellow marrow. Finally, the articulating (joint) surfaces at the ends of long bones are covered with a thin layer of articular cartilage, a material presenting extremely low friction coefficient.

1.1 Bone Composition

Bone is composed of 65% (in weight) mineral and 35% organic matrix, cells and water.
The inorganic mineral fraction is in the form of small crystals with shape of needles, plates, and rods located within and between collagen fibers.It is largely impure hydroxyapatyte mineral $Ca_{10}(PO_4)_6(OH)_2$, containing carbonate, citrate, fluoride and strontium adsorbed onto the crystal surface.
The organic matrix consists of 90% of collagen and about 10% of various non collagenous proteins.

1.2 Bone Morphology

In long bones the diaphysis, a cylindrical shaft of compact cortical tissue, connects two wider ends, called epiphysis, as it can be seen in figure 1.1. The connections between diaphysis and epiphysis are conical regions called metaphysis. In the diaphysis, a central cavity, called marrow cavity, holds yellow marrow. Epiphysis are composed mainly of spongy tissue surrounded by a thin layer of cortical bone. Trabecular cavities are filled with red marrow.
At a microscopical observation, bone tissue of adult mammals reveals to be composed of multiple packages formed of layers of collagen fiber and hydroxyapatyte. Unit layers are called lamellae.
Typically, lamellae are 3 to 7 μm thick and collagen fibers are disposed approximately parallel to each other. Within adjacent unit lamellar plates, the main fiber orientation can differ by as much as $90\,^{\circ}$.

1.2.1 Cortical Bone

Cortical bone is a dense and compact structure that constitutes approximately the 80% of the whole mass of the skeleton system. In long bones, cortical bone composes the diaphysis and the external surfaces of epiphyseal regions. Because of its high stiffness it is the main responsible for the support and protective tasks of the skeleton and for bone's mechanical strength.
Depending on anatomical site, the lamellae of cortical bone present the follow-

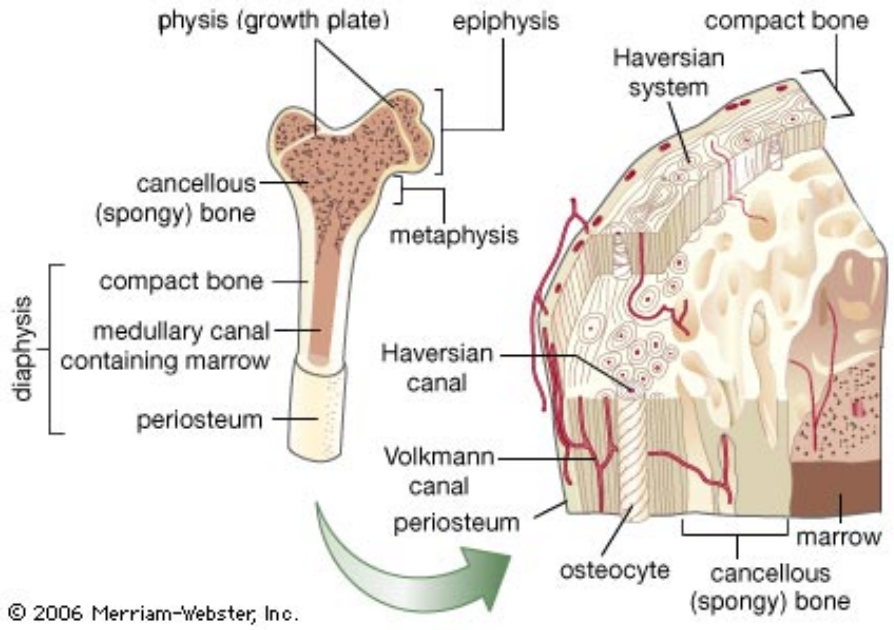

Figure 1.1: Bone morphology: organization and anatomy of cortical and cancellous bone in human femour is shown. Morphological differences between epiphyseal and diaphyseal regions should be noted.

ings different structural patterns:

- *Concentric lamellae* forming circular rings, in the osteon.
- *Circumferencial lamellae*: a thin lamellar layer enveloping bone external surface.
- *Interstitial lamellae*: angular fragments of concentric lamelale, residuals of previous Haversian systems eroded by bone remodelling.

1.2.2 Cancellous Bone

Cancellous bone is a low-density structure that composes metaphyseal and epiphyseal regions in long bones. In cancellous bone (also called trabecular bone),

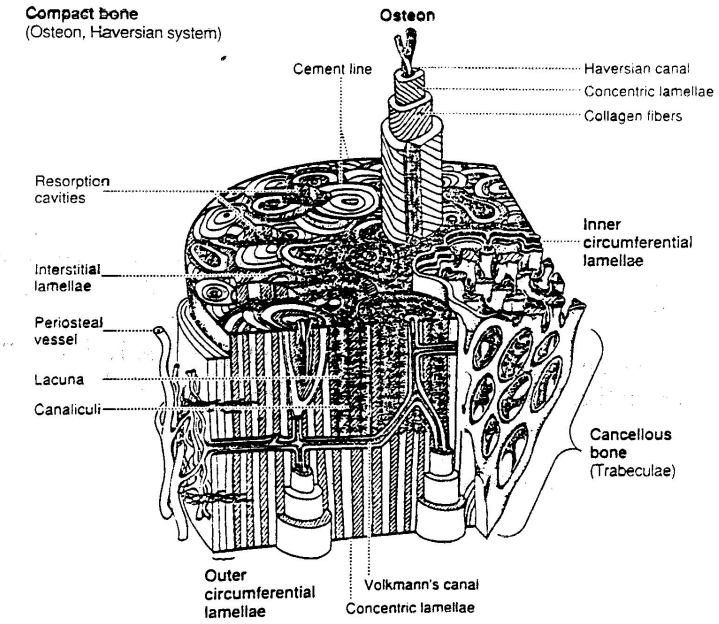

Figure 1.2: Long bone shaft compact bone representation with a detailed view of the Haversian system. Cortical bone forms the outer wall of all bones, being largely responsible for the supportive and protective function of the skeleton. Approximately 80% of the skeletal mass in the adult skeleton is cortical bone.

bone tissue is organized in a complex, high-connected net of small elements called trabeculae. In this structure, cavities are filled with red bone-marrow. Morphology of cancellous bone differs consistently depending on several factors such as subject age, skeleton regions and pathologies. Trabecular mean morphology can vary between a thin, regular, rod-type shape and a plate-like geometry.

The structure has a principal, uniform orientation of trabecular geometry which is aligned with main loading directions of the bone.

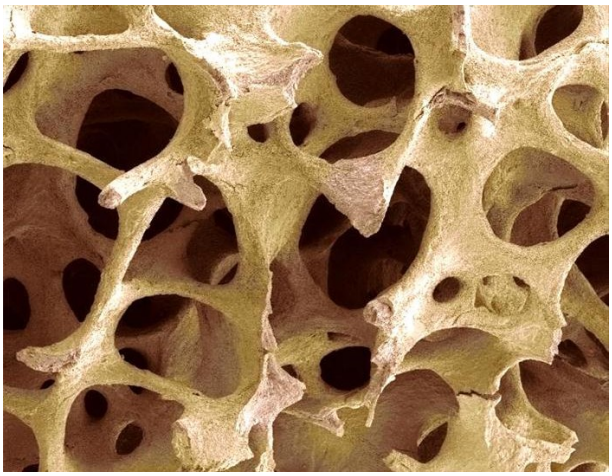

Figure 1.3: Coloured scanning electron micrograph of cancellous bone. A percentage of around 20 % of the bone mass is cancellous bone: a lattice-type structure of plates and rods. The structural unit of cancellous bone has typical mean thicknesses ranging between 50 μm and 300 μm and is known as trabecula. Trabecular bone is found in the inner parts of the skeleton.

1.2.3 Bone Structural Units

The main structural unit of cortical bone is the osteon, a cylindrical, hollow column formed of concentric rings of lamellae.

In the osteon (see figures 1.2 and 1.4), the central canal (called Haversian canal) allows blood and lymphatic vessels and nerves to pass.

Haversian canals are connected to each other as like as with marrow and periosteum by transverse Volkmann's canals.

The typical osteon has an external diameter of 200 to 250 μm with a lamellar circular wall of approximately 70 to 100 μm thick [44]. It's esternal surface is covered with a 1 to 2 μm thick layer of mineral collagen fibers, called cement line.

In addition, cortical bone shows a dense net of small cavities running longitudinally inside osteon's walls called lacunae. Lacunae are connected with eachother by transverse canals called canaliculi.

The dense, interconnected net of lacunae and canaliculi, contains a network of bone cells (Osteocites) entrapped as a result of osteon formation.

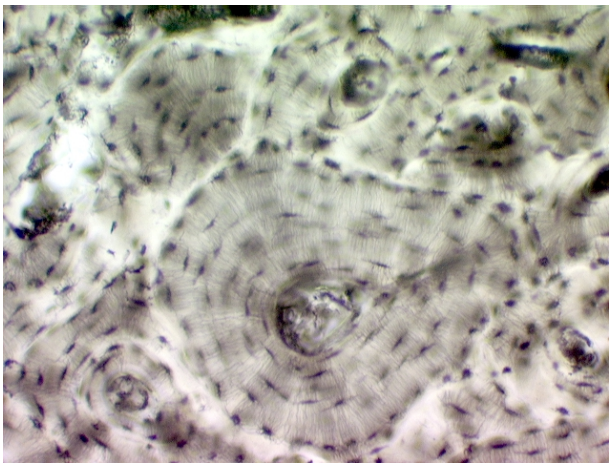

Figure 1.4: Detail of compact bone tissue.

It has been suggested that the osteocite network acts as a detector of bone microfracture and can activate, through biochemical signals, the mechanism of bone resorption and remodelling.
In cancellous or trabecular bone the structural unit is the trabecular packet itself, also called emiosteon (see figure 1.5).
The ideal trabecular packet is a 1 mm long and 50 μm thick cilinder-like bar connected with the structure with a radius of about 600 μm.

As with osteons in cortical bone, a cement line covering holds trabecular packets in cancellous bone.
Lamellar tissue of the hemiosteon appears to be aligned parallel with trabecular surface and hosts the typical lacunae with osteocites inside.

1.3 Cancellous Bone Mechanics

Bone is a non homogeneous material composed by both organic and inorganic substances. Its mechanical behavior is the result of the interaction of its inorganic solid (mineral) phase with the organic phase, which is made of collagen fibers. Trabecular composition is generally similar to the composition of osteons in cortical bone, but with a lower degree of mineralization and con-

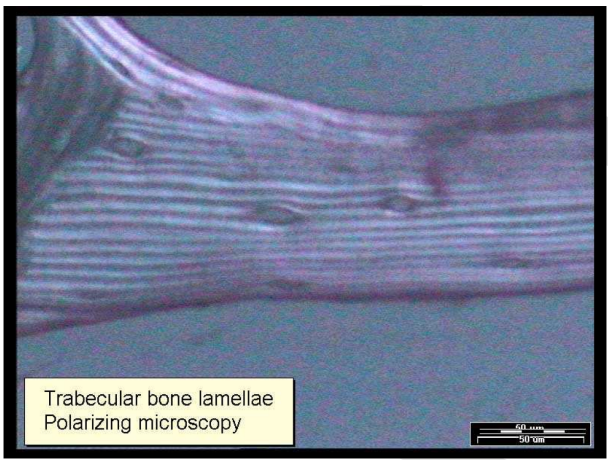

Figure 1.5: Polarizing microscopy image of the longitudinal section of an emiosteon. Lamellar fibers with different orientation present different brightness under polarized light. The presence of lacunae hosting osteocite cells can be noted.

sequently lower density (1.874 g/cm^3 for trabecular tissue versus 1.914 g/cm^3 for cortical tissue). The content of water being slightly higher in cancellous tissue (cancellous = 27 %; cortical = 32 %).
It is no doubt true that the main feature distinguishing cancellous from cortical bone is the typical trabecular organization in an interconnected and high porosity structure. As consequence of this fact, cortical bone volume fraction ranges between 85 95 %, as opposed to 5 60 % for trabecular bone.

1.3.1 Architecture

In trabecular bone, geometrical as well as physical properties can vary with anatomic site, age, gender, pathologies and more. It is therefore fundamental to possess solid methods for the estimation and the characterization of the trabecular structure. This can be done through the description of the following properties of cancellous bone:

- bone density
- main trabecular orientation

- trabecular thickness
- trabecular geometry

The estimation of the above mentioned characteristics of cancellous structure is a point of prior importance for the understanding of bone tissue mechanical properties and of phenomena like bone resorption and remodelling.
Two different approaches exists for the estimation of such parameters:

- 2D histomorphometric methods
- 3D reconstruction methods

Let's have a more detailed view of both methods and relative bone indexes that can be defined with.

Traditional 2D histomorphometric methods

Histomorphometric methods are based on the direct microscopical observation of specimens from hystological sections. This kind of method is considered as "gold-standard" for the direct determinations of structure parameters.
Bone biopsies have to be embedded in a resistant cement (commonly polymethylmetacrylate, PMMA) to allow 20 μm thick sectioning for microscopic observation (see figure 1.6). Images obtained with gold-standard technique (figure 1.7) can reach a definition of 4 μm per pixel.
After selection of the region of interest (ROI) the gray-scale image undergoes to a binarization process called segmentation where bone pixels are distinguished from non-bone ones by selecting a gray-scale value as limit level for bone tissue. From the binary image (figure 1.7), the following parameters describing trabecular architecture can be estimated:

- **Tissue Area** T.Ar $[mm^2]$ Total area of the ROI.
- **Tissue Volume** TV $[mm^3]$ Total volume of the ROI.
- **Bone Area** B.Ar $[mm^2]$ Total area of bone in 2D cross-section.
- **Bone Volume** BV $[mm^3]$ Total volume of bone in 3D cancellous model.
- **Bone Perimeter** B.Pm $[mm]$ Bone perimeter in 2D cross-section.

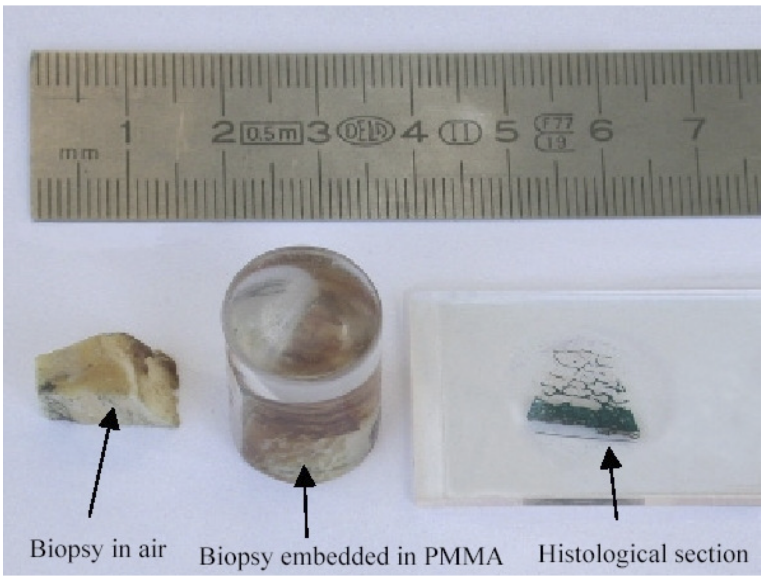

Figure 1.6: Bone biopsy and preparation of the histological observation procedure.

- **Bone Surface** BS $[mm^2]$ Total bone surface in 3D trabecular model.

From a stack of images a 3D ROI is assembled and the following primary indexes calculated:

- **Bone Volume Fraction**

$$BV/TV = \frac{Bone\,Volume}{Total\,Volume} \tag{1.1}$$

  Bone density, or bone volume fraction, can be calculated equivalently by the area fraction, the line fraction or the point fraction [4]. This means that there is no requirement for the orientation of planar or linear section probes. Typically, trabecular bone BV/TV varies between 10% and 30%.

- **Bone Surface Density**

$$BS/TV = \frac{Bone\,Total\,Surface}{Total\,Volume} \tag{1.2}$$

  BS /TV allows the quantification of bone-marrow interface of trabecular bone. Considering a section of the bone specimen, BS/TV is related to

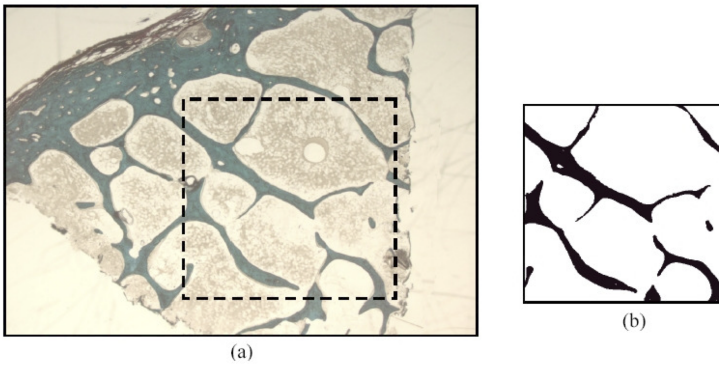

Figure 1.7: (a) Histological section of a bone sample containing both cortical and cancellous bone. The dashed line include the region of interest (ROI) ($4mm$ x $4mm$ in size) containing only cancellous bone. (b) Binary ROI: black pixels identify bone, the white ones identify background.

the linear length of the interface between bone and marrow per section surface.

A set of secondary indexes is useful for the description of trabecular geometry. It is common, in literature [4], to characterize cancellous bone structure by the assumption of two opposite ideal trabecular models. These are the plate-model and the rod-model.
For the calculation of the following secondary indexes, the plate-model assumption is used for trabecular bone.

- **Trabecular Thickness** (μm) The main trabecular thickness with the plate-model structure assumption.

$$Tb.Th = \frac{2}{1.199}\frac{B.Ar}{B.Pm} = \frac{1}{2}\frac{BV}{TS} \tag{1.3}$$

- **Trabecular Number** (or trabecular density) ($1/mm$) The number of trabecular planes (in a plate-model structure) per unit length, along a direction normal to the plates.

$$Tb.N = \frac{1.199}{2}\frac{B.Pm}{B.Ar} = \frac{1}{2}\frac{BS}{TV} \tag{1.4}$$

- **Trabecular Separation** (μm) Is the distance within two plates in the plate-model trabecular structure.

$$Tb.Sp = \frac{1}{Tb.N} - Tb.Th \tag{1.5}$$

A condition for the histomorphometric observation, is the analysis of entire bone cross-sections. The observation is usually conduced over a reduced number of sections, due to the difficulties in slice's extraction. For this reason, the applicability of 2D histomorphometric methods is generally reduced.

3D methods

Three dimensional methods are based on the direct calculation of structure indexes on a 3D reconstruction of the bone specimen. Later, in this chapter, we will se how a 3D model of trabecular bone can be obtained from a micro X-ray Computed Tomography (micro-CT) data set.
Bone indexes can easily be obtained from 3D reconstructions with no use of structure geometrical assumptions. They're affected by an uncertainty witch is related only to the resolution of the micro-CT scan. We will introduce, here, structure indexes from 3D reconstructions of cancellous bone, refering to section 2.2 for a detailed view of the generation of 3D cancellous bone reconstructions from micro-CT data sets.

- **Model Independent Trabecular Thickness** ($Tb.Th*$) (μm) Taken a trabecular structure and a point of it, trabecular thickness can be locally defined as the diameter of the maximum sphere fully included within the structure and including the point itself. A mean value for $Tb.Th*$ is obtained by averaging over the whole volume.

- **Model Independent Trabecular Separation** ($Tb.Sp*$) (μm) Can be calculated with the same technique described for Tb.Th considering points of the marrow cavity.

- **Mean Intercept Length** (MIL) MIL method quantifies the structure interface anisotropy.
  A linear grid is placed onto the selected Region Of Interest (ROI) of the

trabecular structure with orientation ω. The number of interseptions of the bone-marrow interface with the grid ($I(\omega)$) is counted. The mean length separing two interseptions is calculated as:

$$MIL(\omega) = \frac{L}{I(\omega)} \tag{1.6}$$

Where L is the total length of the grid line. It is clear how MIL(ω) varies with the angle ω for structures with a certain rate of anisotropy.
A generalization of this technique for the 3D specimen space leads to the definition of an ellipsoid that can be expressed as the quadratic form of a second-rank tensor **M**. Cowin defined a *MIL fabric tensor* **H** witch as the inverse square root of **M** [4]. The **H** eigenvalues coincide with the *MIL* values in the main directions and it has been found that the larger values of **H** are associated with Young's Modulus maximum values of the structure.

- **Degree of Anisotropy** (DA) It can be calculated as the ratio between the length of the major and minor axes of the ellipsoid described by the vector *MIL*.

$$DA = \frac{MIL_{max}}{MIL_{min}} \tag{1.7}$$

Further seondary indexes can be obtained from 3D reconstructions. These are measures of *Trabecular Connectivity* and *Bone Apparent Density*. It is clear how 3D reconstruction allows an insight into trabecular structure and an accurate description of its properties thanks to the introduced indexes. Informations on trabecular bone morphology and anisotropy are prior for the better understanding of bone stress behaviour and mechanical properties, as it will be seen later with more details.

1.3.2 Apparent Mechanical Properties of Cancellous Bone

As we have seen in the previous paragraphs, cancellous bone presents a porous an interconnected structure which can vary largely, in shape and organization, with several subject-specific and zone-specific factors.
At a certain scale (4 to 5 mm for cancellous bone)[8, 1], a porous material can

be studied as a continuum media independently of its microscopic mechanical behavior. At this scale, trabecular bone exhibits mean mechanical properties that can be referred to the volume of bone under examination. These properties are commonly known as "apparent" properties.

1.3.3 Asymmetry

At the apparent level, trabecular bone exhibits strength asymmetry as well as asymmetry in its failure behavior between compressive and tensile loading.
In figure 1.8 the stress-strain curve is plotted for a compressive test of human cancellous bone.
In compression, yield is generally reached around $\epsilon = 0.05$. A plateau of deformation with constant stress is present and failure strains can reach the 50 %[4].
For tensile loadings, failure occurs earlier ($\epsilon < 0.03$) and the material presents brittle failure behavior. On the other side, its elastic modulus is substantially the same in tension and compression.

1.3.4 Anisotropy

The mechanical apparent anisotropy of cancellous bone is inherently connected with the highly anisotropic nature of its geometrical organization.
The degree of structural anisotropy of cancellous bone (for which an estimation can be calculated with equation 1.7) can vary with age, bone site and pathological factors, between others [4]. Similarly, the elastic modulus of cancellous bone can vary significantly with bone site and, coherently with trabecular organization, with the direction of applied load.

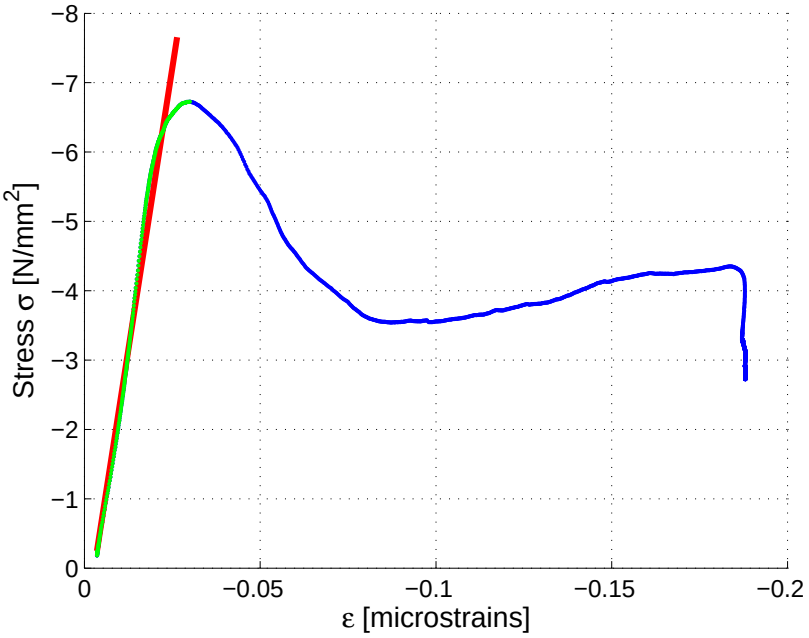

Figure 1.8: Stress-Strain curve for an experimental failure compressive test. Apparent modulus is obtained from the slope (in red in the graph) of the initial quasilinear loading region of the curve.

1.3.5 Relations between bone volume fraction and elastic properties

From the previous paragraphs it is clear how the elastic properties of cancellous bone vary with its density, geometrical organization and with the composition of its tissue. It has been demonstrated how bone density and trabecular organization (through the coefficients BV/TV and MIL presented in section 1.3.1) can account for between the 85 % and the 97 % of the variability of cancellous bone elastic properties [4]. Both linear and exponential relations have been proposed for the dependency between stiffness and bone volume fraction, the coefficients of the equations varying with bone site.

1.3.6 Assessment of Cancellous Bone Tissue Elastic Constants

The small dimensions of cancellous bone structural units (trabecular thickness = 50 μm), make the investigation of tissue level mechanical properties of this kind of bone an extremely hard task for the researcher. As we presented above, the proportionality between apparent stiffness and bone density have been suggested, thus considering the tissue elastic modulus of cancellous bone homogeneous and generally similar to cortical tissue modulus.
Recently developed experimental techniques, based on the combination of mechanical tests with FEM modeling, have made it possible to characterize the trabecular bone tissue modulus[19, 38, 10, 34, 13]. On one side, this kind of investigation have led to a wide range (from 0.76 to 20 GPa) of cancellous tissue modulus values reported in the literature [34](3.5 - 8.6 GPa), [19](5.5 - 7.7 GPa), [33, 26, 10, 46]. On the other hand, investigators seem to agree in reporting a cancellous modulus lower than cortical modulus of between 10 % and 20 % [4].
We will present here most common techniques in use for the characterization of trabecular tissue modulus of elasticity.

Uniaxial Tensile and Bending Tests

Several delicate tensile testing systems have been designed for the determination of cancellous tissue modulus. Testing of such small specimens is associated with several technical difficulties like the irregular specimen's geometry and the alignment of the sample with the external load. For these reasons, tensile and bending tests seem to underestimate trabecular tissue modulus [4].

Ultrasonic Techniques

The origin of these techniques is found in the principle by which the speed at which sound travels through solid matter depends on its elastic properties and density. Ultrasonic technique can be applied either to the continuum level cancellous volume or to a microspecimen to measure the stiffness of cancellous tissue. In both cases, its application provide very similar modulus values for

cancellous bone tissue, which are significantly lower than the corresponding cortical bone modulus.

Micro-Indentation and Nano-Indentation

Micro-indentation of bone tissue was first introduced in the fifties. During the last 20 years Nano-indentation has been used for the determination of bone tissue properties. With an indenter of 2 μm in size and a depth-sensing resolution of nanometers, the unloaddisplacement curve is used to calculate a material elastic modulus. Roughly speaking, nano-indentation has given the higher values for the bone tissue modulus [4].

Numerical Back-calculation with Finite Element Models

From the early seventies the modeling of bone has been proposed as a tool for the investigation of its mechanical behavior.
With the advances introduced by new micro-imaging technologies such as micro-CT, it became possible to accurately describe the 3D microscopic structure of trabecular bone. At the same time we assisted to the development of powerful supercomputers that are now able to solve FEM models characterized by millions of nodes.
The direct conversion of microscopic images from tomographic techniques into hexahedral element based micro-FEM models is at the date a standard approach for the investigation of trabecular bone tissue properties[38, 37, 13, 39, 41].

The process is based on non-destructive mechanical tests (generally uniaxial compression) of cubic or cylindrical trabecular bone samples.
The experimental apparent modulus of cancellous bone ($E_{app\,exp}$) is calculated from the results of mechanical test.
Assuming a tentative value for the cancellous bone tissue modulus of the μ-FEM model ($E_{t\,FEM}$), the predicted apparent modulus $E_{app\,FEM}$ of the model can be determined by simulation of the same boundary conditions as in compressive tests. Within the assumption of linear elasticity, the effective cancel-

lous bone tissue elastic modulus $E_{t\,eff}$ can then be determined by:

$$E_{t\,eff} = \frac{E_{app\,exp}}{E_{app\,FEM}} E_{t\,FEM} \tag{1.8}$$

In this process, errors may be introduced by experimental artifacts such as fastening of the specimen's endcaps and the measurement of trabecular displacements with the use of an extensometer.
Recently, the development of experimental layouts free of this kind of artifacts, has led to the estimation of values of cancellous bone tissue modulus the 10 % lower than the modulus of the cortical component of the corresponding bone section.

In the next chapter, we will introduce the experimental based technique used at Rizzoli's Orthopedic Institute Laboratory of Medical Technology for the determination of cancellous bone tissue mechanical properties. As we will see, the process in use is based on the reconstruction of micro-FEM voxel models of trabecular samples from the data sets obtained through micro-CT scanning. The estimation for the tissue modulus is obtained by use of the back-calculation procedure introduced here.

Chapter 2

From *Micro-CT* data sets to 3D *Micro-FEM* models

Trabecular bone distributes load from articular surfaces to cortical bone through its bone matrix. The trabeculae in this matrix constitute the actual load-carrying construction.
In the previous chapter we've seen how the material properties of the trabeculae, in combination with their architecture, determine the strength and stiffness of trabecular bone under loading.
From the late eighties, several attempts have been described in the literature to determine the trabecular tissue material properties. The purposed techniques include traditional tensile and bending tests applied to single trabeculae, four point bending experiments, microtensile and ultrasonic techniques.

A more precise way for the determination of tissue stresses and strains can be achieved if the architecture of a large portion of cancellous bone can be represented in detail through a numerical 3D finite element model.
Computed Tomography and the recent introduction of micro-CT enable the scanning of bone specimens at high-resolution (10-30 μm), which allows detailed visualization of the trabecular structure.
By use of a "pixels to voxels" conversion technique, high-resolution (or micro-) FE models incorporating trabecular architecture can be generated.
The advancement in computer hardware and solving strategies obtained in the

nineties made it is possible to analyze now the elastic behavior of large[1] bone regions with micro-FEM models [38, 1, 9, 30, 37, 36, 39, 40].

In the present chapter we will follow the steps that lead to the generation of a *micro-FEM* model of a trabecular bone specimen from its high resolution *micro-CT* scanning.

2.1 Computed Tomography

X-ray computed tomography (CT) is a medical imaging technique which allows reproduction of cross-section (tomographic) images of a certain part of the body. The process (invented by nobel prize Sir. Godfrey Hounsfield in 1967) is based on projection data obtained from the attenuation of X-rays radiations. Algorithms allow back-calculation of cross-section images of the object from projection data. With proper calibration of the system, cross-section images can then be converted in density (Hounsfield Units) images.

[1] In recent studies [42], the in-vivo scanning through pQCT (peripheal quantitative computed tomography) was proposed as the basis for the reconstruction of micro-FEM models (isotropic voxel size = 82 μm) of entire bone regions whole bone segments (generally distal radius). the micro-FEM modeling of the distal radius as a comparison with homogeneous bone FEM models.

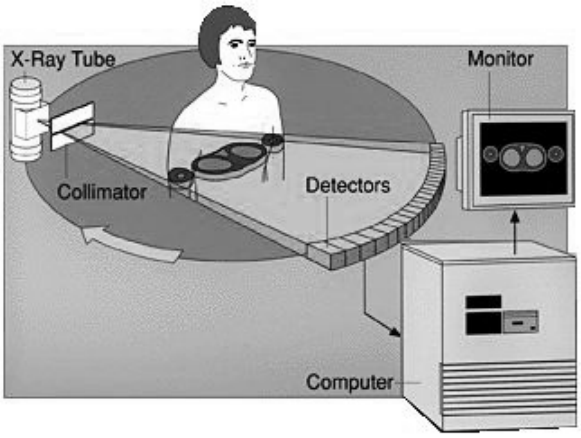

Figure 2.1: Computed Tomography: scheme. Projection data obtained from the attenuation of X-rays radiations is converted in density (Hounsfield Units) images from proper algorithms.

Micro CT was introduced in the late 1980's. Its process is based on a compact fan-beam type of tomograph and the full 360°rotation of the mechanism around the specimen to be scanned.
Each micro-CT image (figure 2.2) reproduces a 2D distribution of linear attenuation coefficients dependent on the atomic composition of the scanned material. In modern devices, this leads, after proper calibration and convertion of attenuation coefficients, to a cross-section density image of extraordinary nominal resolution (pixel size = 4 to 30 μm for gold standard devices).
For high resolution micro-CT scanning of cancellous bone, cylindrical or prismatic specimens with a diameter (or side length, respectively) of the order of 5 to 10 mm should be used.

In this thesis, we will refer to the micro-CT scanning procedure in use at the Medical Technology Laboratory of Rizzoli Orthopaedic Institute.

2.2 Imaging of micro-CT data-sets

The technique in use at Rizzoli's Institute facilities is based on the scanning of cylindrical cancellous bone specimens (generally: Height = 20mm; Diameter

$= 10mm$, [27, 28]) from biopsy of human femural head thank to a Skyscan micro-CT[2] with 0,90°rotation step over a total acquisition angle of 185°.
The result of the reconstruction from micro-CT attenuation data is a stack of 1024 x 1024 [pixels] grey-scale slice images (pixel size = $19.5\mu m$), with a z-axis step of $19.5\mu m$. An example of cross-section image is shown in figure 2.2.

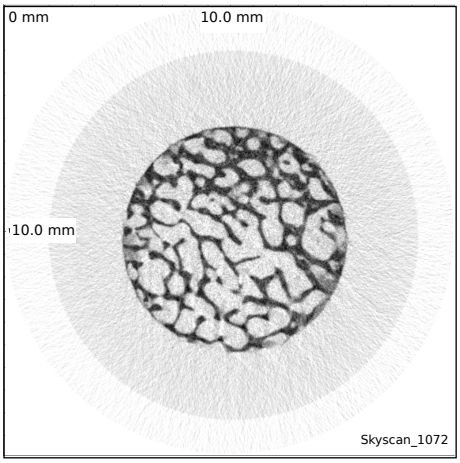

Figure 2.2: Micro-CT scan output: cancellous bone cross-section grey-scale density image. The region of interest (ROI) represents only the central part of the output image.

2.2.1 Binarization of cross-section images

The distribution of grey-scale attenuation coefficients of a typical cross-section micro-CT reconstruction image is shown in figure 2.3. Grey levels are inherently related with the density of the media which is scanned. The higher peak of the histogram corresponds to image background and marrow regions, while the lower peak to bone tissue.

It is important, when analyzing the histogram of cancellous bone cross section attenuation coefficients (figure 2.3), to focus on the wide range of grey-scale values that is displayed. This is caused by bone density's natural variabil-

[2]Skyscan 1072®, BRUKER, Kontich, Belgium

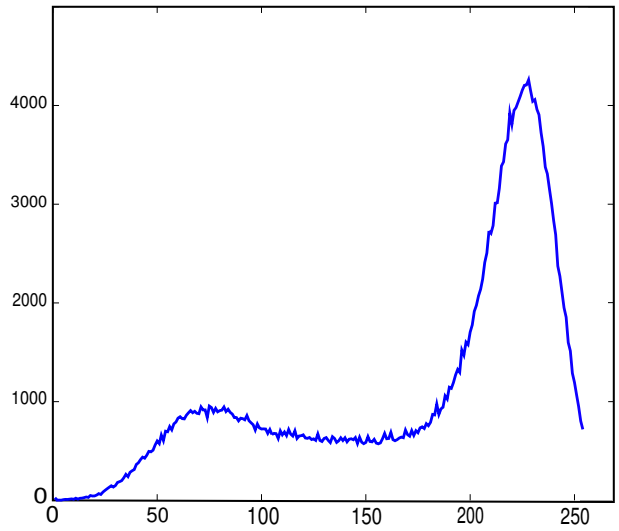

Figure 2.3: Density histogram of the grey-scale attenuation coefficients from the cross-section micro-CT scanning of cancellous bone. The monochromatic grey scale is related with density of the media which i scanned. The lower density peak represent bone tissue while the higher bone marrow and background.

ity and the uncertainty related to the micro-CT process of data acquisition and conversion. In reconstruction images (see figure 2.2), bone edges are blurred. This makes not trivial the task of tracing bone-marrow interface. In order to permit 3D reconstruction of cancellous bone structure, every image of the stack must undergo a binarization process called *segmentation* or *thresholding*, where bone tissue is distinguished from the non-bone background.

Different thresholding techniques have been proposed in the literature [17, 7, 43]. A distinction is usually made between local and global methods.

- **Global threshold** Global thresholding techniques assume a unique thresholdign gray-scale value for the binarization of the data set. The information on the thresholding level can derive from external histological observations. Alternatively, the level can be chosen so as to match BV/TV from 3D reconstruction calculation with BV/TV determined from direct

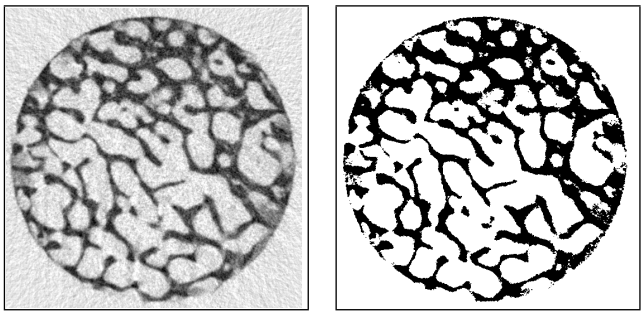

Figure 2.4: Binarization of cancellous bone cross-section data sets: on the left, the region of interest is shown before its binarization. On the right, the same reconstruction image is shown after the segmentation process. Localization of the bone-marrow interface will depend on the grey value chosen as threshold.

observation through histomorphometric methods (see section 1.3.1).

- **Local threshold** Local methods try to escape the difficulty of global matching by locally detecting the bone-non bone interface. This can be obtained with an imaging differential analysis for geometry detection. An example of local technique is the iteration of gradient-based geometry detection and connectivity test processes [43].

Kim, Zhang and Mikhail [17], investigated the effects of different thresholding techniques on micro-CT based trabecular bone models. Particularly, three thresholding procedures were considered: the global (standard) thresholding technique, a Match-global technique, based on matching of bone volume fraction from physical data, and an Adaptive technique, where severeal thresholds are obtained from regional histograms. Their findings suggest that predictions of mechanical structural properties of cancellous bone agree well with experimental measurements regardless of the choice of thresholding methods.
On the other hand Hara, Tanck, Homminga and Huiskes [7], investigated the influence of global threshold variations on the estimated mechanical and structural properties of cancellous bone. Their results confirm how threshold selection is important for the accurate determination of volume fraction and mechanical properties, especially for low bone density.
The thresholding procedure holds a primary role in the reproduction of a

subject-specific cancellous bone structure determining trabecular thickness and, consequently, trabecular connectivity. Separate thresholding methods may lead to different models with substantially different mechanical properties [17]. Similarly, for the global approach, the choice of the gray-scale thresholding value may have an impact on the resulting properties of the model [43, 7].

2.3 Generation of a 3D micro-FEM model

The stack of cross-section images obtained from micro-CT scanning is assembled, by use of a dedicated software, to generate a 3D gray-scale model of the trabecular structure. After this, the segmentation is realized with a determined global threshold.

The procedure performed in Rizzoli's Medical Technology Laboratory follows the points that are detailed below.

1. **From pixels to voxels** The stack of cross-section reconstruction images from micro-CT is imported to a medical imaging manager software. Every image pixel is converted to a volume voxel, where (cubic) voxel size is equal to the native image pixel size (19.5 μm) (see figure 2.5). Each voxel of the 3D model is assigned with the grey value possessed by the corresponding pixel of the original image.

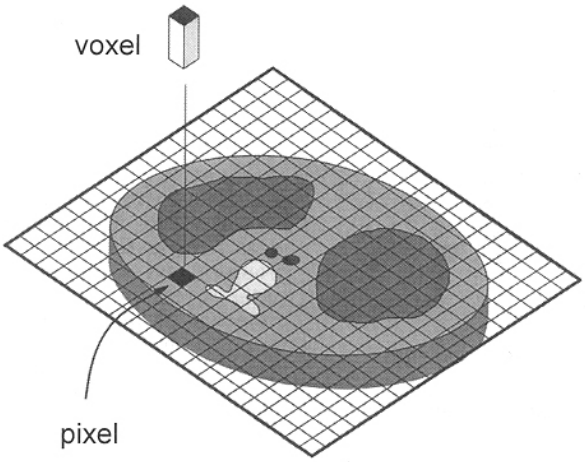

Figure 2.5: From pixels to voxels: each pixel of the reconstruction absorption image is converted to a cubic voxel. The height of each voxel corresponds to the distance between each section given by the scanner: 19.5 μm with Skyscan 1072 (Skyscan 1072®, BRUKER, Kontich, Belgium)

2. *Volume re-sampling* To reduce the total number of nodes of the FEM model together with computational cost, the assembled volume can be re-sampled to lower resolution: from the native voxel size of 19.5 μm to 39.0 μm. In this case, each re-sampled voxel will be assigned with the average grey-scale value of all native voxels included by this one. A sensitivity analysis have been conduced on a random set of specimens to investigate the influence of the re-sampling procedure on the estimation of the tissue elastic properties of cancellous bone (see section 4.2). This was found to be negligible for all the considered cases.

3. **Thresholding** The segmentation of the 3D volume is performed by use of a global thresholding technique, applied a fixed gray-sacle threshold value of *144* (see figure 2.6). The grey-level for the threshold have been obtained from a robust analysis previously realized at IOR's laboratories[29]. This was based on a comparison between the reconstructed micro-CT images (after their segmentation) and microscopic pictures of the corresponding histological sections.
   All voxels characterized by a gray-scale level greater then 144 represent

marrow cavity ad have to be excluded.

While for CT data, a standard calibration tool [14] is available for the conversion of Hounsfield Units (section 2.1) into mineral density, at the date, such a feature is not accessible for the micro-CT in use at Rizzoli's Medical Tecnology Laboratories. For this reason, no information is available on bone density at the microscopic scale and all voxels will be assumed to possess the same material properties.

4. **Connectivity test** A connectivity test is performed (figure 2.6). Here, only a single, interconnected cluster of voxels is maintained, eliminating non-connected bodies and thus defining a contiuous mono-connected structure model (this is a requirement for the FEM numerical analysis). Usually, the portion of non-connected structures discarded by the connectivity test represents between the 0.5% and the 2.5% (in number of elements of the micro-FEM model) of the entire reconstruction.

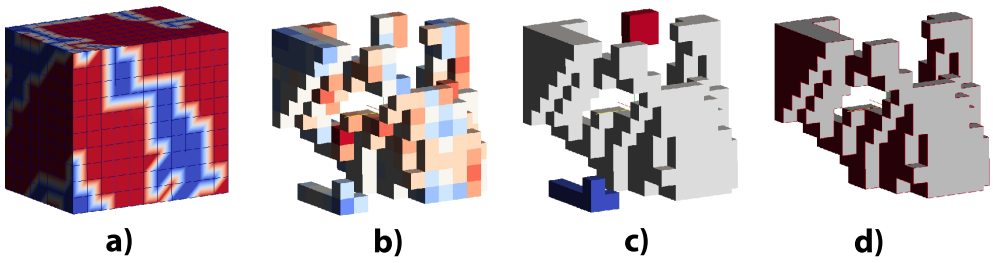

Figure 2.6: Segmentation and connectivity test for the generation of continuous trabecular structure voxel model: a schematic view. The voxel volume (a) is assembled from reconstruction images: a grey-scale value is assigned at each voxel. Segmentation process: all voxels with a grey level lower than the threshold level are removed (b), uniform property is assigned to all remaining voxels and the remaining non-connected regions are removed through connectivity test (c). A uniform voxel-based model (d) is obtained.

5. **Meshing, assignment of material properties and boundary conditions** The mesh of the 3D FEM model can then be defined. Each

voxel is assumed to be an hexahedron-shaped 8-nodes finite element (see section 2.3.1), usually referred to as brick element. Elements will be cubic due to the isotropic nature of voxels obtained from micro-CT dataset reconstructions. The basic model material (bone tissue) will be considered to be isotropic and homogeneous and generally characterized by a linear-elastic behaviour. Therefore, the constitutive law for bone tissue is uniqueley defined by only two parameters: elastic modulus and Poisson ratio. Tentative value are assumed for the parameters ($E_{t\,FEM}$ [GPa] and ν). The first is set at a uniform value of 19 GPa while the latter at 0.3 .

Once geometry and material properties of the hexahedral brick element FEM model are defined, external loading and boundary conditions are applied consistently with the experimental layout:

- *Lower boundary* Considering the bottom of the model of figure 2.12, displacements of all nodes laying under the PMMA cement height are fully constrained leaving no degree of freedom.
- *Upper boundary* At the same time, all nodes laying on the upper surface of the cylinder-shape model have horizontal displacement fully constrained. The vertical displacement is imposed, to simulate the uni-axial compressive behaviour of the experimental test

2.3.1 The eight-node hexahedral element

For the micro-FEM analysis of bone, tissue is modeled through the linearized elasticity equations. As it has been shown above, the procedure is based on equally shaped micro finite elements, obtained by simply converting all bone voxels to equally sized 8-node brick elements. The discretization of the elasticity equations on this domain by means of piecewise trilinear polynomials leads to a linear algebraic system of the form:

$$KU = R \tag{2.1}$$

where **K** denotes the *global stiffness matrix*, and is obtained through the assembly of the stiffness matrix of each element.

Figure 2.7 represents the 8-node hexahedral element with the system of natural coordinates (ξ, η, ζ). According to this coordinate system, the element's faces are defined by: $\xi = \pm 1, \eta = \pm 1$ and $\zeta = \pm 1$.
The coordinates x of each point of the hexahedral element e can be expressed through the interpolation of its nodal coordinates X with the coordinate shape functions $N_C^{(e)}$:

$$x^{(e)} = N_C^{(e)}(\xi, \eta, \zeta)X \tag{2.2}$$

Similarly, the displacement field can be expressed through the interpolation of nodal displacements U with the displacements shape functions $N_D^{(e)}$:

$$u^{(e)} = N_D^{(e)}(\xi, \eta, \zeta)U \tag{2.3}$$

Invoking the isoparametric concept, it is possible to use the same shape functions for the description of both element coordinates and displacements:

$$N_C^{(e)}(\xi, \eta, \zeta) = N_D^{(e)}(\xi, \eta, \zeta) = N^{(e)}(\xi, \eta, \zeta) \tag{2.4}$$

Being the displacements discretized by means of a trilinear polynomial of the form:

$$u(\xi, \eta, \zeta) = a_0 + a_1\xi + a_2\eta + a_3\zeta + a_4\xi\eta + a_5\eta\zeta + a_6\xi\zeta + a_7\xi\eta\zeta \tag{2.5}$$

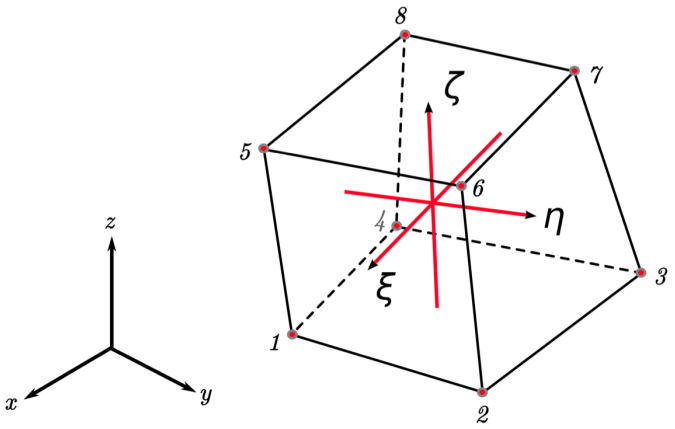

Figure 2.7: 8-node hexahedral "brick" element: the system of natural coordinates is defined by centroids of opposite faces, laying its origin on the element's centroid. In the natural system (ξ, η, ζ) each point of the element has coordinates in the range [-1,+1]. Nodes at $\zeta = -1$ are first numbered counterclockwise, followed by nodes at $\zeta = 1$.

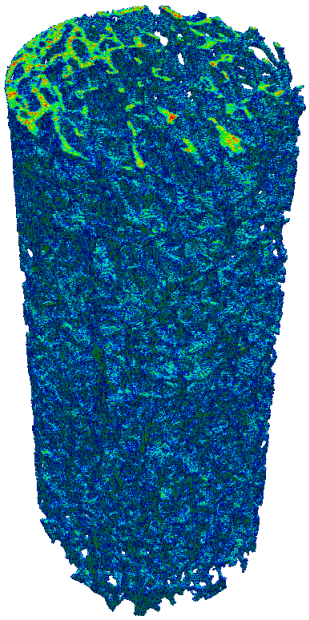

Figure 2.8: A 3D cancellous bone cubic voxel model. The colormap representing the reconstructed micro-CT attenuation coefficient.

2.4 Experimental compressive test

We will consider here the mechanical compressive test procedure performed at the Rizzoli's Orthopedic Institute facilities for the determination of the apparent elastic modulus of each bone specimen [27, 28].

Cylindrical specimens of trabecular bone, with a diameter of $10mm$ and a height of $20mm$, are extracted from donor's femoral heads by means of a bore diamond-coated milling cutter with the cylinder axis aligned with the Mean Trabecular Direction [28] (see figure 2.9). Bone slices are immersed in water during the milling procedure. After their extraction, specimens have to be left immersed in Ringers solution for 24 hours to ensure the rehydratation of the bone tissue. Specimen free length and diameter are measured. Thereafter, each cylinder is scanned by micro-CT (Skyscan 1072®, BRUKER, Kontich, Belgium) following a validated protocol [28], [27].

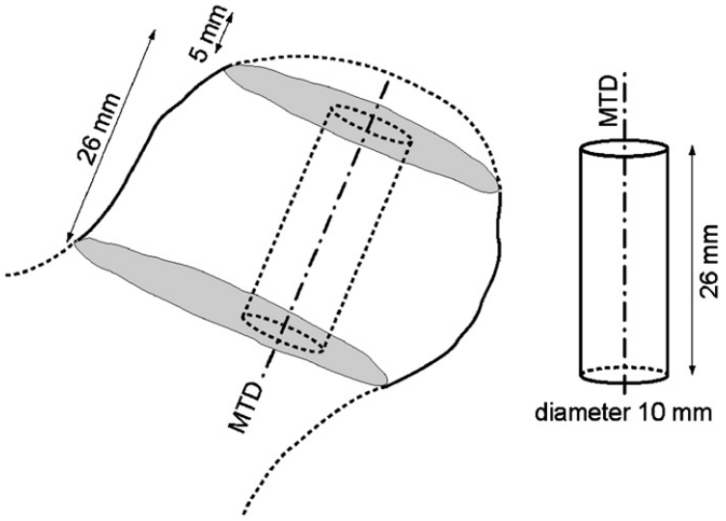

Figure 2.9: (Left) scheme of femural head with the inscribed 26mm thick bone slice, having the planes oriented orthogonally to the main trabecular direction (MTD, dashed-dotted line) determined previously. The bone slice is cut out from the head, and then the cylinder is drilled out from the slice. (Right) The cancellous bone cylinder extracted (diameter 10mm, height 26mm).

Before testing, specimens are immersed in Ringers solution for an additional hour. Bone specimens are cemented directly onto the testing machine (Mod. 8502, Instron Corp., Canton, MA, USA) to ensure the alignment between the loading direction and the specimen axis.
Average strain is measured with an extensometer (Mod. 2620-601, Instron Corp., Canton, MA, USA) attached with two rubber bands directly to the central part of the cylinder. The experimental layout for compressive test and the assembly of the extensometer are shown in figure 2.10. It is important, for the compressive test of cancellous bone specimens, to minimize end-artifacts and side-artifacts which can influence the experimental results [35], [3], [15], [20]. The described technique allows the accurate determination of apparent strain since its measurement is unaffected by end effects [15]. Strain rate[3] is controlled during the test and maintained at $0.01s^{-1}$ [28, 20, 40, 22].

The mean elastic modulus of the specimen, usually referred to as apparent elastic modulus, is calculated as the mean slope of the loading curve in its linear elastic region.
In a late version of the experimental protocol (see chapter 5), the test is repeated four times, along four different angolar positions of the specimen. A system of aluminium markers embedded into the PMMA cement allows the identification of 4 angolar directions on the cylinder-shaped surface of the specimen separated by 90°each. The final elastic modulus will then be extimated as the mean value of the modulus registered for each angolar positioning.
Subsequently, a failure compressive test is performed, to gain further informations on the yielding curve and post-elastic behaviour of the specimen.
In figure 2.11 a plot of the stress-strain curve from experimental failure compressive test of a cylindrical cancellous bone specimen is shown. A first order regression line (plotted in red in the figure) is fitted to the quasilinear region to observe a correlation coefficient $R > 0.99$. The apparent-level elasticity modulus of the bone specimen ($E_{app\,exp}$ [MPa]) is calculated as the slope of this regression line.

[3]Strain rate ϵ represents the speed of the load application during mechanical tests. The apparent elastic modulus of cancellous bone showed a direct dependence with strain rate[4]

Figure 2.10: Experimental layout for compressive test of a cylindrical cancellous bone specimen (diameter = 10 mm; free length = 20 mm). Specimen's endcaps are embedded into PMMA cement. Displacements at two levels of the specimen are registered with an extensometer (Mod. 2620-601, Instron Corp., Canton, MA, USA). The contact between cylinder and extensometer knives is ensured thank to two rubber bands.

2.5 Solution of FEM model

The aim of the micro-FEM model presented in section 2.3 is that of describing the mechanical test of figure 2.10.
Thanks to the linearity of the FEM model, it is possible to determine the effective tissue modulus by scaling the numerical results with those obtained from experimental testing [4, 40, 38, 1].
Displacements are imposed to the upper surface of the model, replicating the loading conditions of experimental compressive tests. The micro-FEM model is solved with the aim of the ParFE[4] iterative solver. The open source ParFE project provides a multilevel solver for micro-FEM bone structures based on the preconditioning conjugate gradient method.

[4]ParFE - Copyright (C) 2006 ETH Zurich, Institute of Computational Science, Uche Mennel, Marzio Sala, and all other ParFE developers

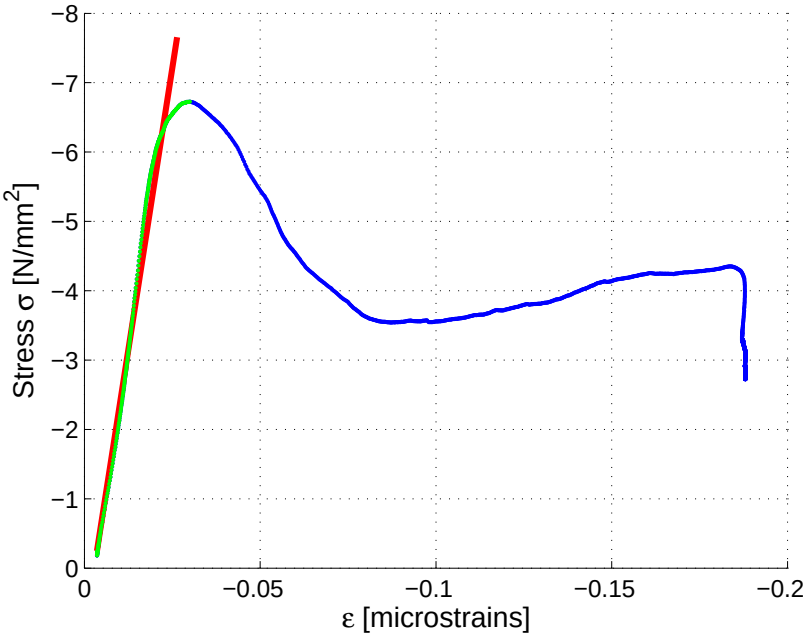

Figure 2.11: Stress-Strain curve from experimental failure compressive test. The elasticity apparent modulus is obtained from the slope (in red in the graph) of the initial quasilinear loading region of the curve.

2.5.1 Calculation of Apparent Modulus

Nodal displacements of all verteces of the micro-FEM model as well as the reaction forces at constrained nodes are registered. Considering the scheme shown in figure 2.13, two meaning heights are chosen (*z1* and *z2*), these corresponding to the extensometer rubber bands. For both levels, all nodes with the z coordinate inside the ($z_{level} \pm$ 0,51 voxel size) range are selected. Mean vertical displacements at levels *z1* and *z2* are calculated from the displacements of the selected nodes. The specimen apparent elastic modulus (E_{app}^{FEM} [MPa]) is estimated as follows:

$$E_{app\,FEM} = \frac{\frac{R}{A}}{\frac{L_2 - L_1}{L_1}} \tag{2.6}$$

Where R is the total reaction force at the two constrained surfaces and A is the nominal cross section of the bone specimen. L_1 and L_2 are the distances

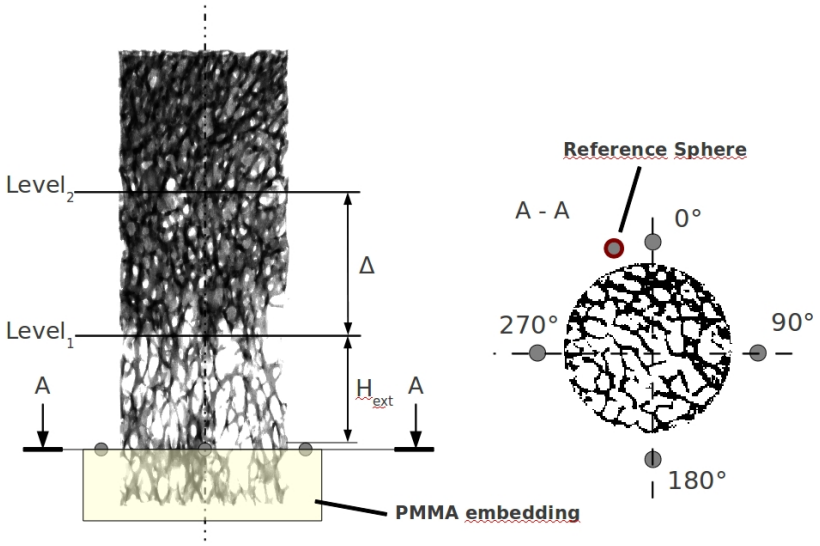

Figure 2.12: Experimental layout scheme for the test of cylindrical cancellous bone specimens (diameter = 10 mm; free length = 20 mm). Specimen's endcaps are embedded into PMMA cement. The two extensometer reference levels are shown. Eventually, a marker system of aluminium spheres allows the repetition of the test along 4 different angolar positions at 0°, 90°, 180°and 270°, respectively, as is shown on the right.

between the extensometer rubber bands before and after solution of the model, respectively.

2.5.2 Back calculation of Tissue Modulus

The effective tissue modulus, in GPa, is finally obtained from the results of FEM analysis and those of mechanical testing, with equation 2.7.

$$E_{tissue}^{EFFECTIVE} = \frac{E_{app}^{EXP}}{E_{app}^{FEM}} E_{tissue}^{FEM} \tag{2.7}$$

Where $E_{app\,exp}$ is the apparent level elastic modulus obtained from mechanical testing, E_{app}^{FEM} is calculated with equation 2.6 and E_{tissue}^{FEM} is the first approxi-

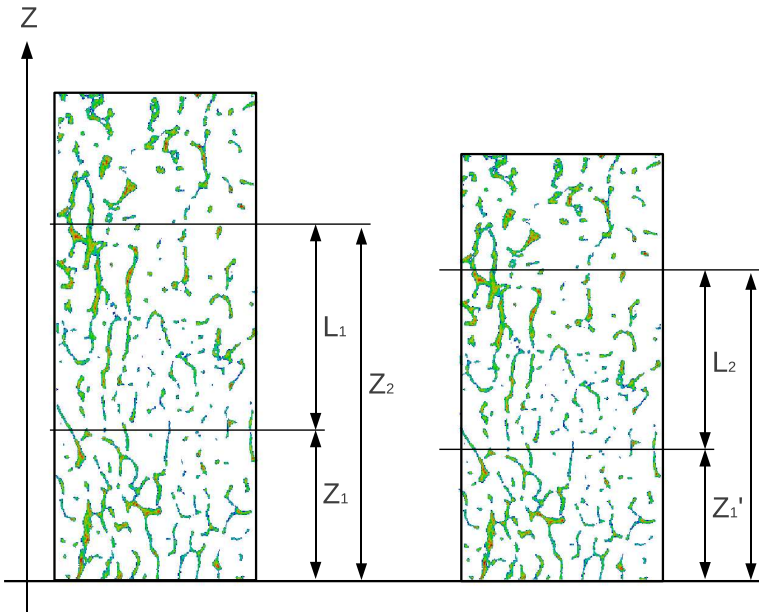

Figure 2.13: Specimen scheme: the model is shown before (left) and after (right) its solution. Levels z_1 and z_2 correspond to extensometer rubber bands.

mation model tissue elastic modulus, in GPa.

The procedure presented in this chapter describes how cancellous bone specimens can be characterized using micro-CT scanners. Using the voxels-to-hexahedral elements conversion technique micro-FEM models can be created. These micro-FEM models incorporate the full trabecular architecture and are capable of predicting anisotropic elastic behavior [13].
The advent of powerful computers together with scalable parallel micro-FEM solvers such as ParFE (Copyright (C) 2006 ETH Zurich, [24]) provide a tool for the specimen-specific investigation of the mechanical properties of cancellous bone tissue.
The predictive behavior of the ParFE based micro-FEM analysis will be examined in the next chapters as well as its sensitivity to the following parameters:

- Reconstruction Voxel Resolution
- Threshold Value

Chapter 3

Assessing the ParFE-based modelling procedure

In the pervious chapter, a procedure for the generation of micro-FEM voxels models of trabecular bone specimens from high resolution micro-CT scanning has been described.
The stack of grey-scale micro-CT attenuation images can be converted to 3D finite element models through the direct generation of equally sized cubic voxels from image pixels. The result of this operation is a 3D 8-node hexahedral element based FEM model. For a typical cancellous bone specimen (height = 20 mm; diameter = 10 mm) the obtained micro-FEM model (resolution = 39 μm voxel size; threshold grey value = 144) can be described by up to five millions of degrees of freedom.

Even if the discretization of the elasticity equations on this kind of domain is a well-known problem, on the other side the efficient solution of a model characterized by such a remarkable number of nodes is still a demanding issue. The higher computational time and memory required for the solution of a trabecular bone micro-FEM model makes the use of parallel, distributed memory numerical solvers, a mandatory strategy.

The ParFE Solutor

ParFE is an open source software consisting in a scalable and high paral-

lelization finite element solver for bone modeling. It was developed by the Informatics and Biomedical deparments of the ETH of Zurich[1].
To meet the characteristics of most problems, the ParFE software offers two different solution techniques:

- Preconditioned Conjiugate Gradient based solutor with assembly of the global stiffness matrix of the model;
- Element-by-Element Preconditioned Conjiugate Gradient based solutor.

The technique requires equally shaped hexahedral elements: the cubic voxel nature of micro-FEM models fitting properly with this requirement.
The use of a high parallelization FEM software would permit a significant saving of computational time spent for the solution of cancellous bone micro-FEM models. Being the solution of the system of linear equations associated with the model the bottleneck of the whole modelling process, the use of ParFE would produce a significant speed-up of the entire procedure.

3.1 Aim of the study

Previous analyses conduced at IOR's Medical Technology Laboratory have been supported by the use of Ansys®, a commercial suite for general purpose multiphysics FEM analysis [2]. A large database of cancellous bone specimens had been micro-CT scanned and tested to mechanical compression for the determination of apparent cancellous modulus through the procedure described in chapter 2. 3D voxel models had been reconstructed from stacks of micro-CT images.
These micro-FEM models, replicating the geometrical and mechanical characteristics of bone specimens as well as the compressive test performed in the laboratory, were solved with Ansys. The so obtained database represented the benchmark for the comparison with analysis performed with ParFE which will be presented in the present study.

[1]Copyright (C) 2006 ETH Zurich, Institute of Computational Science, Uche Mennel, Marzio Sala, and all other ParFE developers

[2]ANSYS® Academic Research, Release 14.0

On one side Ansys do not offer, at the current version, options for the desirable massive scaling of the process over all the available processors. On the other, the reliability of the ParFE[3] based modeling procedure, should be assessed on an existing cancellous bone database.
In this contest, the aims of the work presented in this chapter were two:

1. To confirm the use, for later studies, of the open source ParFE scalable software for the modeling of cancellous bone specimens, permitting this way the propitious reduction of total computational time.
   This would be obtained by:

   - finding acceptable agreement with the results previously obtained with the Ansys® Software and
   - assessing the predictive nature of the results obtained with ParFE for the cancellous tissue bone modulus.

2. To find conformation, at the same time, for the data base of cancellous bone tissue modulus previously calculated with an Ansys® based modelling procedure.

3.2 Materials and Methods

3.2.1 Trabecular bone specimens

For this work, 34 cylindrically shaped cancellous bone specimens from human femoral head was used.
The protocol for the specimen's extraction and its preparation is described in detail in section 2.4 of the previous chapter. No more than a brief summary will be provided here.

Specimens (9.65 to 10.0 mm in diameter and 15.5 to 20.6 mm in free length) were extracted from femur's diaphyses [27, 28]. A polymethylmethacrylate (PMMA) endcap was applied onto one end of all specimens. Finally, this was placed in Ringers solution for microCT scanning[27].

[3]ParFE is an open source project currently under development.

3.2.2 Micro-CT scanning

Trabecular specimens were acquired (*Skyscan 1072®, BRUKER, Kontich, Belgium*) using a standard protocol [29]: $50kVp$, $200\mu A$, $1mm$ aluminium filter, exposure time $5.9sec$, image averaged on 2 projections, rotation 180 °, rotation step 0.9°, field of view $20mmx20mm$ and an isotropic pixel size of $19.5\mu m$. Cross-section images were saved in 8 bit format (256 grey levels), 1024 x 1024 pixels in size.

3.2.3 Reconstruction of Micro-FEM models

Hexahedral elements models were reconstructed with a resolution lower than the μ-CT imaging resolution. (Voxel size = 39.0 μm instead of 19.5 μm).
Later, in section 4.2, we will discuss the validity of this approximation.
A uniform global threshold (grey scale value = 144) and the consequent connectivity test were applied to all models. A homogeneous tentative value for tissue elastic modulus was set at 19 GPa.

3.2.4 Experimental tests

The experimental compressive test procedure performed at the Rizzoli's Orthopedic Institute facilities for the determination of the apparent elastic modulus of trabecular bone specimens [27, 28] has been described previously in this document (see section 2.4) and will be only summarized here.
An extensometer was fastened to the central part of the cylinder thanks to two rubber bands (see figure 3.1). Strain rate was maintained at $0.01s^{-1}$ [28, 21, 16, 22].
The technique allows the accurate determination of apparent strain: the layout design minimizing end artifacts [15].

3.2.5 Solution of micro-FEM models

Boundary conditions were imposed to the model according with mechanical test layout (see figure 3.1): considering the bottom of the model, displacements of all nodes laying under the PMMA cement height were fully constrained. At

the same time, all nodes laying on the upper surface of the model had horizontal displacement forbidden and vertical displacement imposed to simulate the uni-axial compressive behaviour of the experimental test.
FEM models were solved with the use of the ParFe multilevel iterative solver (Iteration limit = $1E^{6}$; Tolerance = $1E^{-11}$). The complete run of a typical model (height = 20 mm; diameter = 10 mm; voxel size = 39.0 μm; threshold grey value = 144) required between 20 and 30 minutes and was executed over 32 processors on a dedicated calculus server.
By contrast, the same run with Ansys required at least 4 hours over 4 processors of the same IOR's server.

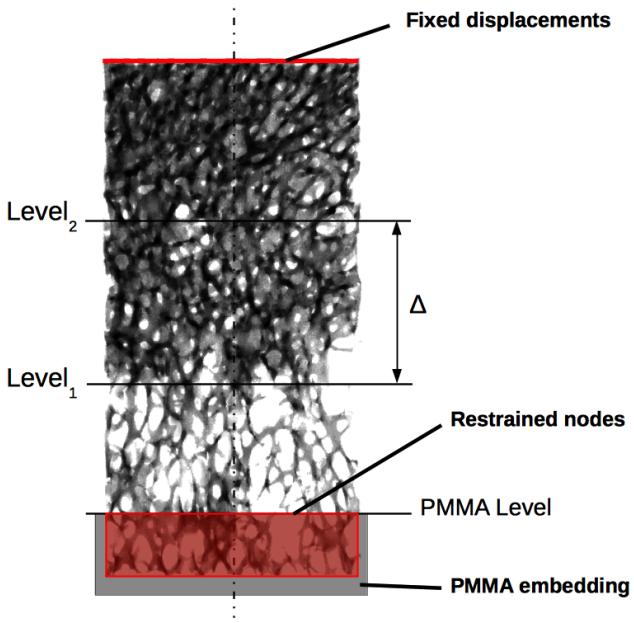

Figure 3.1: Experimental layout scheme for compressive test of cylindrical cancellous bone specimens (diameter = 10 mm; free length = 20 mm). Specimen's endcaps are embedded into PMMA cement. The two extensometer reference levels are shown. All nodes laying below the PMMA cement are fixed with no degree of freedom. A vertical displacement is imposed to all nodes of the upper surface to reproduce the compressive nature of the experimental test.

3.2.6 Determination of apparent elastic modulus from FEM results

In the sketch of figure 3.1, the two heights ($Level_1$ and $Level_2$) represent the estimated contact points between extensometer knives and trabecular surface. According to the experimental protocol in use, no angular reference for the contact regions was registered. As a consequence of this, the only measurable parameter is the initial distance Δ between the extensometer knives.
The z coordinates of ($Level_1$ and $Level_2$) were therefore estimated considering the cement level as height 0 and adding (or subtracting) one-half of the measured distance Δ from the specimen's midpoint.
The displacements of all nodes nearest to the planes cutting the specimen at z_{Level_1} and z_{Level_2}, respectively, were selected. The average displacement was calculated for each level and the apparent modulus from micro-FEM results was determined as follows:

$$E_{app}^{FEM} = \frac{\frac{R}{A}}{\frac{L_2 - L_1}{L_1}} \tag{3.1}$$

Where R is the reaction force at constrained surfaces and A is the nominal cross section of the bone specimen. L_1 and L_2 are the distances between the extensometer knives before and after solution of the model, respectively.

3.2.7 Back-calculation of cancellous tissue modulus

An estimation for the real trabecular tissue elastic modulus E_{tissue}^{EFF} is obtained from the postprocessing of the solved micro-FEM model and from the results of mechanical testing. This is done imposing (equation 3.2)that the numerical value of apparent stiffness obtained from the FEM model (which value is linearly dependent on the tentative tissue modulus E_{tissue}^{FEM}) corresponds to the experimentally derived value of E_{app}^{EXP}.

$$E_{tissue}^{EFF} = \frac{E_{app}^{EXP}}{E_{app}^{FEM}} E_{tissue}^{FEM} \tag{3.2}$$

3.2.8 Estimation of the cancellous tissue modulus of best fit

From the analysis described above, an estimation for the cancellous tissue elastic modulus is obtained by back-calculation for every specimen available in the database.
To obtain a value for cancellous tissue stiffness best fitting the apparent level elastic moduli of the whole database, the least squares method was used.
This was done through minimization of the sum of all squared residuals between experimentally and numerically determined apparent moduli. Being the residual defined as:

$$\varepsilon_i = E_{app,i}^{EXP} - E_{app,i}^{FEM}(E_{tissue}^{FEM}) \tag{3.3}$$

We already introduced the assumption of linear elasticity that gives, for every specimen i of the database:

$$\frac{E_{app,i}^{FEM}}{E_{tissue}^{FEM}} = \frac{E_{app,i}^{EXP}}{E_{tissue,i}^{EST}} \tag{3.4}$$

Where $E_{app,i}^{FEM}$ and $E_{app,i}^{EXP}$ are the apparent level cancellous bone moduli predicted by micro-FEM analysis and experimentally determined, respectively, for the specimen i. E_{tissue}^{FEM} is the tentative value for the tissue stiffness of micro-FEM models (this was set at 19 GPa) and $E_{tissue,i}^{EST}$ is the resulting estimation for the real tissue modulus of elasticity, for specimen i, in GPa.
Considering equation 3.4 it is possible to write the sum of squared residuals as follows:

$$\begin{aligned} F = R^2 &= \sum_{i=1}^{n} (E_{app,i}^{FEM} - E_{app,i}^{EXP})^2 \\ &= \sum_{i=1}^{n} \left(\frac{E_{app,i}^{EXP}}{E_{tissue,i}^{EST}} E_{tissue}^{FEM} - E_{app,i}^{EXP} \right)^2 \end{aligned} \tag{3.5}$$

Being n the number of specimens of the whole cancellous bone database from micro-CT scanning.
The best fit for the tissue modulus can be obtained by imposition of:

$$\frac{\partial F(E_{tissue}^{EST})}{\partial E_{tissue}^{EST}} = 0 \tag{3.6}$$

From 3.5 this is:

$$\frac{\partial F(E_{tissue}^{EST})}{\partial E_{tissue}^{EST}} = \sum_{i=1}^{n} \left(\frac{E_{app,i}^{EXP}}{E_{tissue,i}^{EST}} \right)^2 E_{tissue}^{BEST-FIT} - \sum_{i=1}^{n} \frac{E_{app,i}^{EXP\,2}}{E_{tissue,i}^{EST}} \tag{3.7}$$

We have:

$$E_{tissue}^{BEST-FIT} = \frac{\sum_{i=1}^{n} \frac{E_{app,i}^{EXP\,2}}{E_{tissue,i}^{EST}}}{\left(\frac{E_{app,i}^{EXP}}{E_{tissue,i}^{EST}} \right)^2} \tag{3.8}$$

Once the best fitting value of tissue modulus has been calculated, it is possible to obtain from this an estimation for the apparent level modulus of the micro-FEM model. From 3.4, we have for the i^{th} specimen:

$$E_{app,i}^{FEM}(E_{tissue}^{BEST-FIT}) = \frac{E_{app,i}^{EXP}}{E_{tissue,i}^{EST}} E_{tissue}^{BEST-FIT} \tag{3.9}$$

3.2.9 Statistic Cross-validation

Cross-validation is method for the estimation of the predicitve behavior of the results of statistic analysis on the application of a model. It is commonly used to asses how the results of a modelling procedure will perform on a different specimen's sample [6, 31].

2-fold cross-validation Is one of the most commonly used and simplest cross-validation procedure. The sample is randomly partitioned into two equally sized subsets. The statistical analysis is performed on the first subset (also called *training set*) and the variable of interest is estimated. The results are then validated on the second subset (which is also called *testing set*).

Leave-one-out cross-validation In Leave-one-out cross-validation procedure, only one specimen is used as testing group and all the remaining specimens constitute the training subset. The analysis is repeated for all specimens: the i^{th} specimen is excluded from the training subset and the i^{th} tissue modulus of best-fit is calculated from the remaining part of the whole sample.

3.2.10 Analysis of Predicitvity of ParFE on a database subsample

For this analysis the whole cancellous bone database was analyzed with ParFE. A schematic recap the procedure for the predictivity analysis of ParFE on the whole database is reported in figure 3.2

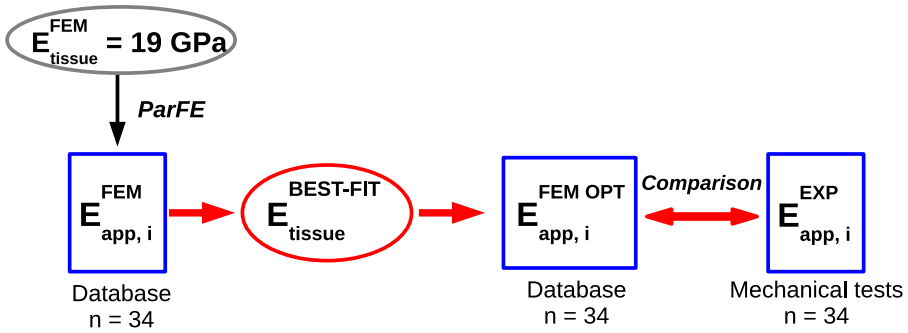

Figure 3.2: Predictivity analysis of ParFE on the whole database: the block diagram represents the procedure that led to the comparison between apparent moduli estimated from micro-FEM models and the results of mechanical tests.

Referring to the diagram of figure 3.2:

1. The best fitting tissue modulus was calculated over the whole 34 specimens database by use of equation 3.8.
2. Estimated apparent moduli for all micro-FEM models were calculated by use of equation 3.9.
3. The apparent modulus estimations were used for a direct comparison with the experimentally determined apparent stiffness.

At the same time, the 2-fold cross-validation method was applied.
A training subset of 17 specimens was randomly selected from the full database and the best best fitting tissue modulus was calculated (3.8). This value was used for the determination of the micro-FEM apparent modulus of the testing subset of the 17 remaining specimens.
The so obtained prediction for the second subset was compared with apparent moduli derived from compressive tests.

3.2.11 Comparison with the results obtained with Ansys

For this study, the same modeling procedure was followed twice for all micro-CT data-sets (34 specimens scanned).
Micro-FEM models were obtained independently for the solution with Ansys® and ParFE.
The comparison between the results obtained with the two different FEM solvers was based on the following points:

- Comparison of the best fitting tissue modulus calculated on the entire cancellous bone database with the least squares method.
- Comparison of the best fitting tissue modulus obtained through leave-one-out cross-validation technique for all cancellous bone specimens. The best fit for tissue modulus was calculated by means of the least squares method, excluding only one specimen of the database. The procedure was repeated for all n specimens.
- Comparison of the prediction of apparent modulus (E_{app}^{FEM}) for all specimens obtained with the two FEM solvers.
- Direct comparison of E_{app}^{FEM} predicted by the two softwares with experimental data.

3.3 Results

3.3.1 Predicitvity analysis

Comparison with experimental results

The best fitting tissue modulus $E_{tissue}^{BEST-FIT}$ obtained from the whole sample with the least squares method of (equation 3.8) was 18.25 GPa.
With this value (see block diagram of figure 3.2), a prediction for the *optimal* apparent level modulus $E_{app,i}^{FEMOPT}$ was estimated from equation 3.9 for every specimen.
In figure 3.3, the apparent moduli predicted for all specimens by the ParFE

based micro-FEM analysis with $E_{tissue}^{BEST-FIT}$=18.25 GPa are compared with the corresponding results of the mechanical tests.

Analysis of residuals[4] with respect to the affine linear regression of figure 3.3

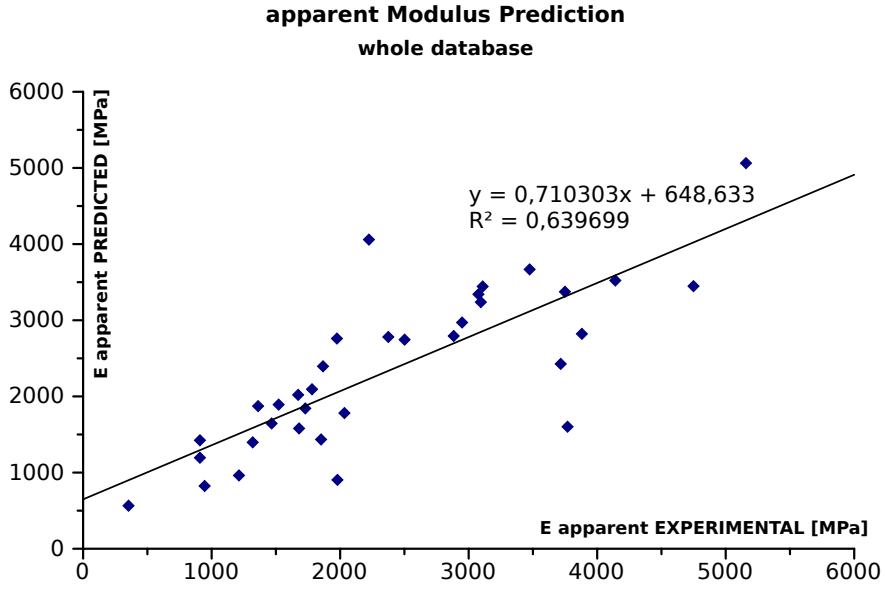

Figure 3.3: Comparison between predicted and experimentally determined apparent moduli for the whole database. (specimen number = 34; $E_{tissue}^{BEST-FIT}$ = 18.25 GPa; $R^2 = 0.64$). Affine linear regression of equation: Y=0.71+648.63

was conduced for the apparent level modulus predictions. The results of the residuals analysis are reported in figure 3.4.

2-fold cross-validation

For the 2-fold cross-validation predictivity analysis, a random subset of 17 specimens was partitioned from the original 34 specimens database.

[4]Residual were calculated as:

$$\varepsilon_i = \frac{|E_{app,i}^{FEM} - E_{app,i}^{REGRESSION}|}{E_{app,i}^{REGRESSION}} \tag{3.10}$$

where $E_{app,i}^{FEM}$ and $E_{app,i}^{REGRESSION}$ are the FEM prediction of apparent modulus and the corresponding value on the linear regression, respectively.

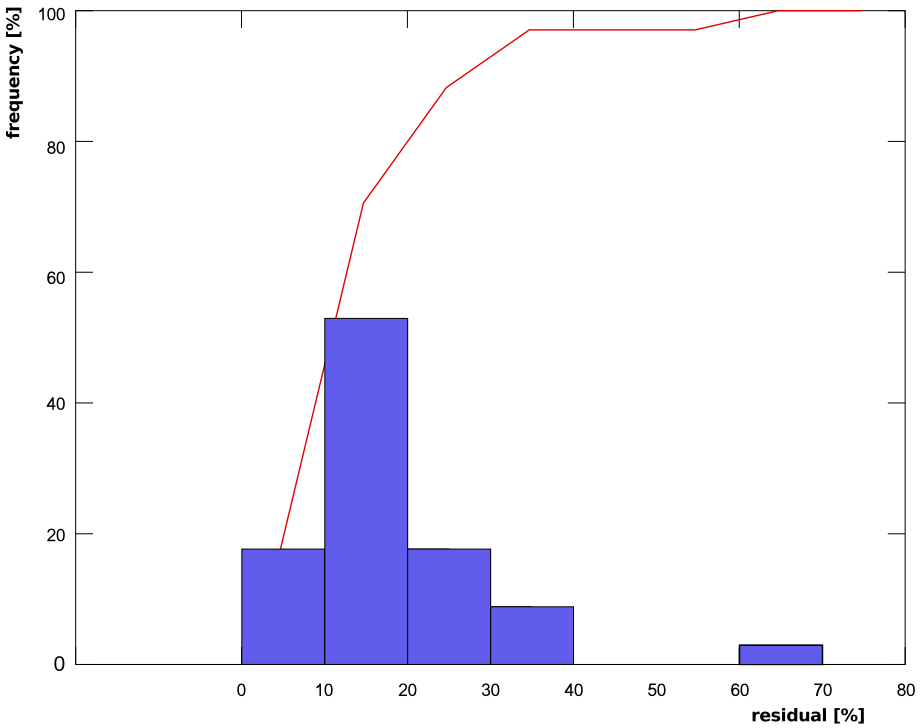

Figure 3.4: Residual analysis on the predicted apparent level modulus of elasticity for the investigated sample. The histogram represents the variance frequency. BLUE COLUMNS: absolute (percent) frequency; RED LINE: cumulative (percent) frequency. Residuals were obtained from the comparison with regression line of figure 3.3 (specimen number = 34; $E_{tissue}^{BEST-FIT} = 18.25$ GPa).

In table 3.1, experimentally determined apparent moduli and micro-FEM calculated tissue moduli for the training subset are reported.

A 18.95 GPa best fitting value for tissue modulus $E_{tissue}^{BEST-FIT}$ was obtained through least squares method from the training subset of table 3.1.

The resulting prediction of apparent modulus for the testing subset is reported in table 3.2.

ID	E_{app}^{EXP} **[MPa]**	**BV/TV (%)**	E_{tissue} **[GPa]**
1	3749	36,11	20,28
2	2033	29,42	20,82
8	2883	29,95	18,83
9	2948	32,05	18,11
13	5157	50,07	18,59
15	2374	30,95	15,58
17	3881	30,06	25,10
21	1319	21,99	17,24
22	1466	24,65	16,27
23	1978	15,82	39,94
25	3109	32,18	16,47
26	1781	25,17	15,52
27	1673	27,42	15,11
28	3769	26,09	42,93
29	1361	25,34	13,26
31	1521	23,57	14,67
33	945	14,38	20,94

Table 3.1: Training subset for the apparent modulus prediction with ParFE (specimen number = 17; $E_{tissue}^{BEST-FIT}$ = 18.95 GPa).

ID	E_{app}^{EXP} **[Mpa]**	**BV/TV (%)**	E_{tissue} **GPa**	$E_{app}^{PREDICTED}$ **[Mpa]**
3	1680	25,87	19,41	1640
4	3716	32,35	27,94	2521
5	2223	37,71	10,00	4216
6	4141	38,57	21,45	3658
7	3474	36,22	17,28	3810
10	2501	28,58	16,63	2851
11	909	24,14	11,65	1479
12	3075	34,20	16,80	3470
14	1728	21,68	17,12	1913
16	1866	28,54	14,22	2488
18	3094	33,74	17,44	3363
19	1975	28,69	13,06	2867
20	4749	35,86	25,13	3581
24	1851	20,51	23,55	1490
30	908	19,60	13,88	1241
32	1212	21,12	22,99	1000
34	353	11,67	11,41	586

Table 3.2: Apparent modulus prediction with ParFE: testing subset (specimen number = 17; $E_{tissue}^{BEST-FIT}$ = 18.95 GPa).

Data of table 3.2 is showed in figure 3.5. Here, the comparison between apparent moduli predicted with ParFE micro-FEM analysis and experimental data is presented. The plot reports the apparent modulus prediction (E_{app}^{FEM}) versus the corresponding experimentally determined value, for the 17 cancellous bone specimens of the testing subset.

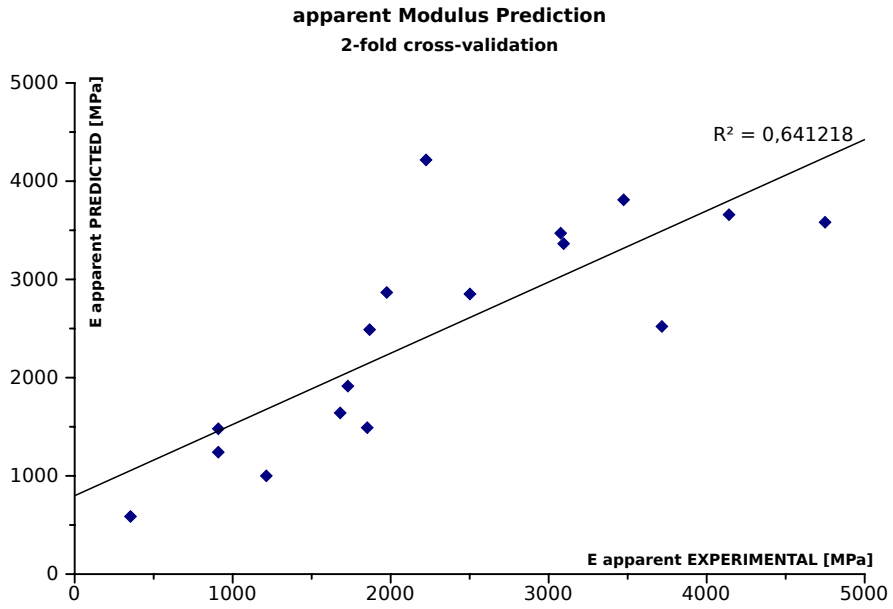

Figure 3.5: Comparison between predicted and experimentally determined apparent moduli for the testing subset. (specimen number = 17; $E_{tissue}^{BEST-FIT}$ = 18.95 GPa; R^2 = 0.64).

3.3.2 Comparison with the results obtained with Ansys

Cancellous tissue moduli were calculated for the entire database from micro-FEM analysis, independently with ParFE® and ANSYS®.
These values were used for the direct determination of a best fitting apparent modulus (equation 3.8).
The best fitting value obtained for the models solved with ParFE was **18.25 GPa**, while for the data processed with the ANSYS this value was **18.72 GPa**.

In table 3.3 predicted apparent moduli and micro-FEM calculated tissue moduli are reported for either the ANSYS® and the ParFE® based procedure.

Id	BV/TV	$E_{apparent}$ [MPa]			E_{tissue} GPa		Leave-one-out test E_{tissue} GPa	
			BEST-FIT					
	[%]	EXP	ParFE	ANSYS	ParFE	ANSYS	ParFE	ANSYS
1	36,11	3749	3374	3208	20,28	19,53	18,09	18,57
2	29,42	2033	1782	1802	20,82	20,18	18,17	18,68
3	25,87	1680	1580	1578	19,41	19,00	18,19	18,71
4	32,35	3716	2427	2414	27,94	27,01	17,94	18,45
5	37,71	2224	4059	4392	10,00	9,75	18,85	19,48
6	38,57	4141	3522	3603	21,45	21,74	18,01	18,56
7	36,22	3474	3668	3465	17,28	17,54	18,26	18,72
8	29,95	2884	2793	2832	18,83	18,06	18,18	18,71
9	32,05	2949	2970	3011	18,11	17,34	18,21	18,73
10	28,58	2501	2745	2787	15,64	15,97	18,30	18,79
11	24,14	909	1424	1443	11,65	11,26	18,26	18,78
12	34,20	3076	3341	3377	16,80	15,82	18,28	18,80
13	50,07	5158	5063	5110	18,59	18,87	18,15	18,70
14	21,68	1729	1842	1868	17,12	17,34	18,22	18,74
15	30,95	2375	2781	2682	15,58	15,15	18,30	18,79
16	28,54	1867	2396	2466	14,22	13,03	18,31	18,84
17	30,06	3881	2821	2834	25,10	23,19	17,95	18,47
18	33,74	3095	3238	3116	17,44	16,27	18,24	18,72
19	28,69	1975	2760	2668	13,06	11,85	18,38	18,87
20	35,86	4749	3448	3409	25,13	25,54	17,82	18,33
21	21,99	1320	1397	1526	17,24	17,52	18,21	18,75
22	24,65	1467	1645	1587	16,27	16,69	18,23	18,73
23	15,82	1979	904	896	39,94	41,14	18,12	18,64
24	20,51	1852	1435	1433	23,55	24,08	18,15	18,67
25	32,18	3109	3444	3375	16,47	16,87	18,30	18,79
26	25,17	1781	2094	2133	15,52	14,23	18,26	18,78
27	27,42	1673	2020	1949	15,11	14,46	18,26	18,76
28	26,09	3769	1602	1574	42,93	39,08	17,92	18,43
29	25,34	1362	1873	1909	13,26	12,22	18,28	18,81
30	19,60	909	1195	1192	13,88	14,30	18,23	18,75
31	23,57	1521	1892	1934	14,67	14,73	18,26	18,79
32	21,12	1213	963	939	22,99	24,27	18,18	18,70
33	14,38	946	824	820	20,94	21,58	18,19	18,71
34	11,67	353	565	558	11,41	11,85	18,21	18,73

Table 3.3: Apparent Modulus Prediction and LEAVE-ONE-OUT test: comparison of the results obtained with ANSYS and ParFE. Percentual difference in E_tissue prediction between ParFE and ANSYS: MEAN = 2.04 %; MAX = 7.05 %. Leave-one-out test results, E_tissue MEAN: ANSYS = 18.72 GPa; ParFE = 18.20 GPa.

Predictions of apparent modulus obtained with ANSYS® and ParFE® are compared in figure 3.6.

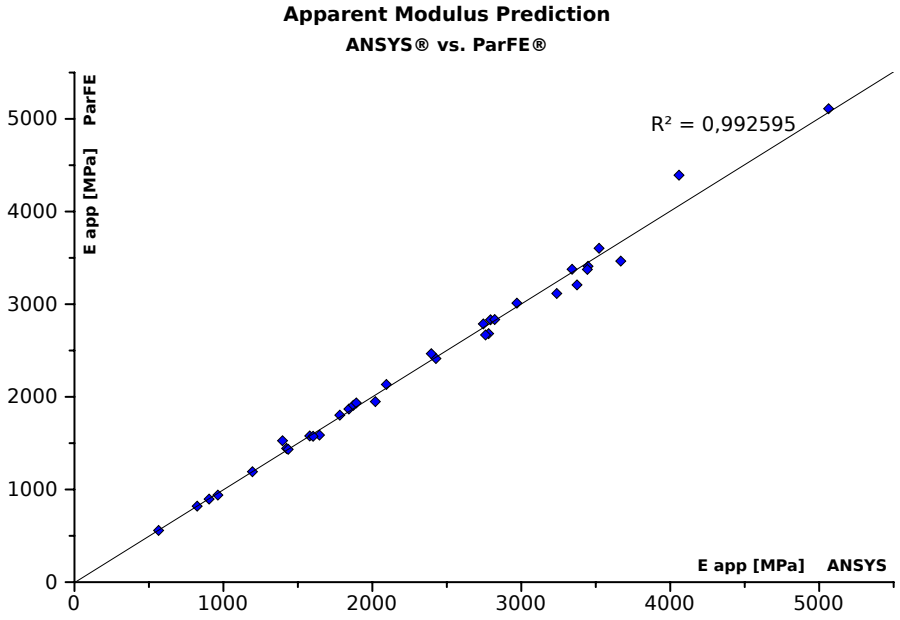

Figure 3.6: Prediction of cancellous apparent modulus from micro-FEM analysis: comparison between the results obtained with ParFE and ANSYS solvers. (specimen number = 34; $R^2 = 0.99$).

The same predictions for apparent modulus of figure 3.6 are compared with experimental results in figure 3.7.
The results of the application of the leave-one-out cross-validation technique on the whole cancellous bone database are shown in figure 3.8.
The bar chart reporting the best fitting value of cancellous tissue modulus obtained by exclusion of only one specimen from the training subset.

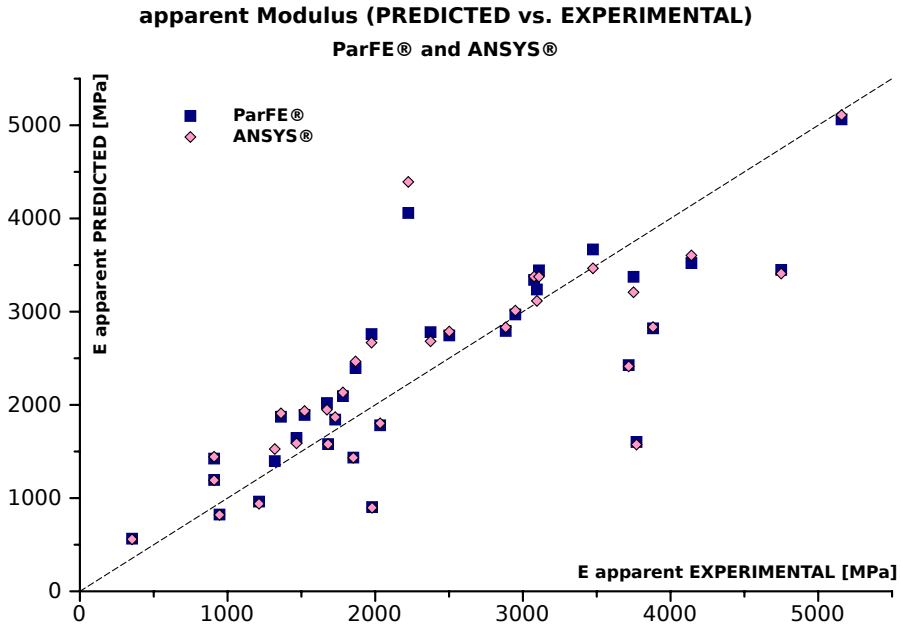

Figure 3.7: Prediction of cancellous apparent modulus from micro-FEM analysis: comparison with experimental results. (specimen number = 34).

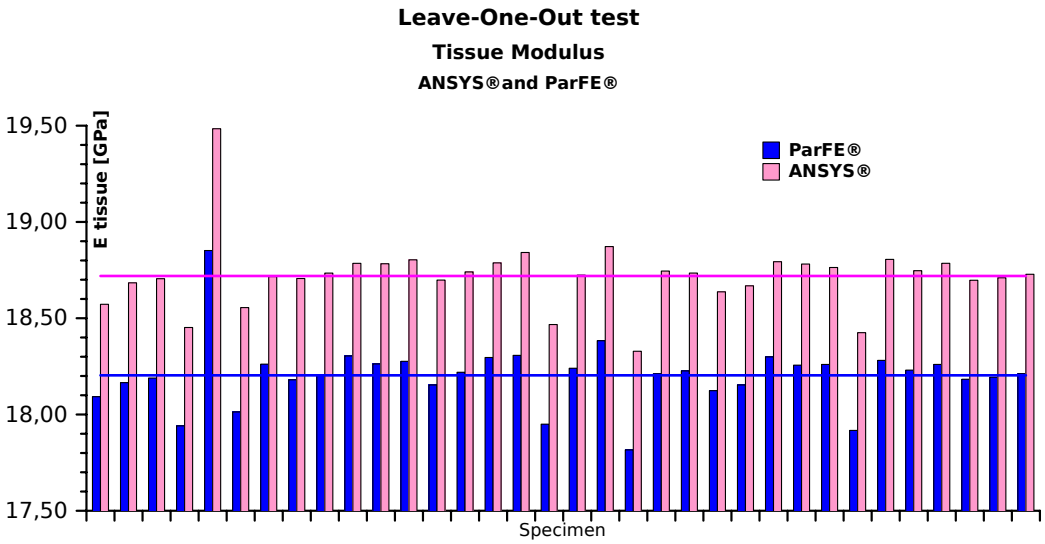

Figure 3.8: Best fitting values of cancellous tissue modulus obtained by exclusion of one specimen from the training subset. The best fitting value was obtained by mean of the application of least squares method. (specimen number of training subset = *n-1* = 33; MEAN: Ansys = 18.72 GPa, ParFE = 18.20 GPa).

3.4 Discussion

Comparison with the results obtained with Ansys In the second section of this chapter, a comparison between micro-FEM ParFE based predictions of cancellous bone mechanical properties with the equivalent properties previously estimated through an Ansys-based modeling procedure has been proposed.

The aim of the analysis conduced here, was to assess the coherence of the ParFE-based modelling procedure for the prediction of tissue modulus, through the comparison with the preliminary procedure which had been set up with Ansys. The consistency of the ParFE solutor had been previously verified on a benchmark problem of known solution available in a closed form, and was then out of the aim of this study. The source of information for the two modeling procedures was the same micro-CT scanning database at level of stack of bmp

reconstruction images. The graph of figure 3.6 shows the correspondence of apparent modulus predictions obtained with the ParFE and Ansys-based modeling procedures, suggesting the absence of software bugs afecting the ParFE. In figure 3.7, apparent modulus predictions of ParFE and Ansys are compared with experimental results. It is clear how both FEM solvers produce similar estimations of trabecular specimen's stiffness, supporting the hypothesis on the coherence of ParFE results with those obtained with Ansys. The results from the leave-one-out cross-validation test reported in figure 3.8 confirm the agreement (which has been found for all specimens) of the ParFE predictions of tissue modulus with those obtained with the use of a commercial FEM solver of high reliability as the Ansys. Both tests pointed out that some identical samples have great influence in the determination of an optimal value of tissue modulus $E_{tissue}^{OPTIMAL}$ for the whole sample. The coherence of the compared procedure is then confirmed.

The differences in the estimations of tissue elastic modulus observed between the two procedures could be attributed to the following issues:

- difference between the solvers implemented by the Ansys and the ParFE open source project which, additionally, was set with different tolerance limit ($1E-9$ for Ansys solver; $1E-11$ for the ParFE solver);

- difference in the post processing technique applied for the calculation of strains from nodal displacements in the two procedures. On one side, with Ansys, average displacements at the control levels (see description of section 2.5.1) were calculated selecting only nodes on the boundary of the structure: inner nodes were not considered.
  On the other, the post processing of ParFE results was performed with an algorithm developed at IOR for the optimal replication of experimental reality. This procedure, which considers all the nodes included in the considered cross section, can be considered more reliable;

- discrepancies introduced by the user: the two procedures (from the reconstruction of micro-CT data sets to the prediction of tissue modulus) have been conduced, independently, by two different users starting from the same stak of images. As a consequence, discrepancies between the

resulting micro-FEM models could have originated (e.g. the manual elimination of cross-sections affected by noise led to models different in length; then, the reference levels chosen for the post processing differ too).

Considering the coherence of the results obtained with the two different procedures, the replication in Ansys of the post-processing strategy applied for the ParFE-based modeling procedure, have been considered unnecessary. The reliability of our micro-FEM modeling procedure based on the use of the ParFE solver is assessed. From this point on, ParFE will be adopted at IOR's Medical Technology Laboratory, as standard numerical solver, for the modeling procedure aimed at the estimation of cancellous bone's elastic properties.

Analysis of Predicitvity of ParFE on a database subsample The results of the analysis on the predictive behavior of the ParFE based modeling procedure are reported in section 3.3.1.

A cancellous tissue modulus of 18.25 GPa was found through best fitting of apparent moduli from mechanical tests of all specimens of the available database. Observing the graph of figure 3.3 (comparison between predicted and experimentally determined apparent moduli for the whole database), two issues should be noted:

- A correlation was found between micro-FEM predicted and experimentally measured apparent moduli, the correlation coefficient being $R^2 = 0.64$.
- For a limited number of specimens, significant incongruity is shown between the modulus predicted by the FEM model and the corresponding value derived from mechanical tests. This resulting in a relatively low coefficient of correlation R^2.
- From the residual analysis of figure 3.4, it can be observed how for the 90% of the tissue modulus predictions, the resulting variance is lower than the 30% with respect to the regression line of figure 3.3. At the same time, the 70% of the statistical sample shows a variance lower than the 20%.

The results of the 2-fold cross-validation test seem to confirm what has been reported above: the correlation between FEM and experimentally determined

apparent moduli for a 17 specimens subset (figure 3.5) showed an essential agreement with the full-database estimation.
The coefficient R^2 resulted unvaried (0.64) and for a restricted number of specimens a large discrepancy between prediction and measurement was found.
For the training subset of the 2-fold cross-validation test, the resulting cancellous modulus best fitting experimental measurements was 18.95 GPa. This is a 3.69 % variation with respect to the modulus of best-fit for the whole database (18.25 GPa).
Finally, the same level of correlation between FEM results and experimantal measurements ($R^2 = 0.64$) was found through apparent modulus fitting, considering 17 or 34 specimens (see plots of figure 3.3 and figure 3.5).

High discrepancies between experimental measurements and numerical results were found for a restricted group of specimens. Distinct causes and issues should be taken into account for the understanding of this lack of accuracy:

1. The uncertainty affecting experimental measurements of apparent level modulus from mechanical tests. This was roughly of the order of 10% of the measured value of stiffness and derives from the propagation of errors affecting the experimental procedure.

2. The claimable incongruity between the process of determination of apparent modulus from micro-FEM modeling and the physical reality of experiments. While during compressive tests, displacements are measured at the surface of the specimen (on contact points between trabecular structure and extensometer knives), in numerical modeling, these are averaged on the entire cross section of the specimen. This can cause a significant inaccuracy of the prediction of apparent modulus. In chapter 5, the uncertainties connected with this kind of approach will be detailed and an alternative experimental layout will be proposed for the reduction of model discrepancies.

3. The height at which the extensometer was fastened for the measure of displacements. Since the experimental layout does not take into account the registration of the height of the two extensometer's knives, during numerical post-processing this input could only be approximated.

4. The incompleteness of the reconstructed architecture. Since the micro-CT's field of view was not sufficient for the scan of the entire specimen's length, only the central portion of it (roughly up to the 70%) could be reconstructed.

The tissue modulus prediction obtained thanks to our modeling procedure, is included in the range (2 - 20 GPa) which is reported in literature[34](3.5 - 8.6 GPa), [19](5.5 - 7.7 GPa), [33, 26, 10, 46]. The value of 18.25 GPa is in particular coherent with the last values reported in literature[1]($18.0 \pm 2.8GPa$) and with studies reporting the similarity between cancellous bone tissue and cortical bone tissue[33]($23.6 \pm 1.5GPa$). As it has been discussed above, a good predictivity of apparent level modulus is confirmed, being high residuals restricted to a small number of specimens. These cases can be related to the incomplete characterization of the experimental counterpart (e.g. lack of accurate extensometer's height reference, incomplete micro-CT acquisition.). In addition, the obtained modulus predictions are based on the hypothesis of a unique value for the tissue modulus common for all specimens. These, indeed, derive from different donors and different age category (MEAN: 65.73, MIN: 49, MAX: 83).
Even though the majority of the cited works which propose apparent level modulus predictions rest on the hypothesis of the invariance of E_{tissue}, the literature support too the hypothesis of an E_{tissue} dependency with the age[45, 19] and with the donor[46]. In effect, the dependency between tissue modulus and causes of variability of the bone tissue constituents (bone mineralization, collagenic component's properties) is commonly suggested. However Jaasma[11][5] suggest that when the variation coefficient of E_{tissue} is smaller the 20%, negligible errors are introduced in the $E_{apparent}$ prediction with micro-FEM modeling. It could therefore be supposed that incongruities in $E_{apparent}$ predictions are related with singular values of tissue modulus, deviating from the so considered unique value of E_{tissue}.Although the stability of the values obtained for E_{tissue} from the leave-one-out test of the present study, the question on the consistency and effectiveness of a single value of E_{tissue} is far from being closed.

[5] who isolate too the intra-specimen variability of E_{tissue} for the determination of apparent level modulus predictions

Chapter 4

(A couple of) Sensitivity studies

In chapter 3, the use of the scalable FEM software ParFE for the fast solution of micro-FEM models deriving from micro-CT scans of cancellous bone specimens has been described.
The coherence of the ParFE based procedure's results with respect to those obtained with the commercial FEM solver Ansys was assessed.
At the same time, the predictive character of trabecular modulus estimations obtained with ParFE resulted to be confirmed.

In chapter 2 the complete procedure for the characterization of linear micro-FEM voxel models of trabecular bone was detailed.
Here, the importance for the resulting FEM models of two user-defined parameters has been introduced:

1. the grey value *threshold level*. This parameter has an interaction with the thickness of the trabecular structure considered for the reconstruction of the 3D cubic element model

2. the *reconstruction resolution* of the model. Representing the size of the cubic elements (voxels) that constitute the basis of the 3D micro-FEM models.

It is no doubt true that both variables are directly connected with the geometrical coherence of the FEM model to reality and, by consequence, with the

accuracy of the estimation of trabecular bone mechanical properties.

The choice of an optimal value for the *threshold* is linked to the comparative study of the bone volume fraction of micro-CT reconstructions with the bone volume fraction deduced by histological observation of the same cancellous cross-sections. The experience developed at the Rizzoli Orthopedic Institute (IOR) showed the robustness of this strategy for the threshold determination in terms of its reliability for the estimation of cancellous tissue elastic properties. By the way, no mathematical confidence is available, at the date, for the procedure, being this based on the best fitting of a cancellous cross-section statistical sample. The question on how the uncertainty affecting the threshold determination influences the tissue modulus estimation of cancellous bone from micro-FEM linear modeling is still open.

The *voxel size* chosen for geometry reconstruction influences intrinsically the characteristics of the micro-FEM model. On one hand, full resolution (19.5 microns) models are able to describe (against remarkable computational efforts) the micro-CT scanned trabecular structure with no loss of information on its geometrical characteristics. On the other, general agreement is found in the literature, on the reliability of tissue modulus estimations obtained through micro-FEM models with voxel size of 40 microns or more. The question should be analyzed, however, with respect to the procedure in use at IOR's Medical Technology Laboratories.

In this chapter, two different sensitivity studies will be presented:

1. on the *effects of thresholding variation on the calculated elastic modulus of trabecular bone tissue*, and

2. on the *influence of the micro-CT reconstruction resolution on the estimated tissue elastic modulus of cancellous bone.*

4.1 Effects of the selected threshold on the calculated elastic modulus of trabecular bone tissue

In chapter 2, it has been shown how a stack of micro-CT grey values images can be assembled obtaining a 3D solid volume codyfing the attenuation coefficients of the scan of a trabecular structure.
It has then been explained how the application of a threshold to the reconstructed volume leads to the definition of a 3D voxel model of the trabecular structure of the scanned specimen.
Since micro-CT attenuation images are blurred because of the scanner sensibility, the procedure of segmentation has to deal with an uncertainty on the location of the bone non-bone interface.
There is no doubt that an approximation is introduced here, the exact location of the interface remaining undefined to the user.
Reconstructed structures approximate the overall trabecular thickness, implying a level of uncertainty on the characteristics of the reconstructed trabecular model such as Bone Volume Fraction:

$$BV/TV = \frac{Bone\,Volume}{Total\,Volume} \tag{4.1}$$

and Trabecular thickness under plate-model structure assumption:

$$Tb.Th = \frac{1}{2}\frac{BV}{TS} \tag{4.2}$$

Where BV corresponds to the total bone volume and TS to the total trabecular surface (see paragraph 1.3.1).
At the same time, the reconstructed frame can differ from the geometrical reality of the cancellous bone specimen in terms of local trabecular connectivity.
The uncertainty introduced by the thresholding procedure is propagated to the calculated tissue elastic modulus through the solution of the linear 3D micro-Finite Element Model.

In this section, an investigation on the effects of a small variation of the global threshold value on the predicted elastic properties of cancellous bone tissue is

proposed.

4.1.1 Aim of the study

Different thresholding techniques have been proposed in the literature, with distinction between global and local methods[1] (see section 2.2.1).
In a work dated 2007 [17], Kim, Zhang and Mikhail investigated the effects of different thresholding techniques on micro-CT based FEM models of cancellous bone. The authors of this work suggested that "[...] *apparent mechanical properties and structural properties agree well with experimental measurements regardless of the choice of thresholding methods or the format of micro-CT images*".
The thresholding procedure in use at IOR's facilities is based on a global value obtained from a best fitting statistic study on the comparison of BV/TV from reconstructions and histological observations.
The best-fit value has to be referred to a statistical sample of cancellous bone cross-sections and, as a consequence, is affected by statistical uncertainty. The results obtained at the date suggest the reliability of the technique in use at IOR. However, the finding of a low sensitivity of cancellous bone elastic properties estimations to the threshold variation, would confirm the reliability of tissue modulus predictions obtained at IOR.

In the literature, it has been reported too[7] that the effects of a variation of the threshold value on tissue modulus are related with the specimen bone volume fraction, these being higher for low BV/TV indexes.
The finding of a confirmation for this trend through the thresholding and modeling procedures in use at IOR, would permit to fully characterize the reliability of our thresholding strategy.
Informations would be obtained too, about the level of uncertainty on experi-

[1] Global thresholding techniques assume a unique gray-scale threshold value for the binarization of the data set.
Local methods try to escape the difficulty of global matching by locally detecting the bone-non bone interface through strategies of imaging analysis.

mental results that we should expect when the thresholding level is varied.

4.1.2 Materials and methods

Trabecular bone specimens

For this study, a subset of 10 cylindric cancellous bone specimens from human femoral head was selected from the database of 34 specimens used for the study described in chapter 3.
The procedure for the obtainment of cancellous samples for mechanical tests is reported in chapter 2 in detail. For the reconstruction of micro-FEM models, the 3D voxel based stack was resampled at 39 microns voxel size.
Since a relation between the effects of a threshold variation and bone density is expected, it was important to take into account and represent the whole range of BV/TV displayed by the original 34 specimens.
Figure 4.1 represents the BV/TV normal distribution of whole the specimen pool: the Bone Volume Fraction varying between a minimum of $15,69\%$ and a maximum of $51,28\%$. The sensitivity test sub-set was chosen to fully represent the bone volume fraction distribution of the whole sample (BV/TV varying between 19.53% and 37.63%), (see table 4.1.3 for more details).

Thresholding

The reference threshold value was set at 144. As it was presented in section 2.2.1 the grey-levels of an 8 bit image are in the range [0 - 255].
The 144 grey level threshold had been calculated in a previous study conduced at the Rizzoli's Medical Technology Laboratory[29].
In this research, the optimal threshold value was found through the comparison between reconstructed thresholded micro-CT images and histological cross-section microscopic pictures, 144 corresponding to the level best fitting the resulting bone volume fraction for the whole comparison group.
In a previous study by Hara [7], the threshold value was varied in 5 steps of $0,5\%$ each. Researchers found that such a small variation of the threshold level could account for a 9% maximum variation of the calculated bone stiffness, for

specimens with $BV/TV < 15\%$. For test presented here, the threshold value was varied in the range 136 to 148, by steps of 4 gray levels each. This resulting in a $-3,2\%$ to $+1,6\%$ variation with respect to the optimum value of 144, for the obtainment of a threshold variation covering almost the 5% of the available range.

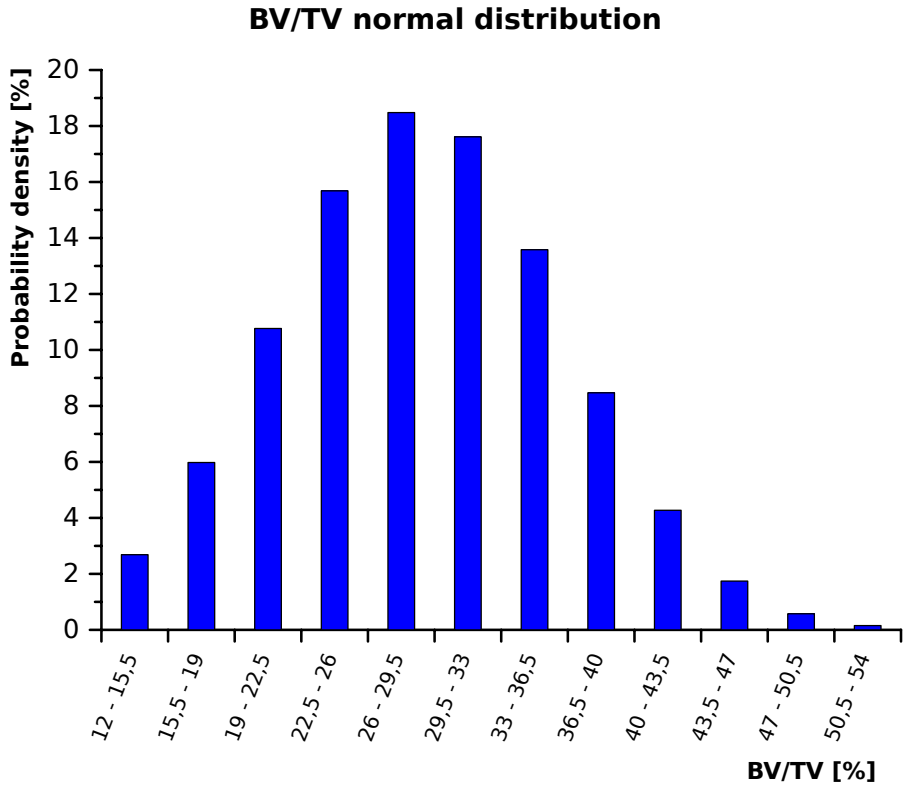

Figure 4.1: Specimens BV/TV Normal Distribution. Number of specimens: 34. BV/TV: MEAN = 29,60; SD = 7,53. Selected specimens: 10.

Trabecular modulus determination

Apparent-level elastic modulus of each specimen was experimentally obtained through mechanical axial compressive test (see paragraph 2.4) performed at IOR's Medical Technology Laboratory with a (Mod. 8502, Instron Corp., Canton, MA, USA) testing machine. Bone samples were cemented in PMMA (see

section 2.4; [27, 28]) directly onto the testing machine to ensure the alignment between the loading direction and the specimen axis.
Experimental layout took into account one single angolar positioning of the extensometer for each test: compressive experiments were repeated once (strain rate = $0.01s^{-1}$) for each specimen and sample failure was reached. ([28, 20, 40, 22]))

Four hexahedral-elements micro-FEM models were generated independently for each specimen from micro-CT data-sets by the application of a threshold value of $[136, 140, 144, 148]$, respectively. This resulted in a total number of 40 micro-FEM trabecular bone models.

A linear elastic constitutive law was assigned to the model material by means of a constant tissue elastic modulus of $19GPa$ (see section 2.5 for further details). Models were solved by use of the Parfe solver[2] (Iteration limit = $1E^6$; Tolerance = $1E^{-11}$).
Thanks to the linear-elastic assumption:

$$E_{tissue}^{EFFECTIVE} = \frac{E_{app}^{EXP}}{E_{app}^{FEM}} E_{tissue}^{FEM} \tag{4.3}$$

Where $E_{tissue}^{EFFECTIVE}$ corresponds to the estimated trabecular tissue modulus and E_{tissue}^{FEM} the tentative value for it.
E_{app}^{EXP} and E_{app}^{FEM} correspond to the apparent moduli, from experimental tests and micro-FEM analysis, respectively.
Effective trabecular tissue elastic modulus was back-calculated (equation 4.3) from the results of the micro-FEM analysis and the experimentally determined apparent modulus (see section 2.5.2 for more details on the procedure).
The relative variation of the effective tissue modulus calculated with different threshold levels was obtained by comparison with the result of the 144 threshold models.

[2]ParFe - Copyright (C) 2006 ETH Zurich, Institute of Computational Science

4.1.3 Results

In table 4.1.3, the back-calculated tissue moduli of the selected 10 specimens are reported for each threshold level.
Results are reported together with the specimen's bone volume fraction BV/TV.

	BV/TV	**Tissue Modulus [GPa]**			
Id	[%]	**thres.=136**	**thres.=140**	**thres.=144**	**thres.=148**
1	19,53	27,14	24,92	22,99	21,35
10	21,86	20,08	18,58	17,24	16,09
6	22,95	13,37	12,44	11,65	10,93
2	24,64	22,57	20,87	19,41	18,16
5	28,84	20,44	19,59	18,83	18,12
8	30,26	17,51	16,47	15,58	14,80
9	34,72	27,29	26,17	25,13	24,20
7	35,50	18,70	17,68	16,80	16,00
4	37,52	19,24	18,23	17,28	16,44
3	37,63	23,94	22,62	21,45	20,40
Mean	29,35	21,03	19,76	18,64	17,65
St. Dev.	6,82	4,32	4,08	3,87	3,72

Table 4.1: Back-calculated tissue moduli and BV/TV of the selected 10 specimens. thres. = [136, 140, 144, 148]

Table 4.1.3 reports the estimated tissue modulus relative variation for threshold values of **136, 140 and 148** with respect to the value obtained with threshold = 144 which has been taken as reference for the comparison. Results are reported in terms of percentual variation of the estimated stiffness.

The variation of the determined tissue elastic properties of cancellous bone caused by the variation of the threshold level parameter are shown in figure 4.2.
The relative variation of tissue modulus is plotted as function of the specimen's

	BV/TV	E_{tissue} relative variation [%]		
Id	[%]	**thres.=136**	**thres.=140**	**thres.=148**
1	19,53	+18,05%	+8,42%	-7,13%
10	21,86	+16,51%	+7,76%	-6,64%
6	22,95	+14,84%	+6,82%	-6,11%
2	24,64	+16,28%	+7,52%	-6,43%
5	28,84	+8,53%	+3,99%	-3,78%
8	30,26	+12,36%	+5,68%	-5,00%
9	34,72	+8,58%	+4,11%	-3,73%
7	35,50	+11,31%	+5,26%	-4,75%
4	37,52	+11,32%	+5,45%	-4,86%
3	37,63	+11,61%	+5,45%	-4,89%
Mean	29,35	+12,94%	+6,05%	-5,33%
St. Dev.	6,82	+3,32%	+1,52%	-1,18%

Table 4.2: Back-calculated tissue modulus variation for the selected 10 specimens. Threshold levels thres.=[136, 140, 148]. Reference threshold = 144. The dependence with BV/TV of the modulus variation should be noted: a 4 $1,6\%$ variation of the threshold level leads to a minimum variation of the effective tissue modulus of the 3,73 % (for a specimen with BV/TV = 34.72 %), and to a maximum variation of the 8,42 % (for the specimen with BV/TV = 19.53%.). When the threshold level is set at 136 ($-3,2\%$ with respect to the optimum), a variation of at least 8 percent points of the estimated tissue modulus occurs: minimum variation = 8,53 % for BV/TV = 28.84%; maximum variation = 18.05 % for BV/TV = 19.53%.

bone density.
Different series correspond to different threshold values. All data is reported in the form of a ratio with the results obtained with threshold value = 144. As it has been introduced above, this level was taken as reference threshold.

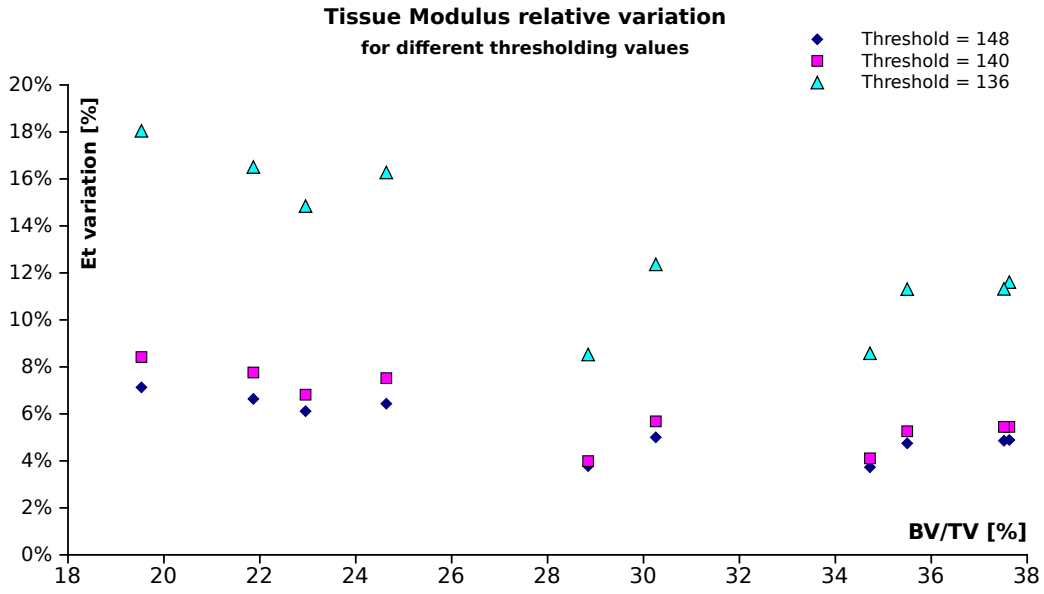

Figure 4.2: Results of a threshold level variation from the optimal value of 144 on the estimated tissue elastic modulus. Relative variation of the absolute value of the resulting bone stiffness is plotted as function of bone apparent density BV/TV. Rhombus series: threshold = 148; square series: threshold = 140; triangle series: threshold = 136.

4.1.4 Discussion

From the results reported in table 4.1.3 and figure 4.2 it can be noticed that a relation between the effects of a threshold variation and the specimen's bone density exists, being the modulus variation higher for specimens with low bone volume fraction.
The results described above seem to confirm what was expected: that a threshold variation has stronger effects on the estimation of the cancellous tissue

elastic properties for low density samples.
The reported observations could be explained as follows: when, during the process of micro-FEM model reconstruction, the gray-scale threshold level is modified, a certain part of bone is added to (or removed from) the resulting structure. The amount of bone added (or removed) is related with the magnitude of the threshold variation and with the total bone surface of the sample. For specimens with low BV/TV, the ratio between bone surface density[3] and bone volume fraction is higher. This means that for the same variation of the trheshold level, a higher ammount of bone (relatively to the total fraction of the specimen) will be added (or removed) to those samples with low BV/TV. In other words, the relative increase (or reduction) of the specimen's bone volume and, directly with this, of the specimen's stiffness, is higher for low density samples and thinner structures.

The effect of a threshold variation for specimens with different bone density is shown in figure 4.3. Here, the same cross section is shown after reconstruction with different threshold values and for two specimens of different bone volume density.

Secondly, another observation can be done on the sensitivity results. From the results of figure 4.2 it can be gathered that a reduction of the threshold from its reference level causes a variation of the calculated tissue elastic modulus which is higher than the variation obtained by an increase of the threshold of the same quantity.
This issue can be explained assuming a monotone decreasing relation between predicted tissue modulus variation and BV/TV. The bone volume fraction of the reconstructed model varies with the threshold level: increasing the threshold value the resulting BV/TV is increased too. Even if in figure 4.2 the histomorphometric determined BV/TV is plotted, an horizontal shift for the markers should be considered: markers representing increased-threshold mod-

[3]**Bone Surface Density**:

$$BS/TV = \frac{Bone\,Total\,Surface}{Total\,Volume} \tag{4.4}$$

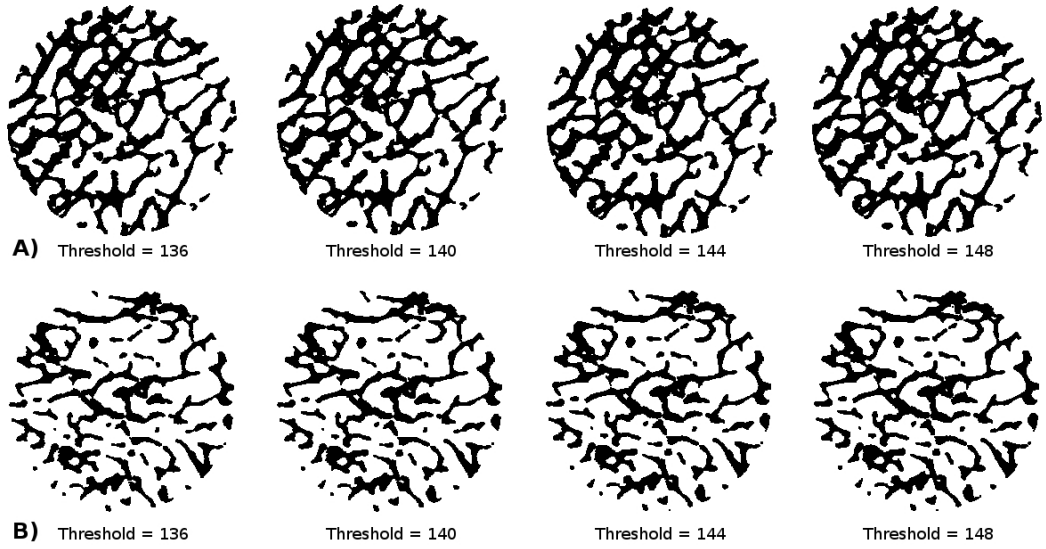

Figure 4.3: Effects of the threshold variation on a reconstructed cross section of specimens with different bone density: A) BV/TV = 34.7 %, B) BV/TV = 21.9 %. Increasing the threshold level of the same amount, the enhancement in area of the trabecular cross-section is higher for the specimen (B) with lower BV/TV. For this reason, the stiffness increase is higher too for the specimen with higher BV/TV.

els should report a BV/TV increase too (right shift), while the markers representing models reconstructed after threshold reduction should display also a reduced BV/TV (left shift).
This explains why, for the same cancellous bone sample, the reduction and the decrease of the threshold level for its reconstruction do not cause exactly the same magnitude of variation of the predicted bone tissue stiffness: because an inherent variation of the bone volume fraction is originated at the same time.

In conclusion, it has been found that a variation of the 1.6% of the threshold level around the reference value of 144[29] (140 to 148 grey levels), causes a maximum variation of the 8% in the prediction of cancellous bone tissue modulus. The error committed in worst case scenario is therefore characterized.
In addition, a confirmation of the relation proposed by Hara et. al. [7] was found, recognizing the suggested inverse proportionality between bone volume

fraction and the variation of the micro-FEM based estimations of cancellous bone mechanical properties induced by threshold modifications.
However, the desirable definition of a mathematical law connecting the variation of the estimated tissue cancellous modulus due to the threshold modification with the specimen's BV/TV remains an open issue. In this contest, the influence of trabecular structure characteristics which are not included in the BV/TV parameter should be considered too for the proposal of a correlation law.

From a different point of view, the results of this sensitivity study suggest future developments of the threshold influence analysis for the best characterization of the prediction of cancellous tissue modulus.
On the chance that a characterization of the uncertainty related with the optimal threshold determination will soon be available, the sensitivity analysis of a larger statistical sample would provide the characterization of the experimental error associated with the back-calculation of cancellous tissue modulus from micro-FEM modeling.

4.2 Influence of the micro-CT reconstruction resolution on the estimated tissue elastic modulus of cancellous bone

In section 2.3 it has been reported how the process of reconstruction of 3D micro-FEM models from micro-CT datasets can introduce uncertainties related with voxel size.
A first uncertainty is introduced by the micro-CT scanner resolution (see chapter 2). With the scanner available at IOR's Medical Technology Laboratory (Skyscan 1072®, Belgium), the highest achievable image resolution is of 19.5 microns pixel size.
The 3D voxel model can be reconstructed at native resolution (cubic voxels of 19.5 microns per side), resulting in a high resolution micro-FEM model (taken as gold standard [43, 12, 19, 3, 25] at IOR's facilities). On the other hand, the need for a reduction of computational costs (related with total number of nodes), suggests the reconstruction of the micro-FEM model at an increased voxel size.

In a study [43] dated 2005, Yeni et. al. investigated the effects of micro-CT voxel size on finite element models accuracy for human cancellous bone. The study showed that the estimated BV/TV does not differ considerably between 21 and 50 *microns* and between 21, 50 and 100 *microns*, scanning and reconstructing resolutions, respectively.
In addition, Yeni et. al.[43] suggested that the observed differences in the estimated modulus are largely attributable to scanning resolution and that the 21/21 results can be predicted from the 21/50 resolution results.
In an even more recent study, Bevill and Keaveny [3] debated on if yield stress estimated by non-linear micro-FEM analyses could improve correlations with bone strength in comparison with the use of elastic modulus from linear analysis as a predictor. In addition, the dependence of bone volume fraction and voxel size on this effect was investigated by Bevill at. al.[3].
In the results of this work, the errors in yield stress and elastic modulus obtained with 40, 80 and 120 *microns* reconstruction resolution (20 *microns*

taken as a gold standard), exhibits a clear convergence with bone volume fraction.

A study on the sensitivity of the estimation of cancellous tissue modulus from micro-FEM analysis to the model reconstruction voxel size will be presented in this chapter. In addition, the dependence of the tissue modulus predictions to the bone volume fraction of the studied sample will be analyzed for models reconstructed at different resolutions.

4.2.1 Aim of the study

Voxel size is one of the most important modeling parameters for the micro-FEM analysis of cancellous bone. It is no doubt true that the size of the reconstructed voxel influences directly the estimated stiffness of cancellous bone tissue [43], [3].
The dependence between reconstruction resolution and the predicted modulus is furthermore related with bone volume fraction[3].
From the review of the available literature, it seems to be confirmed the predictive behavior, for tissue elastic modulus, of models reconstructed at a voxel size between 40 and 50 microns.

Considering the micro-FEM modeling procedure in use at IOR, the reconstruction of 3D micro-FEM models at a resolution of 39 microns has represented, until the date, the acceptable compromise between prediction's accuracy and computational time. We have seen how the recently developed ParFE based strategy, allowed the speed-up of the whole modeling procedure[4]. This permits, for the first time, to verify the accuracy of models reconstructed at 39 microns voxel size with respect to scanner native resolution based (19.5 microns voxel size) models.
This was done through the investigation of the sensitivity of cancellous tissue modulus estimations from micro-FEM analysis to the model reconstruction

[4]The reduction of model resolution leads to a considerable decrease of computational costs (CPU hours needed for the run of one calculus approximately reduced from 50 % to 67 %, for 39.0 versus 19.5 microns voxel size.

voxel size.

4.2.2 Materials and methods

Trabecular bone specimens

For the purposes of this study, a total number of 16 cylindrical cancellous bone specimens from human femoral head from an initial sample of 34 was used. Samples were obtained by use of the procedure which has been detailed in the previous paragraph (see 4.1.2). The extracted specimens varying between 9,65 and 10,00 *mm* in diameter and 15,50 and 20,00 *mm* in free length.
All samples were micro-CT scanned (*Skyscan 1072®, Belgium*), obtaining stacks of binary images of 19,5 microns pixel side. Each stack contained more than 1000 grey-scale (8 bit) images.
Bone volume fraction and bone primary indexes (see section 1.3.1) were calculated from the micro-CT data-set reconstructions. Bone density varying between 14.38% and 37.52% for the selected set of specimens (see table 4.2.3). The procedure for the obtainment of trabecular samples for mechanical tests is reported with more detail in chapter 2.

Micro-FEM models

Stacks were reconstructed both at native (19.5 microns) and resampled (39.0 microns) resolution by use of the LHP Builder software for medical data management [5], obtainging micro-FEM voxel models characterized by 37 to 73 millions of elements for the 19.5 microns voxel size models and by 4 to up to 9 millions of elements for the 39.0 microns voxel size models (see table 4.2.3).

Linear analysis were performed by use of the high parallelization ParFe software [6] on a dedicated server.
Trabecular tissue elastic modulus of the linear elastic micro-FEM models was set initially at 19 GPa [40, 2, 38].

[5] LHP Builder - Multimodal Application for Medical Physics
[6] ParFe - Copyright (C) 2006 ETH Zurich, Institute of Computational Science

The run of each model at native and reduced voxel size required around 50 and 20 CPU minutes, respectively (Iteration limit = $1e^6$; iterative tolerance = $1e^{-9}$). The run of each model was performed over 32 processors on a dedicated calculus server.
The effective trabecular tissue modulus was calculated through equation 4.3 from the ratio between numerical and experimentally determined apparent modulus (see section 2.5.2 of chapter 2) [38].
The tissue modulus percentual variation was obtained considering as gold standard the value calculated with 19.5 microns voxel size model.

4.2.3 Results

Table 4.2.3 reports the trabecular tissue modulus obtained from both native and reduced voxel size models, for each bone specimen.
Tissue modulus variation is calculated as the percentual difference with the modulus obtained from native resolution models (actually these can be taken as gold standard).

The observed variation of the estimated tissue modulus ranges between $-1,28\%$ and $+1,17\%$, with the tissue modulus at reduced voxel size exceeding the 1% limit for only 3 of 16 specimens.
It can be noted how at higher BV/TV correspond higher differences in the estimation of bulk modulus: the models at reduced reconstruction resolution generally underestimate tissue resistance for low density specimens while generally overestimate bulk modulus for high density compact samples.
In general, larger errors were obtained for higher values of bone density.

In the graph of figure 4.4 the tissue modulus variation caused by volume resampling is plotted as function of bone volume fraction. The $\pm 1\%$ errors are plotted as red lines in the chart: it can be noted how the estimation of the tissue modulus made with models reconstructed at 39 microns voxel size exceed the 1% of error for only 3 specimens. For 2 cases of 3, this happens when BV/TV is on an extreme of its range.
A mild correlation between BV/TV and the variation of the prediction of cancellous tissue modulus is observed, higher densities corresponding to larger

	BV/TV	Elements		E_{tissue} [Gpa]		E_{tissue} Variation
Id	[%]	**19.5μm**	**39.0μm**	**19.5μm**	**39.0μm**	[%]
1	19,53	39'851'052	5'006'406	22,91	22,99	-0,34%
2	21,86	42'155'500	5'293'239	17,23	17,24	-0,02%
3	22,95	47'398'965	5'953'683	11,61	11,65	-0,28%
4	24,64	50'020'865	6'282'873	19,57	19,41	0,82%
5	28,84	57'260'925	7'184'792	18,81	18,83	-0,12%
6	30,26	60'479'464	7'596'606	15,73	15,58	0,93%
7	34,72	70'372'839	8'830'750	25,22	25,13	0,34%
8	35,50	66'091'356	8'296'798	16,99	16,80	1,14%
9	37,52	72'543'341	9'100'630	17,40	17,28	0,66%
10	22,66	41'833'217	5'256'969	17,09	17,12	-0,21%
11	29,28	56'302'165	7'371'505	16,67	16,63	0,25%
12	15,69	37'312'596	4'689'861	13,80	13,88	-0,60%
13	25,88	51'096'175	6'420'365	43,48	42,93	1,28%
14	31,25	60'079'997	7'543'847	27,97	27,94	0,11%
15	20,70	40'880'750	5'137'096	18,25	18,29	-0,19%
16	14,38	39'249'474	4'887'926	20,70	20,94	-1,17%
Mean	25,98	52'058'043	6'553'334	20,21	20,16	-0,16%
St.Dev.	6,90	11'596'515	1'465'522	7,42	7,31	0,67%

Table 4.3: Reconstruction resolution sensitivity test results. The predicted trabecular tissue stiffness is reported for models reconstructed with voxel size of 19.5 microns and 39.0 microns.

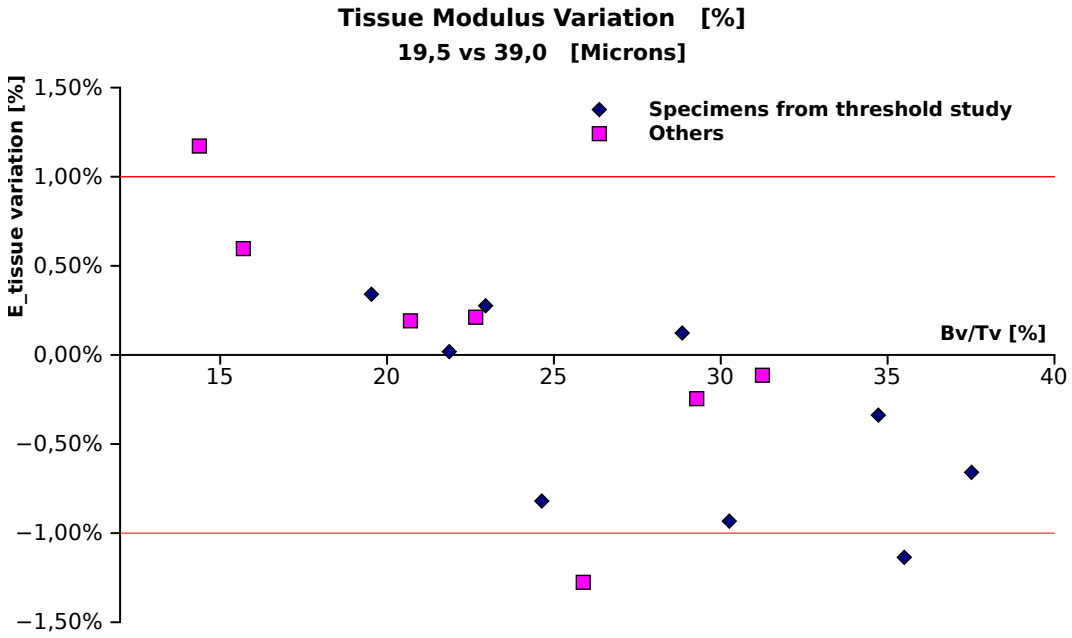

Figure 4.4: Results of a threshold level variation on the estimated tissue elastic modulus. Relative variation of the resulting bone stiffness is plotted as function of bone apparent density BV/TV. The 1% limits are plotted in red: it can be seen how for only 3 of 16 specimens the modulus estimated at 39 microns voxel size reconstruction exceed the 1% of error. This happens for specimens with extremely low or extremely high density. Proportionality between BV/TV and modulus variation should be noted too.

variations of tissue modulus.

4.2.4 Discussion

In this section, the effects of the reconstruction of micro-FEM models at a voxel size of 39.0 microns versus the native (gold standard) resolution of 19.5 microns, on the estimation of the tissue elastic modulus of trabecular bone tissue from linear FEM analysis was investigated.
Existing works [43, 3] suggested the consistency of the results of linear micro-FEM analysis with trabecular bone models reconstructed at a resolution of 40 or 50 microns.

The aim of this sensitivity analysis was that of evaluating the assumption of a 19.5 microns pixel size micro-CT scanning and the reconstruction of micro-FEM cancellous bone models at a reduced voxel size of 39.0 microns[7].
The principal advantage of such a reduction in the model resolution is the decrease of the overall computational time from the 50 % to the 67 %.
This was done through the micro-FEM analysis of 16 cancellous bone specimens micro-CT scanned at a resolution of 19.5 microns and reconstructed both at 19.5 microns and 39.0 microns voxel size.
Tissue modulus estimations from finite element analysis were compared for the two different reconstruction resolutions.

The comparison showed a maximum variation of the predicted tissue modulus of the 1.28 %, the error being included in the $\pm 1\%$ limit for 13 of 16 specimens. This result confirms the high quality of the 39.0 microns voxel size models used for micro-FEM analyses of cancellous bone tissue at IOR.
In addition, it is pointed out how the variation induced in the tissue modulus prediction by the reduction of model resolution from 19.5 to 39.0 microns is of one order of magnitude lower than the uncertainty propagated on the same prediction by the error affecting the experimental determination of apparent modulus from mechanical tests.

On the other hand, the results reported in the graph of figure 4.4 suggest the direct dependency between the specimen's bone volume fraction and the error that can be committed in the estimation of the tissue modulus elastic modulus with micro-FEM models at reduced resolution. These results are in good agreement with findings reported in literature by Bevill et. al. [3].
Anyway, for the procedure in use at IOR's Medical Technology Laboratory, predictions obtained with 39 microns voxel size linear micro-FEM models can be cosidered as accurate as predictions obtained with full resolution (19.5 microns voxel size) models. The applicability of the 39 microns voxel size based strategy is confirmed for the investigation of linear elastic properties of cancellous bone tissue with micro-FEM models from micro-CT reconstructions.

[7]This is the procedure commonly conduced at IOR's Medical Technology Laboratoy

Chapter 5

A new layout for experimental tests

In section 2.4, the experimental layout commonly used at Rizzoli Orthopedic Institute's Medical Technology Laboratory for compressive tests of cancellous bone specimens has been presented.
The described procedure is based on the compressive test with measurement of displacements with the extensometer positioned on a fixed angolar position of the cylindrical specimen.
In this test, displacements do not exceed the tissue elastic limit of the material during the loading-unloading cycle. After the first elastic loading-unloading cycle, a failure compressive test is performed and the collapse of the specimen is reached.

The cancellous bone database used for the sensitivity studies presented in chapter 4 has been tested by use of this experimental protocol, which was presented in 2007 [Ohman, Baleani, Perilli et al. [27]] and is in use from 2006 at IOR's Medical Technology Laboratory.
The experimental procedure, however, was not developed with the aim of supporting the micro-FEM modeling of cancellous bone specimens for the prediction of cancellous tissue modulus. The sinergy between mechanical tests and micro-FEM modeling introduced the necessity of the update of the experimental protocol in use. The aim of this upgrade involves the improvement of accuracy in experimental measurements as well as the detection of more

informations for the characterization of an accurate micro-FEM model able to detect the physical problem in question.

In this chapter, the main features of the experimental layout described in section 2.4 will be listed, with particular attention for those characteristics for which a review of the protocol became necessary. The reasons for an upgrade of the layout will be cleared and new solutions proposed.
Later, the development of a perfected procedure for compressive tests and cancellous bone tissue modulus prediction from micro-FEM modeling will be presented.
In the end, the results obtained at the date from the application of the new procedure will be illustrated.

From this point on, the layout described in section 2.4 will be referred to as *"existing" layout*, while the upgraded one that will be described above will be referred to as *"new" layout*.

5.0.5 Characteristics and problems of the existing procedure

During the years and with the gowth of experience in dealing with mechanical tests of trabecular bone specimens, researchers of the IOR's Medical Technology Laboratory pointed out more than one source of uncertainty concerning the existing layout for experimental tests.
However, even if there were several factors of the procedure of mechanical testing requiring a revision, the complex nature of the process of estimation of the tissue elastic properties of cancellous bone should not be forgotten.
Considering a procedure in which several different phases are inherently connected, it is important to maintain an objective point of view over the overall experimental system and its aims. The processes of micro-CT scanning, assembling of 3D FEM models and mechanical testing should not be treated separately as they are all parts of a unique answer to a modeling question.
In other words, the refinement of a single procedure could be of no help due to the indetermination of one of the others.
For these reasons, the development of a new experimental procedure for me-

chanical tests of cancelous bone specimens, should be guided by the best achievable uniformity between the physical reality of mechanical tests and the numerical representation of the same through finite element models.
For the comprehension of the particular requirements of a new experimental procedure, the following observations with respect to the existing method should be pointed out:

1. *Accuracy of the mechanical compressive test results*
   Compressive tests (with no exceed of the material yielding point) were repeated more than once for the same specimens. This showed that a significant variation of the measured apparent-level strains can occur for the same specimen. In some cases, this suggested that the yielding limit had been reached, with damaging of the trabecular structure.
   However, in most cases, the measured strains (and, with these, the apparent modulus too) showed a stabilization after the firsts compressive cycles. It can be supposed how this behavior is the result of the recovery of assembly plays and of the discontinuous contact of the PMMA cement with press joints.

2. *Indetermination of the bone-extensometer contact*
   From the results of micro-FEM modeling, it has been shown how trabecular displacements can vary consistently with the z-coordinate and on the cross-section plane. For a more accurate determination on the FEM model of the same displacements registered by the extensometer, a reference system is necessary for the measure of the control levels.

   (a) *Extensometer knives positioning*
   According to the existing experimental procedure, only the initial distance between the extensometer's knives is measured (see figure 5.3), remaining the axial position of the contact point between extensometer knives and trabecular structure undefined. This implies an indetermination on the coordinates for the strain calculation on the micro-FEM model in agree with the position of the extensometer's knives. This problem can be appreciated in the sketch of figure 5.5.

(b) *Contact Instability*
In section 2.4 it was described how the contact between extensometer knives and bone specimen is maintained thank to two rubber bands. During the preparation of the experimental setup, the extensometer knives are secured by a block pin. When the block pin is removed, an arrangement of the knives with respect to the irregular trabecular surface is observed. The initial distance between the two knives is detected at this point of the procedure, with a loss of information regarding the arrangement between the two knives. It is necessary to take into account this adjustment of the knives for the accurate determination of the extensometer-specimen contact heights.

(c) *No reference for angular positioning*
According to the experimental procedure in use, the calculation of strains by use of the extensometer is repeated among the four angular positions of the specimen. In some cases, the measure is obtained for one single alignment. In both cases, the exact level of the extensomter's knives with respect to the specimen is not determined.
When calculating the displacements of the 3D bone model from results of the micro-FEM analysis, it has been so far considered the average displacement exhibited by the structure inside the cross-section at two reference levels, these approximating (see above) the extensometer's knives heights. Results showed a large variation of the axial component of the displacement field into a single cross-section of the specimen (see figure 5.1). From these results, researchers inferred on the necessity of an angular reference system, for the precise determination of the extensometer-specimen contact regions and for their accurate detection on the micro-FEM 3D model of the specimen.

3. *Only partial micro-CT reconstruction of the structure*
Due to the unsufficient field of view of the actual micro-CT scanner[1]

[1]Skyscan 1072®, Belgium

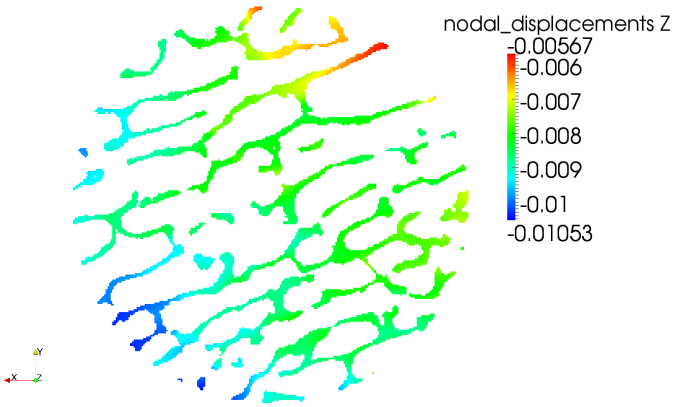

Figure 5.1: Displacements obtained on the control level. The colormap identifies the displacement level. The large variability of the resulting displacements should be noted.

in use at IOR, the specimen's acquisition causes the only partial reconstruction of the tested cancellous structure (see the sketch of figure 5.2).

5.0.6 Development of a new experimental layout

In the previous section, the characteristics determining the uncertainty of the model representation of the experimental mechanical test have been introduced. These features are related with an experimental procedure for mechanical tests which had not been developed, in its origins, considering the needs of a coupled numerical analysis.
The development of a new experimental procedure toke into account each one of these points.
The new layout is based on the repetition of the elastic component of the compressive test (without reaching the specimen's yielding) with the extensometer placed on different angular positions and an higher accuracy in the determination of the effective contact points between extensometer knives and trabecular surface.
The procedure was developed entirely at Rizzoli Orthopedic Institute Medical

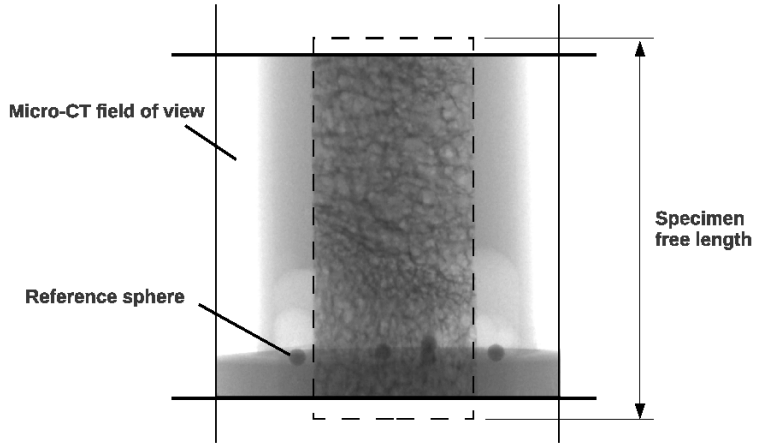

Figure 5.2: Micro-CT field of view: the scheme represents how the total free length of the cancellous bone specimen cannot be acquired by the micro-CT scanner in use. This causes the loss of information regarding the extremities of the bone specimen.

Technology Laboratory and will be briefly presented here. For the methodological as well as technical aspects of the new experimental measuring procedure, the reader should refer to the MS thesis conduced at IOR's Medical Technology Laboratory by Falco et. al.[5].
In this work, the attention will be attributed to the characteristics of the new processing of numerical results from micro-FEM modeling.

Solutions for the new layout

1. *Pre-conditioning compressive cycle*
   Relaxation of the specimen after the initial compressions was observed through the repetition of mechanical tests on the same sample.
   A preconditioning cycle of compressions-decompressions was introduced with the aim of eliminating plays between specimen and the PMMA cement and between cement and machine joints.

2. *Repetition of the test with different angular positioning of the extensometer*

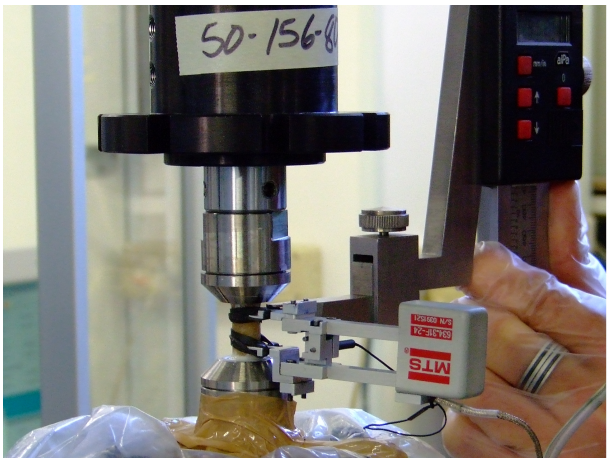

Figure 5.3: Setup for the mechanical compressive test of a trabecular bone specimen. The extensometer is fastened to the bone specimen by use of two rubber bands. The picture shows the process of determination of the extensometer knives vertical positions.

The new procedure is based on the repetition of the axial compressive test, and the registration of displacements with the extensometer arranged along 4 different angular directions (respectively at 0°, 90°, 180° and 270° from the initial direction selected by the user). The the sketch of figure 5.5 for an overview of the solution.

3. *Repetition of the test for the same angular position*
   The elastic compressive test was repeated 4 times for each angular position of the extensometer.
   For each cycle, a total strain of the 0.2 % was imposed. This value was chosen to prevent the exceeding of the yielding strain limit of the structure and to ensure the specimen against plastic deformations. A constant strain rate of $0.01s^{-1}$ was maintained during the test and reaction forces were registered simultaneously.
   When the 16 tests (4 per angular position), a failure compressive test was performed, to detect the failure load characterizing the specific bone specimen.

4. *Angular reference for the positioning of the extensometer*
   Before the μ-CT scanning of the specimen, a system of 5 aluminum spheres is fixed by immersion into the PMMA cement surface (see figure 5.4). 4 spheres (diameter = 1mm) identify the angular reference for the position of the extensometer during each test. A fifth reference sphere identifies the 0° angular position.
   Thanks to the LHP Builder[2] it is possible to fully identify the centers

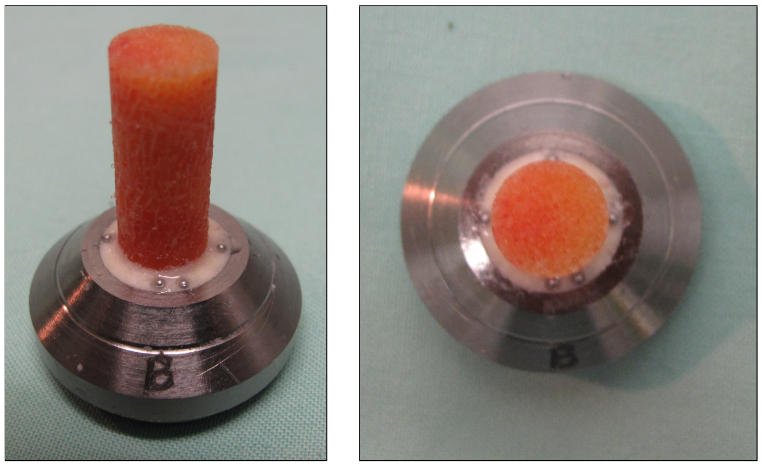

Figure 5.4: Detail of the setup of a trabecular bone specimen for mechanical compressive test. The system of aluminum marker spheres fixed to the PMMA cement surface should be noted.

   of the reference spheres, providing the registration of the micro-FEM 3D model with the experimental compressive test.

5. *Determination of vertical positioning of the extensometer's knives*
   The height of the lower knife is measured relative to the height of the corresponding sphere above the PMMA cement level (see scheme of figure 5.5). Afterwards, the distance between the two knives can be detected identifying this way the heights of the knife-bone contact regions on the micro-FEM model.

6. *Determination of extensometer initial displacement*
   When the block pin of the extensometer is removed, the initial displace-

[2]LHB Builder, medical data management software - LHDL Consortium

ment is registered. This value is considered for the calculation of the levels of the extensometer knives.

Experimental layout scheme

In figure 5.5, a representation of the experimental layout for compressive tests with control of angular positioning of the extensometer is presented. The reference aluminum spheres system and the determination of extensometer knives levels can be observed.

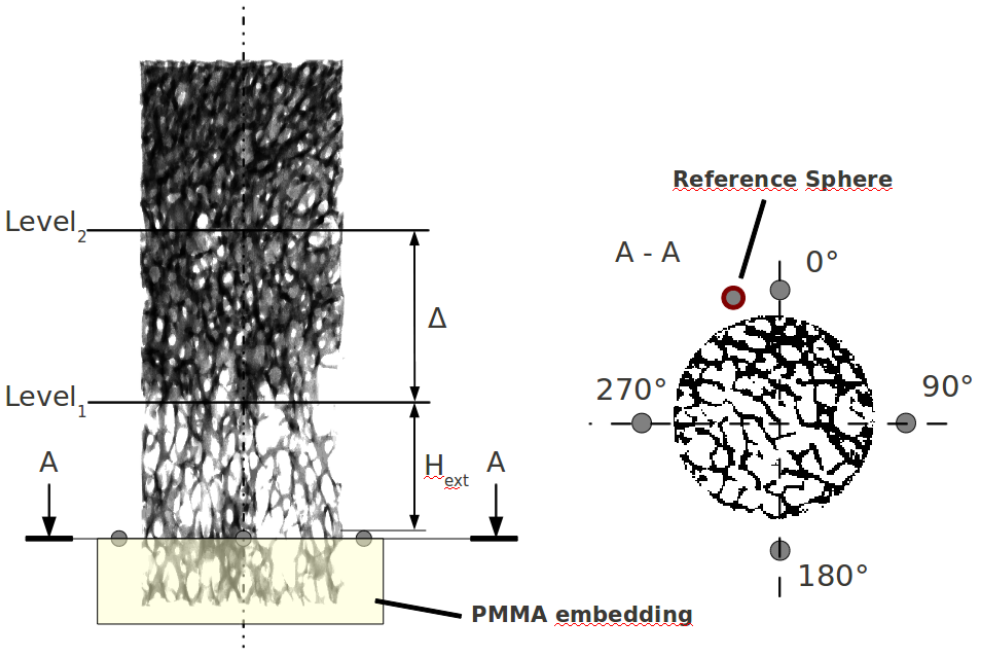

Figure 5.5: Experimental layout scheme. 5 aluminum spheres identifying the angular positioning of the extensometer are embedded into the PMMA cement surface. Initial distance between the extensometer knives (δ) and height of the lower knife (H_{ext}) are registered before each test.

Processing of FEM results

As it has been introduced above, the contact points between extensometer's knives and bone tissue can be identified, on the specimen's 3D model, with reasonable accuracy, thanks to the informations acquired with the new setup before experimental test.
Considering the scheme of figure 5.6, the heights of the two extensometer's knives ($level_1$ and $level_2$) can be determined with an accuracy of $\pm 0.3mm$.

For the calculation of strains from the results of μ-FEM analysis, two contact

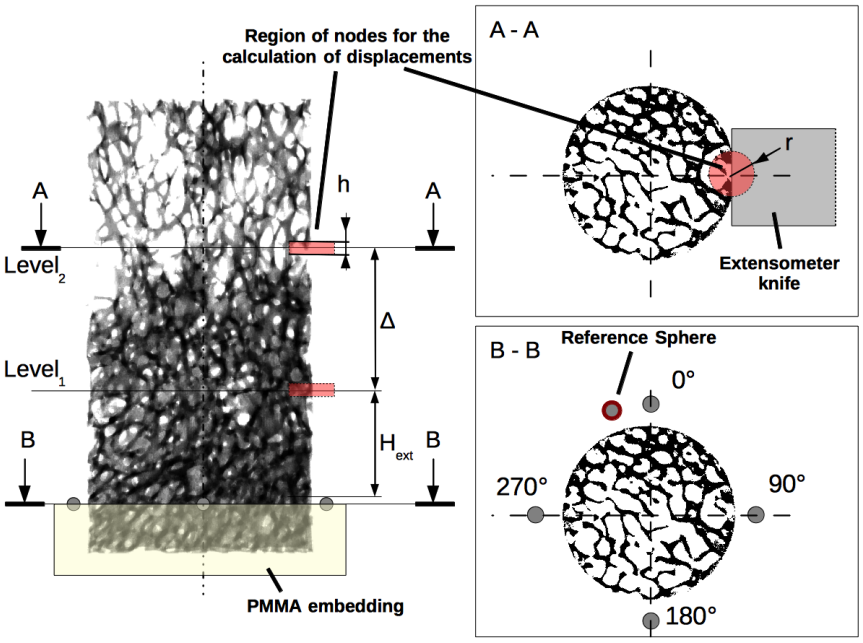

Figure 5.6: Experimental layout scheme: determination of displacements. For each angular position, the extensometer knives levels ($level_1$ and $level_2$, respectively) are obtained thank to data from experimental measures. The contact points are therefore estimated. The figure shows, in red, the two cylindrical regions of points selected for the estimation of displacements for each angular position.

cylindrical regions of the model are defined, these corresponding to two vol-

umes surrounding the effective contact points of the specimen (see figure 5.6). An algorithm situates the midpoint of each one of the cylindrical volumes at the calculated extensometer's knife height and, consequently, in the center of the deduced contact point with trabecular surface.
Axial displacements of all nodes included inside these volumes are considered. For each extensometer level, the average displacement of all nodes belonging to the corresponding volume is calculated. The resulting strain is obtained from the difference between the average displacements of the two regions of nodes.
The two cylindrical regions for the calculation of trabecular displacements are described by cylinder height h and radius r. The values assumed for the parameters h and r correspond to the uncertainty in the determination of the vertical position of each knife and to the assumed contact length, respectively. The actual angular extension of the contact region between extensometer knife and trabecular surface is estimated to be 12°at least. This would correspond to a contact length of at least 1 mm.
To assess the influence of the two parameters h and r on the resulting estimation of cancellous tissue modulus a sensitivity study has been performed. Separately, the determination of the specimen's apparent modulus (and the consequent back-calculation of cancellous tissue modulus), was performed through the postprocessing strategy of the previous experimental layout (see section 2.5.1). This consists in the determination of the average displacement on the specimen's cross-section at the height at which the extensometer's knife is fastened.

5.0.7 Materials and methods

Application of the new experimental layout for mechanical test of trabecular bone specimens

6 cylindrical shaped cancellous bone specimens were estracted from human femur condyles of 2 donors.
Specimens were estracted by means of a holed diamond-coated milling cutter with a nominal diameter of 10 mm, with the bone slice immersed in water during the process.

Specimens measured between 9.47 and 9.68 mm in diameter and 20 mm in free length.
A polymethylmethacrylate (PMMA) endcap was applied onto one end of all specimens by submerging the bone specimen end into curing PMMA mixture. The PMMA surface was leveled as much as possible and 4 aluminum spheres (diameter = 1.0 mm) were positioned on the PMMA surface plane by partial immersion into the cement. The aluminum spheres were fixed at 90 °steps around the bone specimen and a fifth sphere was positioned beside one of the others to identify the 0 °position.
After this, the specimen was put vertically into a polyethylene cylinder filled with Ringers solution for microCT scanning [27].
For further details regarding the processes of specimen's preparation and realization of mechanical tests, the reader should refer to the work: "Caratterizzazione meccanica di tessuto osseo trabecolare: sviluppo di un protocollo sperimentale finalizzato alla validazione di un modello numerico" [5] from Luigi Falco et. al. performed at IOR and presented on the last 21st march, 2013.

Micro-CT scanning

The necessity to reproduce the position of the set of 5 alignment aluminum spheres on the micro-FEM model involved the nesessity of an enlargement of the micro-CT scanning field of view, for their acquisition. Being the scanner[3] available at IOR's Medical Technology Laboratory unable of such an extention of the field of view, two different scans of the same specimen had to be glued together to represent the total height of the specimen.
Each acquisition was performed by use of a standard protocol [29] ($50kVp$, $200\mu A$, $1mm$ aluminum filter, exposure time $5.9sec$, image averaged on 2 projections, rotation 180 °, rotation step 0.9°, field of view $20mmx20mm$, isotropic pixel size of $19.5\mu m$) and the specimen was not removed from its support untill the end of the second scan, to avoid misalignment due to the repositioning of the specimen. Cross-section images were stored in 2 different stacks in 8 bit format (256 grey levels), 1024 x 1024 pixels in size.
The union of the two stacks of micro-CT reconsructions was performed manu-

[3]Skyscan 1072®, Belgium

ally. A shift had to be executed on all images of one of the two stacks to align their respective horizontal position. The shift is potentially caused by a bug of the software controlling the reconstruction of cross-sections from the scanned dataset.
The correction of the shift was performed through optimization of the alignment of the two cross-sections at the interface.
The partitioning of the reconstructed volume in two different micro-CT scans introduced a source of uncertainty the magnitude of which can not be estimated at the date. The presence of an error introduced by the connection of two micro-CT scans is shown in figure 5.7. Here, the alignment between reconstruction images of the interface from two micro-CT stacks derived from the same specimen are shown. It can be seen how the reconstructed geometry is different for the two stacks: the difference appearing in black in figure. The error between the two reconstructions is maximum at peripheral zones, being the accuracy of the micro-CT scanner lower in this area. In table 5.1, the bone

Figure 5.7: Alignment between micro-CT stacks: the reconstructed geometry varies for the two stacks, the difference appearing in black. The accuracy of the micro-CT scanner is lower for peripheral regions, this resulting in a larger difference between the two reconstructed trabecular structures at the border of the specimen.

structure indexes derived from micro-FEM stacks analysis are reported. Due

to the phenomenon of stack discontinuity introduced above, bone indexes were obtained for the two different stacks of micro-CT acquisitions.

Specimen	**Stack**	**BV/TV [%]**	**BS/BV [1/mm]**	**SMI**	**Tb.th [mm]**
1	UP	6,43	31,62	1,52	0,14
	DOWN	8,49	24,43	1,42	0,18
2	UP	23,57	18,95	0,79	0,22
	DOWN	15,44	25,71	0,92	0,173
3	UP	12,44	29,49	1,23	0,15
	DOWN	13	27,89	1,02	0,159
4	UP	6,43	31,62	1,52	0,14
	DOWN	8,49	24,44	1,42	0,18
5	UP	15,13	27,62	1,08	0,152
	DOWN	16,43	30,54	1,24	0,139
6	UP	11,62	31,14	1,54	0,142
	DOWN	16,79	29,89	0,78	0,142

Table 5.1: Bone structural indexes for the 6 specimens tested to uniaxial compression. The values are reported for the two different stacks constituting the micro-CT acquisition.

Reconstruction of Micro-FEM models

The procedure applied for the reconstruction of micro-FEM models from micro-CT datasets is the same that has already been presented in chapters 2 and 3.

Hexahedral elements models were reconstructed with voxel size = 39.0 microns.
Global thresholding (threshold grey scale value = 144) and connectivity test were performed and an homogeneous tentative value for tissue elastic modulus was set at 19 GPa for all models.

The procedure of numerical postprocessing of the results of micro-FEM modeling has been detailed in section 5.0.6. This is based on the definition of two cylinder shaped regions of nodes around the contact point between extensometer's knives and trabecular surface.
The minimum value chosen for the cylindrical height h of this cylinder should be $0.3mm$, this being the uncertainty affecting the measure of the extensometer's knives levels.
On the other side, the base diameter of the cylindrical volume should be at least $1.0mm$, corresponding to this value the estimated extensometer knife-specimen contact length. As a consequence, the minimum value selected for the cylindrical radius r will be 0.5 mm.
For the determination of trabecular apparent modulus from micro-FEM modeling, an height $h = 0.3\ mm$ and a radius $r = 0.5\ mm$ were chosen for the cylindrical region of nodes of interest.

Mechanical compressive tests of cancellous bone specimens

All the six cancellous bone specimens were tested to uniaxial compression [5]. Four tests were performed for each specimen, with the extensometer fastened in 0°, 90°, 180°and 270°angular position, respectively.
A preconditioning cycle of 20 load/unload compressions was performes prior to each angular test. Afterwards, a cycle of 4 compressions was performed for each position. A total vertical displacement of 0.2 mm was imposed. Strain rate was controlled by the testing machine (INSTRON 8502, Instron Corp., Canton, MA) during the test and maintained at $0.01s^{-1}$ [28, 21, 16, 22].
As a consequence, 16 calculations of the apparent stiffness were obtained for each specimen: the mean values of modulus E_{app}^{EXP} for each angular position of the extensometer were obtained from the average of the corresponding four measurements.

Solution of micro-FEM models

Micro-FEM modeling was performed for each angular experimental measurement. The apparent level modulus from linear micro-FEM analysis (E_{app}^{FEM}) was obtained for each angular position of the extensometer, fixed at 19 GPa the tentative value of tissue modulus for the linear analysis.
Predictions for the effective cancellous tissue modulus $E_{tissue}^{EFFECTIVE}$ were back-calculated as:

$$E_{tissue}^{EFFECTIVE} = \frac{E_{app}^{EXP}}{E_{app}^{FEM}} E_{tissue}^{FEM} \tag{5.1}$$

The same method for the back-calculation of tissue modulus was followed with both the results obtained by the newly developed post-processing approach and those obtained through the previous version of post-processing (see section 5.0.6).

Sensitivity test on the micro-FEM results processing parameters

The processes for the determination of model strains from the results of micro-FEM analysis has been presented in its concept in section 5.0.6. As it is shown in the sketch of figure 5.6, the mean value of vertical displacements are extracted from the micro-FEM model considering the two cylindrical regions of nodes located around the estimated contact points between extensometer's knives and trabecular surface.
Since the assumed values for the height h and the radius r of the regions of nodes are arbitrary, a study on the sensitivity of tissue elastic modulus estimations from micro-FEM modeling to these parameters is needed. The investigation would permit to fully qualify the reliability of the procedure that leads to the estimation of cancellous bone tissue elastic modulus from micro-FEM modeling (E_{tissue}^{FEM})[4].

For the sensitivity test, the two parameters h and r were made varying in the range (0.05 - 0.30 mm) and (0.10 - 2.50 mm), respectively, by steps of 0.01 mm for the cylinder height h and 0.05 mm for the cylinder radius r.

[4]Further informations regarding the relation between local strain states and the estimation of cancellous bone elastic properties from micro-FEM linear analysis, would help too in the understanding of the incidence of side artifacts.

The apparent level elastic modulus of the specimen was calculated for each pair of parameters h and r and for each one of the six specimens. For the comparative representation of the results of all tests, the relative variation of the elastic modulus was calculated. The linear elastic assumption descibing the problem implies the substantial agreement between the relative variation of the micro-FEM determined apparent modulus with the corresponding relative variation of the tissue modulus prediction.

5.0.8 Results

16 tests were performed for each one of the 6 cancellous bone specimens of the available database (4 tests for each angular position of the extensometer). The test at 180°of specimen 5 caused the accidential failure of the same due to an operative error in the setting of the testing machine. For this reason, only data from the 0°and 90°tests are available for specimen 5. The reader should refer to the work of Falco [5] for more details on the realization of experimental tests.

Modulus variability for the single angular position

The compressive test was repeated four times for each angular position of the extensometer. The extensometer was fastened accurately at the beginning of each angular test and no interference was introduced during the repetition of each cycle.
In table 5.2 the apparent moduli from experimental compressive tests $E_{app,i}^{EXP}$ are reported for each tested specimen and for each angular position i.
The mean value of apparent modulus was calculated from the results of the 4 compression repetitions performed in each position. Mean apparent moduli are reported together with the corresponding standard deviation.

The variability of the experimentally measured apparent modulus for the single angular position was generally low (mean percent standard deviation = 9.01%, percent standard deviation > 10.0% for only 4 specimens). The mean standard deviation is significantly high due to the great indetermination connected with specimen 3, for which an estremely low mean apparent

Apparent Modulus from experimental tests [GPa]								
	0 °		90 °		180 °		270 °	
Id	$\bar{E}_{app}$	σ	$\bar{E}_{app}$	σ	$\bar{E}_{app}$	σ	$\bar{E}_{app}$	σ
1	595,1	67,9	635,96	54,37	497,84	14,3	490,06	39,45
2	1195,5	264,1	1116,01	5,85	1392,65	9,64	1372,56	7,61
3	281,52	43,88	69,77	63,77	32,81	0,73	43,85	1,81
4	1113,93	29,82	1074,64	34,04	1065,06	22,37	409,99	24,38
5	999,42	35,82	1694,24	67,39	1552,41	83,31	1680,43	10,29
6	767,59	8,73	804,23	12,38				

Table 5.2: Apparent modulus from mechanical compressive tests. Number of specimens = 6. Specimen 6 was damaged during the test at 180°: no data is therefore available for specimen 6 for the 180°and 270°positions. Percentual Standard Deviation for the test on each angular position: MAX=91.40%; MIN=0,52%; MEAN=9.01%.

modulus (MEAN: 106.99 MPa; ST. DEV.: 117.38 MPa) was found. However, for 4 measurements of 22, the modulus showed high variability (percent standard deviation > 10.0%). It could be supposed that the high variability presented by these cases was the result of accidental errors occurred during mechanical tests. The analysis of the load-displacements compression curves should confirm this hypothesis: for the specimens reporting high variability of the measured apparent modulus, the curves displayed unusual discontinuities, suggesting the loss of the bone-extensometer contact during the test, with the consequent wrong determination of trabecular displacements.

Modulus variability for the 4 angolar positions

In table 5.2, the mean apparent modulus from mechanical tests measurements is reported for each of the 4 angular positions and for the 6 specimens tested to uniaxial compression.
The bar chart of figure 5.8 collects the data of table 5.2, representing the apparent level experimental modulus variability with the angular position of the mechanical test.

For specimens 3, 4 and 5, the plot shows a substantial variation of the measured specimen's stiffness with the angular positioning of the extensometer during the test. By contrast, for specimens 1, 2 and 6, a significant agreement was found between measurements performed on different sides of the trabecular surface.

The apparent modulus variability detected for the 0°position could be ex-

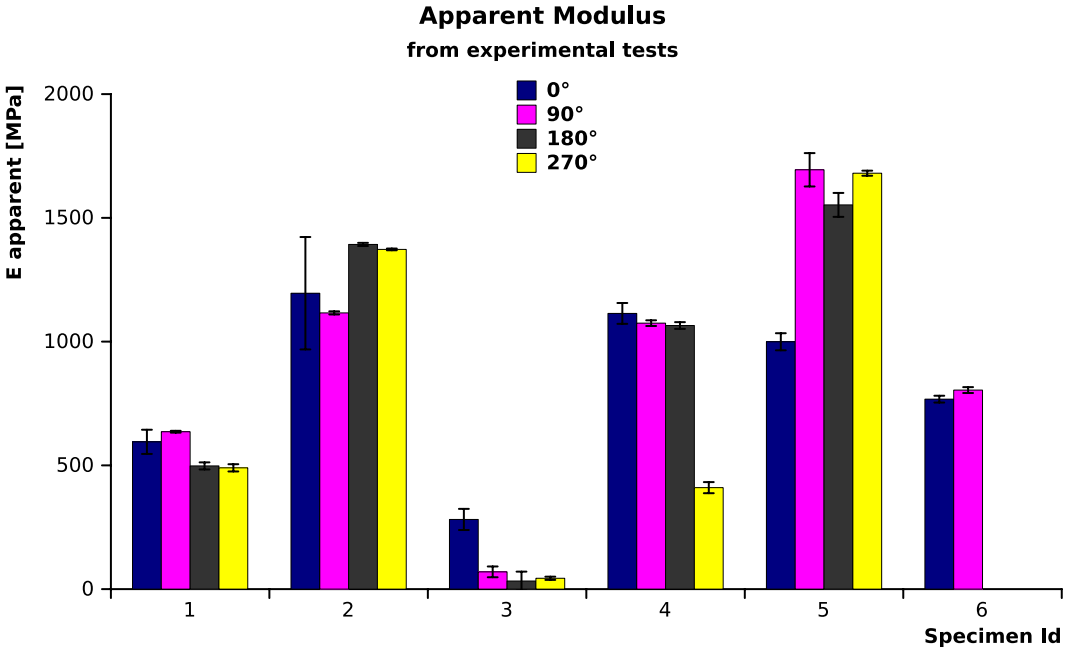

Figure 5.8: Measures of cancellous bone apparent modulus from experimental compresisve tests. Different colors represent different angular positions of the extensometer for the test (BLUE: 0°, PINK: 90°, GREY: 180°, YELLOW: 270°). For specimen 6, results were obtained only for the 0°and 90°positions because of the failure of the specimen during the 180°position test. Standard deviations deriving from the repetition of the compressive test on each position are plotted in black line.

plained with the initial recovery of plays between cement and machine's joints. Similarly, the modulus variation at 270°could be attributed to the premature damaging of trabecular structures. However, for experimental purposes, the measure of the apparent level modulus $E^{EXP}_{apparent}$ from experimental results is obtained as the average value reported by the single specimen on the four an-

gular positions.
Mean values and the corresponding standard deviations for the experimentally measured cancellous modulus for the tested specimens are reported in table 5.3.

	$E^{EXP}_{apparent}$ [MPa]		
Id	**Mean**	**Standard Dv.**	
1	554,74	72,22	13,02%
2	1269,18	135,18	10,65%
3	106,99	117,38	109,72%
4	915,91	337,94	36,90%
5	1481,62	327,75	22,12%
6	785,91	25,91	3,30%

Table 5.3: Mean apparent modulus from mechanical tests. Number of specimens = 6. Specimen 6 was damaged during the test at 180°: no data is therefore available for specimen 6 for the 180°and 270°positions. Average values for the experimentally determined specimen apparent modulus are reported. Mean values and the corresponding standard deviations are obtained from the results of the tests on each angular position. Percentual Standard Deviation: MAX=109.72% (spec. 3); MIN=3.30% (spec. 6); MEAN=32.62%.

Tissue Modulus estimations from micro-FEM analysis

In section 5.0.6, the processing of micro-FEM results has been presented. The aim of this procedure is the obtainment of a prediction of trabecular strains as much as possible in accord with the physical reality detected by the extensometer.
Micro-FEM models were solved for each specimen. Apparent level moduli ($E^{FEM}_{app,i}$) were determined from the resulting trabecular strains derived from the displacement field shown by the model inside the regions which identify the contact points between bone structure and extensometer's knives. The calculation was performed for each one of the four angular positions of the

extensometer.
In figure 5.9, the apparent level moduli from results of micro-FEM analysis are reported for each of the 4 angular positions and for the 6 specimens taken into account for this study. These values were obtained under the assumption of a tentative tissue modulus of 19 GPA.

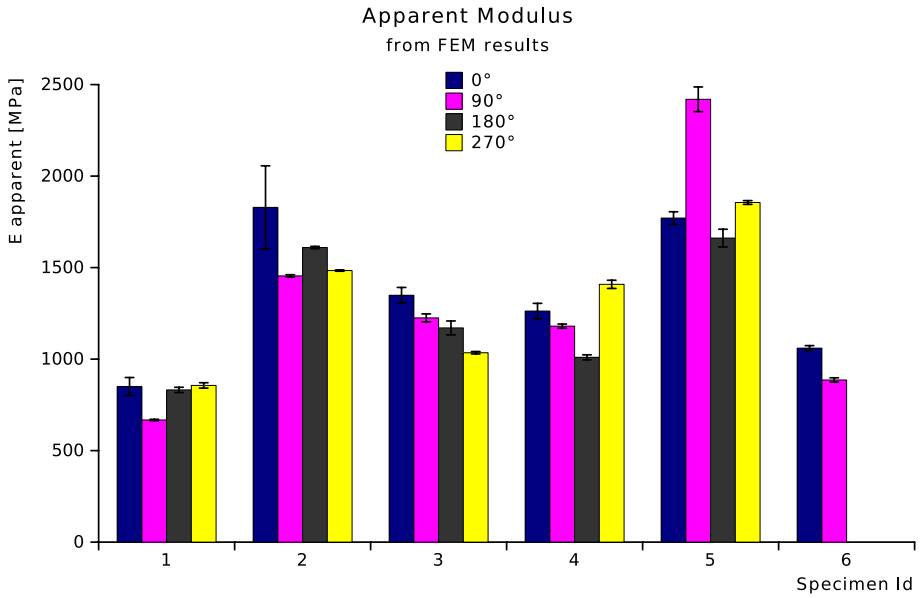

Figure 5.9: Apparent level cancellous bone modulus determined from the results of micro-FEM analysis. Different colors represent different angular positions for strain tracing on the trabecular surface (BLUE: 0°, PINK: 90°, GREY: 180°, YELLOW: 270°). It is important to remember here that the values of apparent level modulus shown by micro-FEM calculations derive from the assumption of a tentative tissue modulus of 19 GPA. The proportion between micro-FEM and experimentally calculated apparent modulus should be observed.

Under the assumption of linear elasticity, estimations of trabecular tissue elastic modulus $E^{EST}_{tissue,i}$ can be calculated from the results of micro-FEM analysis and those of mechanical tests for each angular position test i.
Tissue modulus estimations are reported in figure 5.10, for the six tested specimens and for the four angular positions, in form of a column chart.

Tissue modulus estimations for the 180°and 270°positions for specimen 6 are absent since no experimental data was available for these tests due to the failure of the specimen during the 180°test.

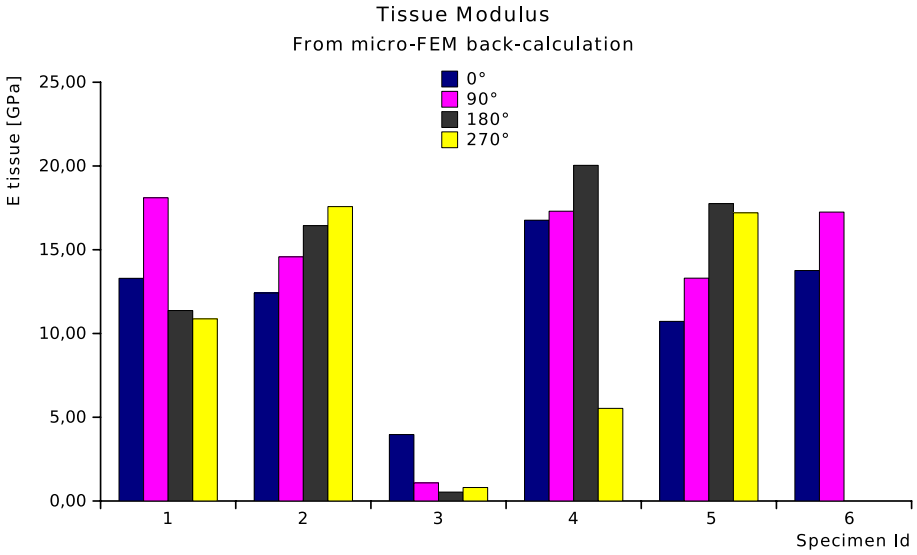

Figure 5.10: Cancellous bone tissue modulus estimations from the results of micro-FEM analysis and experimental measurements. Different colors represent different angular positions for strain tracing on the trabecular surface (BLUE: 0°, PINK: 90°, GREY: 180°, YELLOW: 270°). Results should be compared with experimental data reported in figure 5.9: the similarity of the trend displayed by experimental measures of apparent modulus and numerical predictions suggest an unsatisfactory coherence between experimental reality and FEM models. Actually, homogeneous modulus predictions should be expected, for each specimen, on the four angular positions.

Tissue modulus estimations from cross-section average displacement

The apparent level modulus from experimental results $E^{EXP}_{apparent}$ was averaged on the four angular calculations. The apparent level modulus from micro-FEM results was obtained through average displacements in the specimen's cross-sections at the reference levels of extensometer's knives (heights were averaged for the four angular registrations). From this data, the estimations of tissue

modulus E_{tissue}^{EST} of table 5.4 were back-calculated.

Id	Donor	$\boldsymbol{E_{tissue}^{EST}}$ [GPa]
1	A	14.99
2	A	15.69
3	A	15.38
4	B	14.32
5	B	15.68
6	B	n.a.

Table 5.4: Tissue modulus estimations from average displacements in the cross-section at extensometer's knives reference levels. Number of specimens = 6. Specimen 6 was damaged during the test at 180°: no data is therefore available for specimen 6. For donor A: MEAN = 15.35 GPa; STANDARD DEVIATION = 0.35 GPa.

Micro-FEM apparent modulus predictions

Predictions for the apparent modulus were obtained from the results of tissue modulus estimations of figure 5.10. For values were obtained imposing the correspondence between experimental ($E_{apparent}^{EXP}$) and numerical ($E_{apparent}^{FEM}$) modulus for each angular position. A unique value for the tissue modulus of each specimen was assumed.
Two strategies were used for the calculation of the tissue modulus (assumed homogeneous over the whole specimen) and the consequent estimation of the specimen's apparent stiffness.

- *MEAN tissue modulus* $\overline{\boldsymbol{E}}_{\boldsymbol{tissue}}$: the optimal tissue modulus was calculated as the mean of the tissue moduli estimated for the specimen on the 4 different angular positions.

- *BEST-FIT tissue modulus* $\boldsymbol{E}_{tissue}^{BEST-FIT}$: the optimal value for the tissue modulus was obtained best fitting the apparent modulus predictions on

for the 4 angular positions with the results of mechanical tests through the least square method[5].

In figure 5.11, the apparent level modulus predictions obtained with the two mentioned methods are reported.

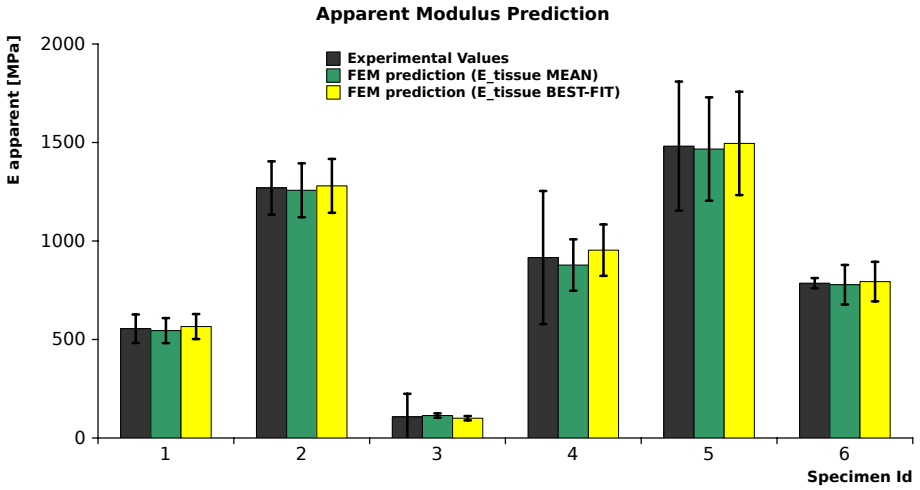

Figure 5.11: Apparent level modulus prediction from the results of micro-FEM analysis. GREY: Experimental results, GREEN: mean tissue modulus method, YELLOW: BEST-FITTING of experimental results, least squares method. Variance from experimental measurements: $\overline{E}_{tissue}$: MAX = 7%, MEAN = 2.67%; $\overline{E}_{tissue}$: MAX = 6%, MEAN = 2.5%.

[5]The statistical operation, already described in section 3.2.8, leads to:

$$E_{tissue}^{BEST-FIT} = \frac{\sum_{i=1}^{n} \frac{E_{app,i}^{EXP\,2}}{E_{tissue,i}^{EST}}}{\left(\frac{E_{app,i}^{EXP}}{E_{tissue,i}^{EST}}\right)^2} \tag{5.2}$$

Once the best fitting value of tissue modulus has been calculated, it is possible to obtain from this an estimation for the apparent level modulus of the micro-FEM model. We have, for the angular position i:

$$E_{app,i}^{FEM}(E_{tissue}^{BEST-FIT}) = \frac{E_{app,i}^{EXP}}{E_{tissue,i}^{EST}} E_{tissue}^{BEST-FIT} \tag{5.3}$$

Sensitivity test

In figure 5.12 the estimated tissue modulus for one specimen and for a single angular position is plotted as function of the parameters h and r. The surface plot shows a substantial independence of the estimation of E_{tissue}^{FEM} from the height h of the cylinder-shaped regions of nodes selected for the determination of average displacements at the two extensometer's levels.
The same behavior was observed for all six specimens and for each angular position of the test: for none of the 24 sensitivity tests a relation between predicted modulus and height h was found.
By contrast, a marked dependence between predicted tissue stiffness and the

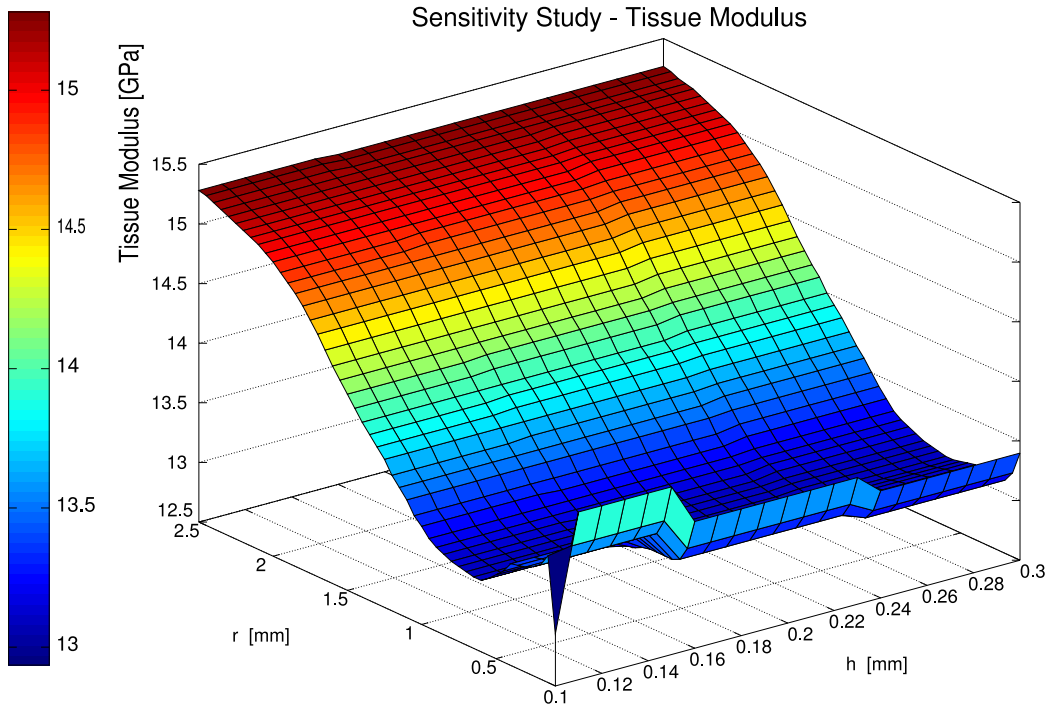

Figure 5.12: Sensitivity study results: the surface represents the variability of the estimated tissue modulus with the parameters h and r. It can be noted how the prediction of tissue modulus is not influenced by the cylindrical height h. Parametric ranges: $h = 0.05$ mm to 0.30 mm; $r = 0.10$ mm to 2.50 mm. Specimen Id: 1.

parameter r was observed for all sensitivity tests.

Being this behavior common to all the examined specimens, the absence of proportionality of the estimated modulus with h was assessed. Results from sensitivity tests were therefore compared at a fixed value of $h = 0.3\ mm$.
In figure 5.13, a comparison of the results from the sensitivity tests of all trabecular bone specimens and for each angular position is proposed.
Curve plots of the relative variation of tissue modulus estimations were obtained for all the 22 specimens for which experimental data was available.

5.0.9 Discussion

For each tested cancellous bone specimen, the apparent modulus determined through micro-FEM analysis $E^{FEM}_{apparent}$ varies with the angular position of the test.
At the same time, contrary to what it was expected, the estimated tissue modulus E^{EST}_{tissue} is not constant for the single specimen. In this section, an interpretation for this unexpected behavior will be offered first; possible reasons for the explanation of discrepancies between numerical and experimental results will be introduced afterward.

Apparent modulus measures from mechanical test of specimen 3 suggest the invalidity of the data for this specimen. A standard deviation of up to the 100% and extremely low values of apparent modulus were observed for this specimen, corroborating the hypothesis of a premature failure of the specimen due to the marked geometrical discontinuity of the same. In figure 5.14 the micro-CT scan of specimen 3 is shown: the appreciable particular discontinuity of the trabecular structure is supposed to be the cause of a premature failure of the specimen with consequent detection of extremely low values of apparent modulus.

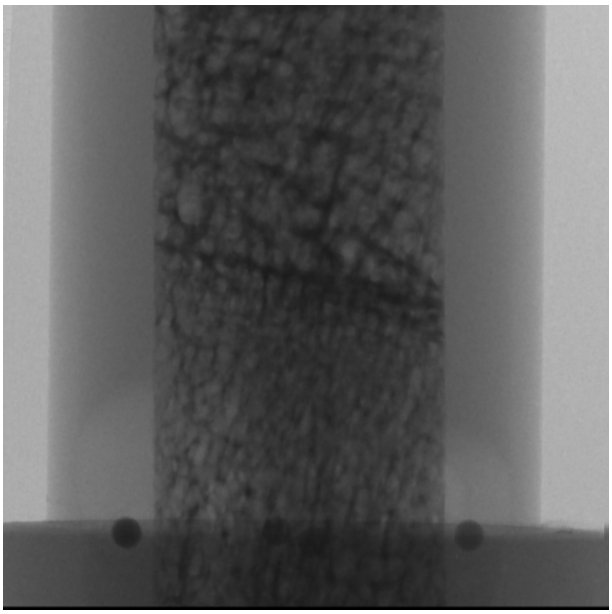

Figure 5.14: Micro-CT scanning of specimen 3. Unusual trabecular discontinuity can be observed.

The experimental measure of apparent modulus on the single angular position of the specimen showed a generally low variability. An average relative standard deviation of 5.29% was found (see table 5.2). High values of standard deviation could generally be linked with discontinuities in the load-displacements curves derived from mechanical tests. These discrepancies could be attributed to a loss of contact between extensometer knife and trabecular structure during the test, suggesting the effectiveness of the remaining measurements.

On the contrary, a considerable variability of apparent modulus was observed for the test with the extensometer fastened on different angular positions among the trabecular surface of the specimen (see figure 5.8). A mean (percent) standard deviation of 17.77% is reported in table 5.3, with a variation of up to the 20% for one half of the investigated specimens.
Together with the experimental variability presented in figure 5.8, the comparison between experimental and micro-FEM results should be considered. The apparent modulus trend exhibited by mechanical tests results for the different

angular positions of each specimen is not replicated by the apparent modulus from micro-FEM analysis. As a result of this, the estimation of tissue modulus from linear elastic assumption reported in figure 5.10, does not produce a uniform value of tissue modulus for the single specimen along the four angular positions. An average (percent) standard deviation of 37.00% was obtained for the E_{tissue} predictions. However, this value is substantially influenced by the 100% standard deviation found for specimen 3, being the percent standard deviation lower than the 25% for 4 specimens of 6.

Three different hypothesis should be considered for the interpretation of the obtained results.

Structural anisotropy

The apparent modulus variability with the position of the investigation among the specimen surface could be explained by means of the natural anisotropy of trabecular structure. The non homogeneous geometry should cause, under this assumption, different displacement's gradients on different angular positions of the trabecular surface.

However, the hypothesis of anisotropy of the apparent level cancellous bone mechanical properties accounting for the variability of the measured stiffness seems to be contradicted by the results of micro-FEM modeling. 3D micro-FEM models should account with precision for the structural anisotropy of the bone, thanks to the great precision whith which the trabecular frame is characterized by the model. The apparent modulus estimation from micro-FEM modeling reported in the plot of figure 5.9 displays inadequate correspondence with the results of mechanical tests. In addition, the expected homogeneous value of tissue modulus characterizing each specimen was not confirmed by the results of figure 5.11.
For these reasons, the anisotropic hypothesis can not account for the behavior observed in the results of this analysis.

Experimental end-artifacts and Boundary conditions

The experimental solutions adopted for the minimization of end-artifacts have been already described in chapter 2 and, referring to the newly developed experimental protocol for compressive tests, in section 2.4. These are, briefly:

1. PMMA cement embedding of the specimen's extremities
2. Detection of displacements with the extensometer positioned on the central portion of the bone specimen, and with the repetition of the measurement among four different angular positions
3. Preconditioning cycle of 20 compressions prior to the test to recover potential plays

Nevertheless, the potential occurrence of end artifacts should not be ignored. Particularly, three kinds of end-artifacts could explain the angular variability of the measured apparent modulus:

1. **misalignment of the testing machine's actuator**: this event would cause the incorrect alignment of loading direction with the orientation of the specimen's axis. The result of the misalignment could be a condition of complex loading of the structure, with the presence of both axial compression and bending of the bone specimen.
2. **residual plays between PMMA cement and machine's supports**: the occurrence of this second type of end-artifact seems to be unlikely thanks to the pre-conditioning compressive cycle introduce for the recovery of latent plays (see section 5.0.6) [5].
3. **Trabecular displacements inside the PMMA cement**: according to the boundary conditions imposed to the micro-FEM model, it is assumed that no vertical displacement occur inside the extremities of the specimen which are embedded into PMMA. However, it has been suggested how this approximation could be erroneous.

The mixed bending and compressive loading state originated by the presence of end-artifacts could not be correctly represented by the micro-FEM model, discretizing its boundary conditions the theoretical uniaxial compressive state

of the test.
The investigation of the influence of such troubling end-artifacts would require multiple mechanical tests on specimens obtained from homogeneous materials of known modulus of elasticity. The design of this kind of experiment should consider the mechanical test to uniaxial compression of a specimen similar in size to the cylindrical shaped cancellous bone specimens of interest. Specimens in homogeneous[6] materials should be tested both with and without PMMA cement embedding of extremities, to gain accurate informations on the influence of misalignment and play end-artifacts on displacements measured at the specimen's side surface.
By the way, the particular presence of a bending loading component, should display experimental evidence in the results of mechanical testing. Pairs of predicted moduli at opposed sides of the specimen should present a typical alternation of corresponding values with asymmetric values. This result is not observed, generally in the available experimental data.

Local effects and side-artifacts

The sensitivity study on the parameters for the calculation of the apparent stiffness E_{app}^{FEM} from micro-FEM results introduced the question on how much the local variability of the displacement field due to the structural anisotropy of the cancellous bone can influence the determination of the apparent level modulus of elasticity of the tested specimen. Together with this argument, a second question should be posed, on how much the experimental measurement of trabecular displacements based on the use of an extensometer, can effectively detect the local characteristics of the displacement field describing the physical problem of interest.
From the results of sensitivity analysis, a great variability of the determined specimen's modulus with the dimensions of the volume of nodes modeling the region contact between extensometer and trabecular surface has been observed for some angular tests. From figure 5.13, a great relative variability of the modulus is observed for specimens 1 and 5.
In particular, a high variability was obtained for the angular positions 90°and 270°for specimen 1 and for the angular positions 0°and 90°for specimen 5.

[6] or regular cellular solid

A correspondence between this result of the sensitivity study can be obsevred, simultaneously, in the results of figure 5.10, where to the tests of specimen 1 and 5 correspond a significant variation of the back calculated tissue modulus. With particular attention for these two specimens:

- **Specimen 1**
  - For the **90°** position, an opposite trend of modulus was presented with respect to the other angular positions.
  - For the **270°** position, a modulus variation of up to the 20% was shown.
- **Specimen 5**
  - For the **0°** position, a significant variability of the estimated modulus was observed, with absence of a uniform trend.
  - For the **90°** position, the results showed a modulus variation of up to the 20%.

This finding suggested the presence of a substantial divergence between the displacements locally detected by the numerical analysis and those registered from the extensometer during mechanical test.
The investigation of local characteristics of trabecular geometry, in combination with the observation of the micro-FEM model's displacement vector field in the regions of bone interested by the contact with extensometer's knives, was possible thanks to ParaView[7].

The observation of local details of the contact region between extensometer knife and trabecular structure, showed how particular situations can be identified for those specimens and angular positions which reported high variation in tissue modulus prediction and, at the same time, non-uniform trend in the sensitivity study.
In figures 5.15 and 5.16, it can be seen what happens for the critical angular positions for specimen 1. When the extensometer is in the 90°and 270°angular positions,the extensometer-bone contact point is situated in the proximity of small trabecular structures showing significant displacement gradient. As a

[7]ParaView - multi-platform data analysis and visualization application

consequence of this, the estimated strain will be affected by a significant variability with the dimensions of the region of points for numerical calculation.
At the same time, it has been observed how, during the compressive tests and the specimen's preparation, the extensometer's metal knives[8] can penetrate deeply into the cylindrical surface of the cancellous bone specimen.
It can be supposed that during the mechanical test, small trabeculaes are broken because of the pressure of knives, this occurring in particular for thin rod-like structures characterized by low BV/TV as those of figure 5.15. The damage of external frames would therefore result in a loss of information on trabecular displacement.
This can be supposed to be the main cause for the considerable variation of the prediction of tissue modulus presented by specimen 1 for the 90°and 270°positions. On the contrary, the estimation corresponding to specimen's sides characterized by plate-like structures would result less influenced by local variability of the displacements field. At the same the contact with thicker structures would mean less penetration of the extensometer knives, with the maintenance of the uniformity between experimental reality and micro-FEM model representation.

A comparable behavior of that observed for specimen 1 and angular positions 90°and 270/textdegree can be observed, in figures 5.17 and 5.18, for specimen 5.
Here, the 0°position is of particular interest. Thin rod-type trabeculaes are in contact with the extensometer's knives. It is easy to suppose that these frames will result broken by the pressur eof the knife after the application of fastening rubber bands to the model. The trabecular connectivity will therefore be interrupted by the experimental tools, causing a heavy interference with the physical reality described by the micro-FEM model. Relevant local variations of the displacement field will be detected during the numerical calculation of strains, while the measure of the extensometer will be insensitive with respect of local phenomenons.

[8]which are developed to perform an optimal grip for the measurement over metallic smooth specimens.

5.0.10 Conclusions

The application of a newly developed experimental layout for compressive tests of cancellous bone specimens has been described in this chapter.
The procedure implements the multiple repetition of linear elastic mechanical test of each specimen with the extensometer positioned among four different angular positions. 3D micro-FEM voxel models discretizing the displacement detection at the contact point between extensometer's knife and cancellous structure were used for the characterization of the modulus of elasticity of the specimen from FEM modeling.

In conclusion, the sensitivity test on the variability of the estimated tissue modulus with the dimension of the region of nodes selected on the micro-FEM model for the calculation of displacements, is a fast post-processing tool for the investigation of local strain variability. The sensitivity study could be introduced as a standard approach for the characterization of the reliability of our cancellous tissue modulus estimations through the investigation of their relation with the local displacement field.

Nevertheless, when an optimal value for the estimated tissue modulus (both through the averaging and best-fitting procedure) is adopted, our predictions of apparent level modulus from micro-FEM analysis agree well, for the whole specimen's sample, with experimentally derived values.

Furthermore, even if local effects influence the calculation of strains, the average displacement inside the specimen's cross-section leads to the determination of plausible and repeatable values of cancellous bone tissue modulus for specimens from the same donor.

Finally, the results showed how the micro-FEM modeling procedure offers the insight which is required for the verification of an experimental hypothesis regarding the structural anisotropy of cancellous bone.

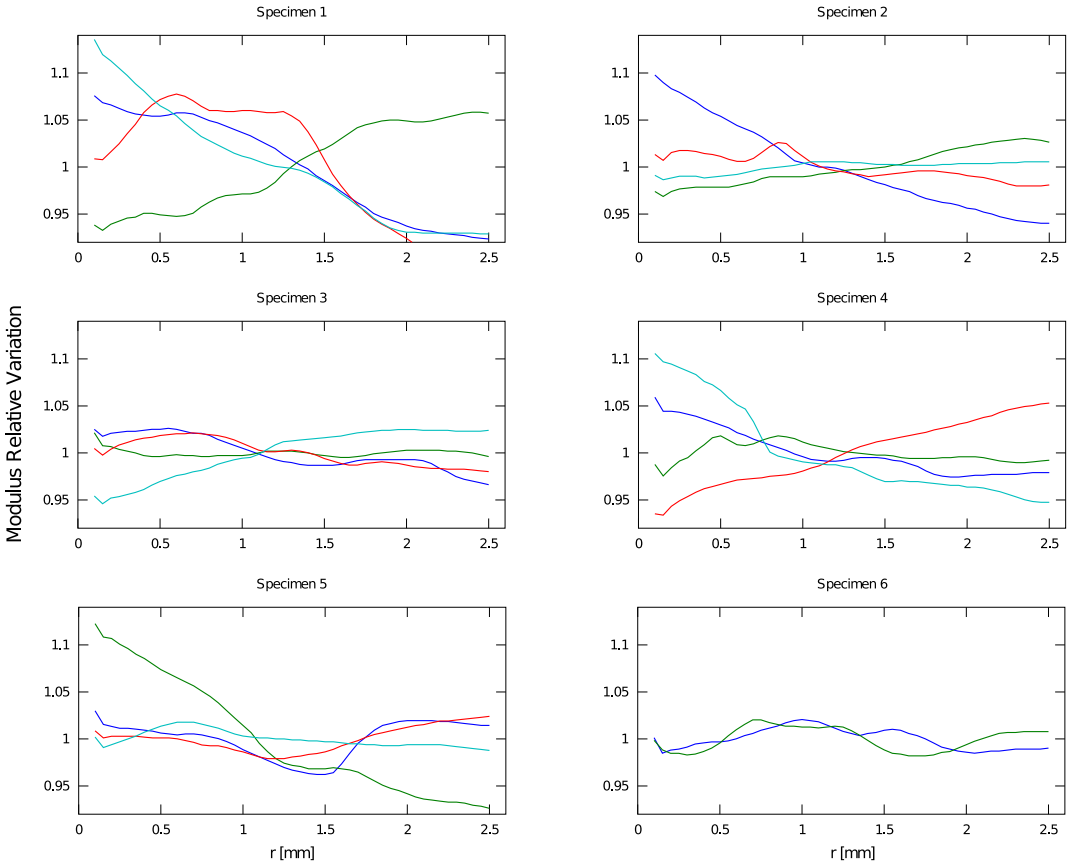

Figure 5.13: Sensitivity study results: 2D plots. The parameter h was fixed at 0.3 mm, according with the results shown in figure 5.12. The relative variation of the calculated apparent modulus is shown as function of the parameter r, for each specimen and angular test position. GREY: 0°, BLUE: 90°, RED: 180°, CYAN: 270°. Only two lines are shown for specimen 5 because of the corresponding lack of experimental information for test positions 180°and 270°. The $E^{FEM}_{apparent}$ relative variation for each plot series is calculated with respect of its mean value. Specimens 2, 3, 5 and 6 exhibit generally low variability for all angular positions of the test (relative variation $< \pm 5\%$) with the exception of position 90°for specimen 2 and position 0°of specimen 6. At the same time the specimens 1 and 4 showed an apparent modulus prediction variability of over the 10% for all positions. Parametric ranges: $h = 0.30$ mm (fixed); $r =$ 0.10 mm to 2.50 mm. Number of specimens: 6. Total number of tests: 22.

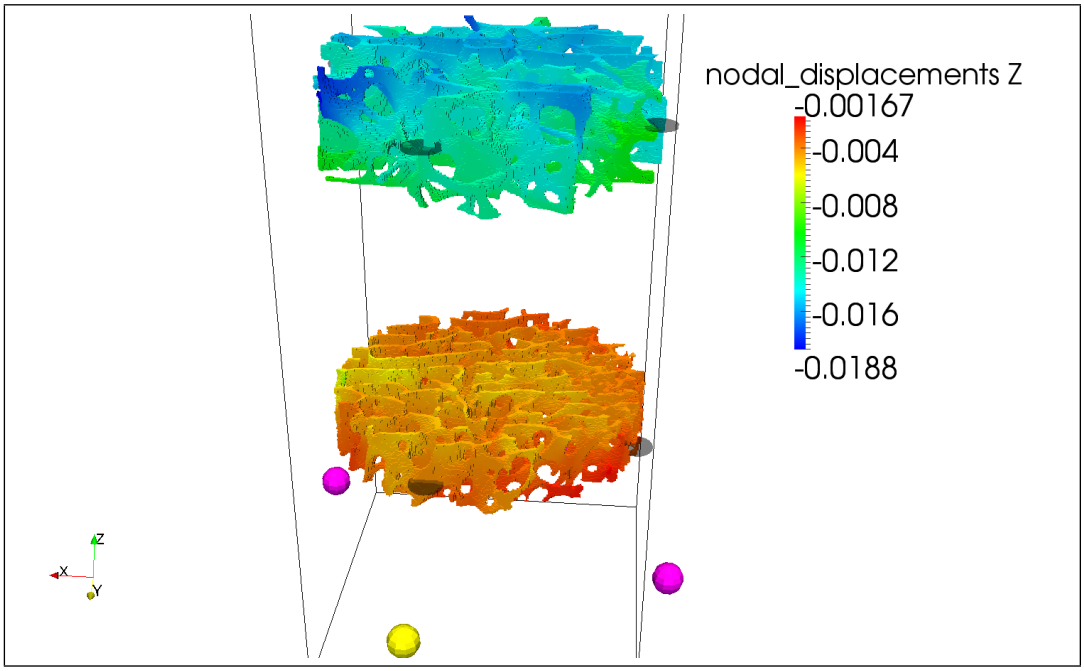

Figure 5.15: Specimen 1. Position 0°. Model visualization with focus on the regions of nodes selected for the calculation of mean trabecular displacements. The colormap codifies the z-component of displacement. The modeled reference spheres are shown as well as the cylinder-shaped regions for the calculation of average displacements (opaque in figure). The plate-like structure should be noted.
Only the bone slices of interest are displayed for visualization requirements.

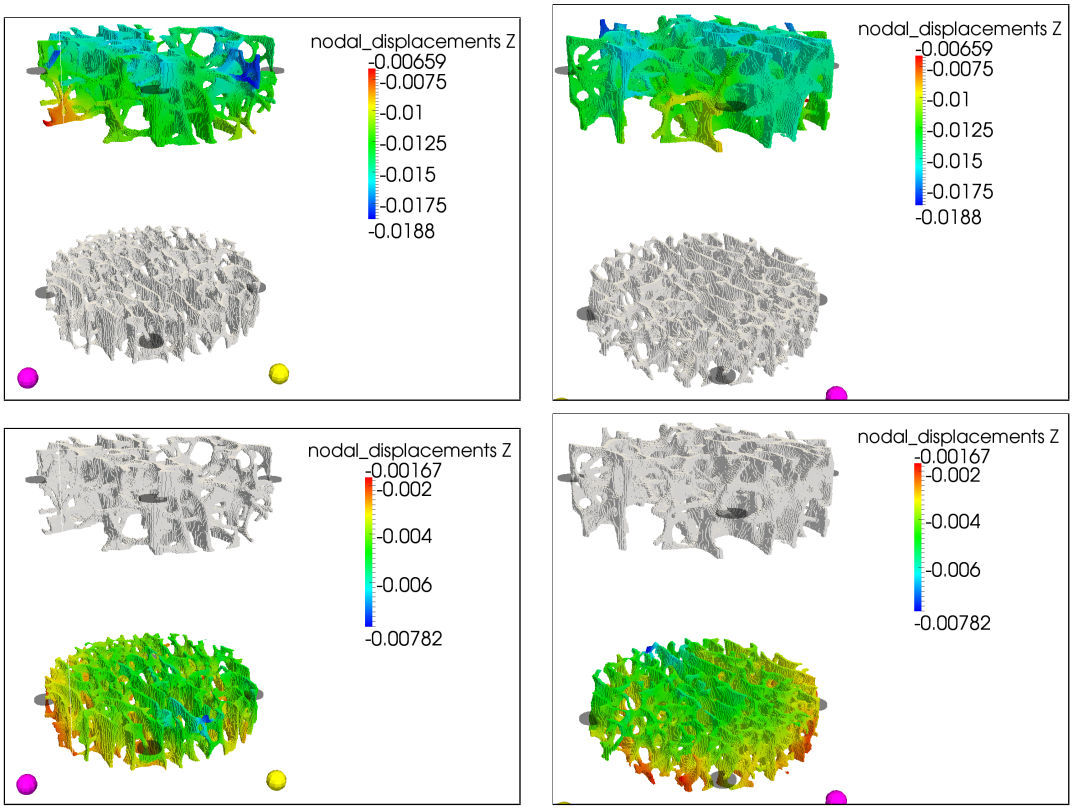

Figure 5.16: Specimen 1. LEFT: detail of the region of nodes selected: 90°position. RIGHT: detail of the region of nodes selected: 270°position. For 90°and 270°positions, small trabecular structures are intercepted by nodes selection around regions displaying high displacement gradient.

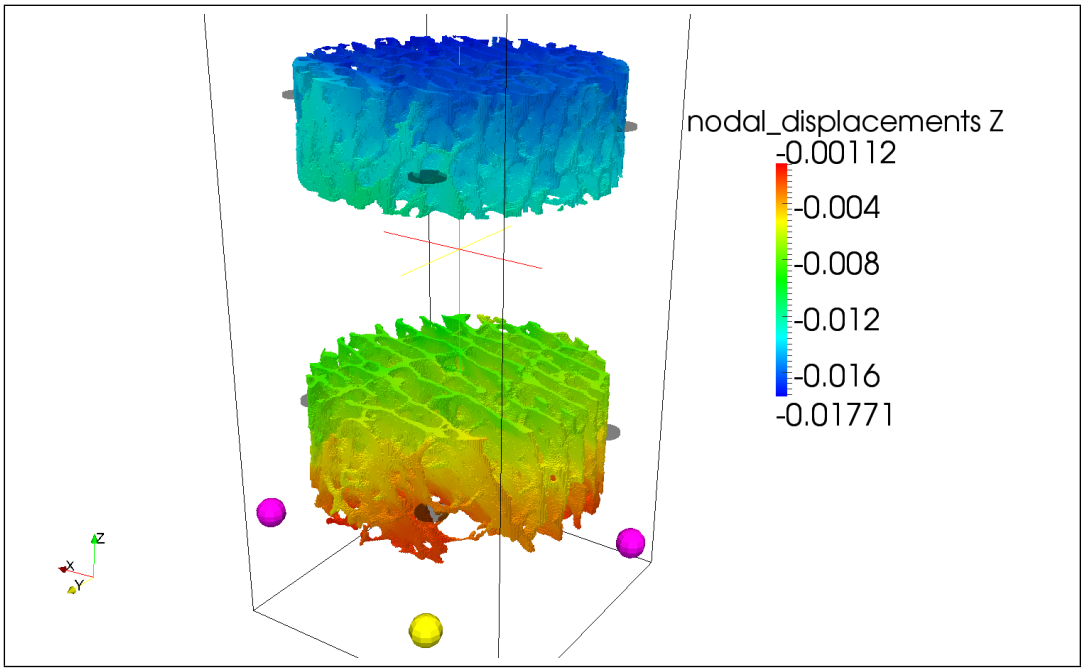

Figure 5.17: Specimen 5. Position 0°. Visualization of the regions of nodes selected for the calculation of mean trabecular displacements (opaque in figure). Local variations of the displacement field should be noted.

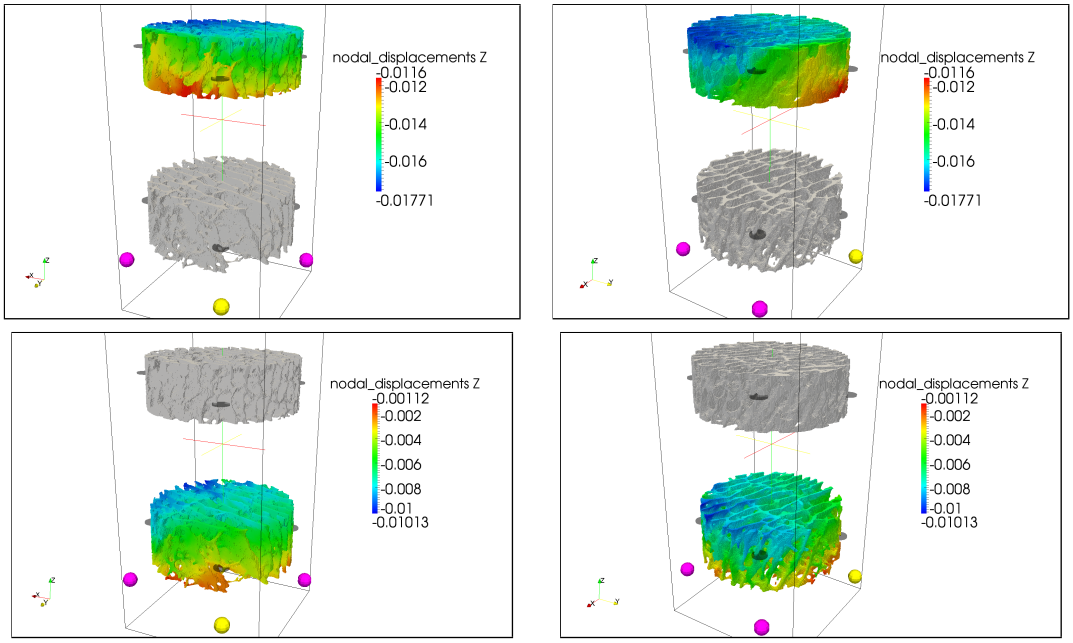

Figure 5.18: Specimen 5. LEFT: detail of the region of nodes selected: 0°position. RIGHT: detail of the region of nodes selected: 90°position. For 0°and 90°positions, small trabecular structures are intercepted by nodes selection around regions displaying high displacement gradient. It can be supposed that these thin structures will result interrupted by the extensometer's knife, which will modify and constrain, locally, the region of contact. As a consequence, the strain determined by the extensometer will differ significantly with the strain derived from the micro-FEM modeling.

Chapter 6

A Digital Image Correlation based experimental layout

In the previous chapter, an experimental layout for mechanical compressive tests of cancellous bone specimens, based on the measurement of trabecular displacements with the use of an extensometer has been presented. It has been illustrated how the main criticality of this kind of experimental procedure, is connected with the same presence of the extensometer's knives.
An alternative technology for the measure of trabecular displacements during compressive test, is actually under development at IOR's Medical Technology Laboratory. This is based on the optical detection of the displacements at the surface of the cancellous bone specimen.
In this chapter, the Digital Image Correlation(DIC) technique will be introduced. It is important notice how the experimental layout for compressive tests of cancellous bone specimens in use at IOR has not been designed for the combination with the Digital Image Correlation technique for the measure of displacements. This is why, at the moment, a lack of information makes hard the task of an accurate numerical postprocessing of micro-FEM modeling results, for the estimation of cancellous bone elastic properties from the measurements performed with the Digital Image Correlation method. In this sense, in the last paragraphs of the chapter, some features of a potential experimental layout for the combination of Digital Image Correlation acquisition with micro-FEM modeling will be proposed.

6.0.11 Principles of digital image correlation for the measure of displacements

Digital Image Correlation (DIC) is an optical imaging technique for the measure of surface displacements (and strains) of an object. 3D DIC is based on the acquisition of a sequence of optical images of the object during its deformation caused by mechanical or thermal loads. From an initial reference state, DIC is capable to identify univocally a group of points belonging to the surface of the body. Through the detection of local grey level's gradients among different frames of the acquisition, the DIC is able to detect the position of each selected point and for each frame. Afterwards, an algorithm calculates the 3D displacement occurred in the time lapse between two acquisitions for each one of the detected points.

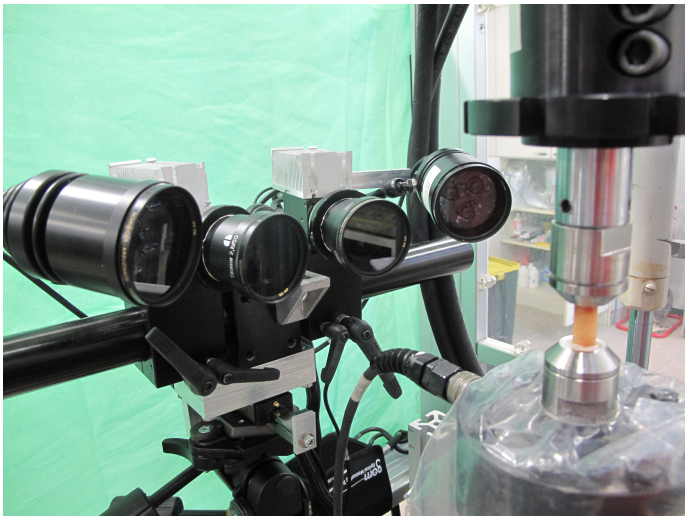

Figure 6.1: ARAMIS 5M. The system of the two digital CCD cameras and the LED lights are shown.

Stochastic pattern

It has been demonstrated how the adoption of some solutions is necessary for the correct development of the DIC acquisition and for the good efficiency of

the operation. The application of a stochastic color pattern to the surface to be investigated is compulsory for the univocal recognition of the points of the object and for the accurate DIC measuring operation[32].

The DIC acquisition device[1] ARAMIS 5M available at LTM is showed in figure 6.1. For further details on the process of calibration and setup of the DIC system for biomedical applications the reader should refer to the MS thesis proposed by Lionello[23] et. al. on 2011 and conduced at IOR's Medical Technology Laboratory: "Messa a punto del metodo di correlazione di immagini per applicazioni biomediche".

6.1 Features of the DIC based layout

In this section, the application of the DIC based procedure for the measurement of the surface displacements of cancellous bone specimens during mechanical compressive tests will be presented. Considering most of its features, the layout described here corresponds with fidelity to the experimental layout[5] introduced in chapter 5.
All specimens were micro-CT scanned and micro-FEM voxel models were reconstructed (threshold grey value = 144; voxel size = 39.0 microns) (see chapters 2, 3 and 5 for more details).

6.1.1 Assembly

The assembly of the layout for experimental tests with acquisition of surface displacements with the DIC procedure is shown figure 6.2. Here, it should be noted how the experimental setup allows the measurement[2] of the cancellous bone specimen's displacements both with the DIC system and with the extensometer based procedure described in chapter 5. This feature of the layout allowed the comparison of the results obtained with the two different strategies, giving this way an important information on the reliability of the DIC

[1] GOM - Optical Measuring Techniques
[2] not simultaneous

system.

The DIC system was calibrated to allow a field of view for the displace-

Figure 6.2: Assembly of the DIC based layout: components and assembly of the ARAMIS 5M system (LEFT) and recording procedures for the extensometer based strategy prior to the mechanical test (RIGHT).

ment detection of 25 x 21 mm[5]. To allow the correct coordination with the 3D geometry of the micro-FEM model deriving from micro-CT reconstruction (see section 6.2.2 below), it was necessary to include one of the aluminum marker spheres into the DIC field of view. The ARAMIS acquisition system had to remain fixed in its calibration position: this is why the test recorded the displacement field on only one side of the specimen. The displacement field was obtained for a surface covering around 120°of the whole cylinder-shaped surface of the specimen.

6.1.2 Realization of the pattern

For the DIC detection of displacements, a high contrast pattern had to be applied on the surface of each cancellous specimen. This was performed in two subsequent phases[5, 23].

1. First, a homogeneous white covering in water paint was applied to the trabecular surface.

2. Secondly, a stochastic pattern was performed with black acrylic spray paint.

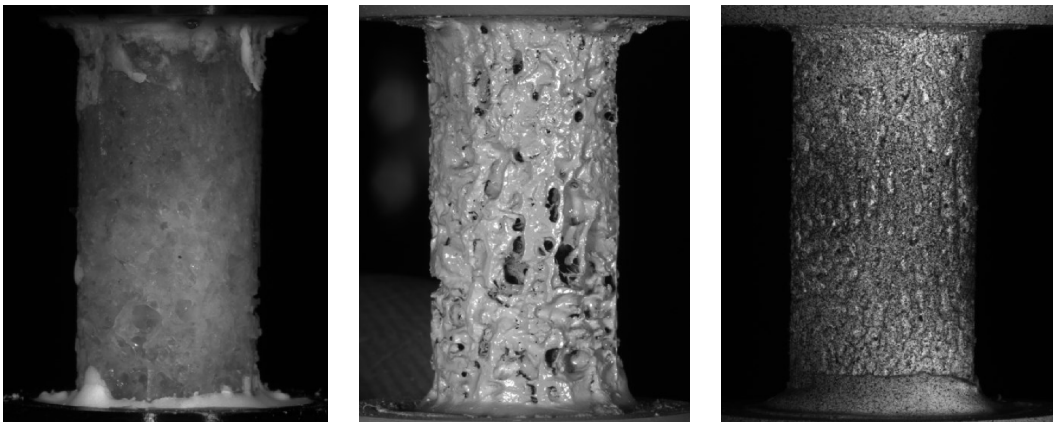

Figure 6.3: Stochastic pattern application: specimen's acquisition before the application of the pattern (LEFT), after the application of the homogeneous covering in white water paint (CENTRE) and after the application of a stochastic pattern in black acrylic paint (RIGHT).

In figure 6.3 the two steps of application of the stochastic pattern are shown. The absence of difference between the results obtained with and without pattern is suggested by Falco[5], together with the reliability of the DIC system for the determination of cancellous bone specimens apparent mechanical properties.

6.1.3 Mechanical tests

All the 3 cancellous bone specimens were tested to uniaxial compression[5]. For the comparative analysis analysis of the results obtained by the DIC procedure with those from the standard (see chapter 5) procedure, compressive tests were repeated with both strategies, following the order:

1. A preconditioning load/unload cycle of 20 compressions was performed.

2. 4 compressive cycles were performed measuring the displacements with the extensometer (see chapter 5 for more details). This was fastened on the single angular orientation which could be acquired by the ARAMIS, obtaining the information for the comparison of the two procedures.

3. 4 cycles were performed with the specimen in the same position acquiring data with the DIC system.

4. Finally, four compressive cycles were performed, with the extensometer fastened in 0°, 90°, 180°and 270°angular position, respectively, for the study detailed in chapter 5.

Strain rate was controlled by the testing machine (INSTRON 8502, Instron Corp., Canton, MA) during each cycle and maintained at $0.01s^{-1}$ [28, 21, 16, 22].

6.1.4 DIC acquisition

In table 6.1, the characteristics of the DIC data acquisition are reported. The shutter time of DIC acquisition was set at 0.1 s. As a result of this, each frame represent the deformed state at intervals of 0.1 seconds.

Facet size [pixels]	40
Facet step [pixels]	10
Field of view [mm]	25x21
Shutter Time [s]	0,1

Table 6.1: Parameters of the DIC data acquisition during mechanical compressive tests.

6.2 Numerical postprocessing

The main features of the experimental layout developed at IOR's Medical Technology Laboratory for the DIC based measure of the displacements of a cancellous bone specimen during mechanical tests have been presented. Together with compressive tests, micro-FEM models of the 3 specimens were solved by use of the ParFE[3] multilevel iterative solver (Iteration limit = $1E^6$;

[3]Copyright (C) 2006 ETH Zurich, Institute of Computational Science, Uche Mennel, Marzio Sala, and all other ParFE developers

Tolerance = $1E^{-11}$).
In this section, a purpose for the methodological approach to the comparison between micro-FEM results and DIC measurements of displacements is presented. The main characteristics of a future layout for the combined use of DIC acquisition and micro-FEM modeling will be described.

6.2.1 Available data

The output of the analysis conduced by use of the DIC technique is a set of 50 frames (one per second) describing the evolution of the displacement field on the surface of the investigated cancellous bone specimen during the complete mechanical test. Each frame of the acquisition is characterized by a point mesh, where each point corresponds to the centroid of one facet and is characterized by the components of the displacement vector averaged on the facet area. In addition, each frame is connected to the first frame, which is assumed as undeformed state. Consequently, the displacement of each point and for each frame, is calculated referring to the corresponding point on the mesh of the undeformed state.

6.2.2 Comparing DIC and micro-FEM displacements

DIC acquirements are registered as a mesh characterized in the reference system of the cameras. On the other hand, the micro-FEM describes the trabecular displacement field in the whole 3D volume, according to the reference system of the micro-CT scanner. For the comparison of the two displacement states, the required operations are:

1. Registration of the two reference systems.
2. Comparison of the two displacement fields on points belonging to the same region.

Registration of the DIC acquisition mesh with the Standard Triangulation Language (STL) file of the micro-FEM model

The process of registration (which is shown in figure 6.4) had the aim of finding a reference for each point of the undeformed mesh on the reference system of

the 3D micro-FEM model.

Thanks to the ARAMIS dedicated software, it was possible to deduce[4] the

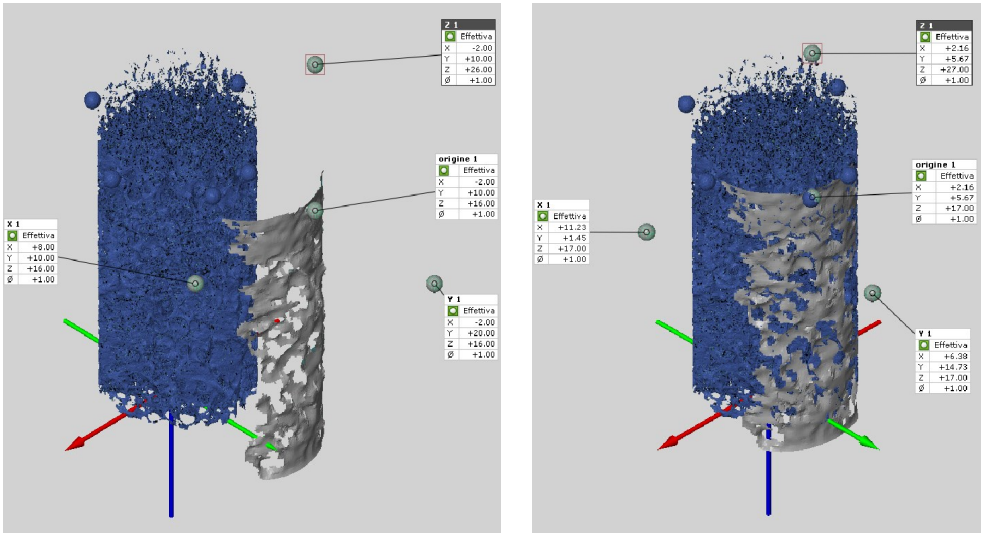

Figure 6.4: Best fitting procedure for the registration of DIC acquisition: before (LEFT) and after (RIGHT) the application of the automatic surface best-fit feature.

coordinates of the center of the aluminum reference sphere laying in the DIC's field of view. Afterwards, the registration was obtained thanks to a feature of surface best-fit of the ARAMIS 5M software[5]. Once the registration was completed, it was possible to locate the points of the DIC acquisition on the 3D micro-FEM model. As it will be illustrated below, the process allowed the direct comparison of local displacements between DIC measurements and results of the micro-FEM modeling.

6.2.3 Comparison of the displacement field in the same region

Displacements from DIC's acquisition were calculated as the difference between the registered coordinates of the mesh at two frames belonging to the linear stage of the mechanical test. From figure 6.5, it can be seen how the unde-

[4]through the interpolation of a spherical volume over points laying on its surface.

formed reference state of the DIC acquisition corresponds to the initial frame of the test, and not to the linear portion of the load-displacement curve. The procedure of displacement calculation was performed in Octave; *frames 0.6 and 0.8 were selected*. For the comparison of DIC measures with micro-FEM

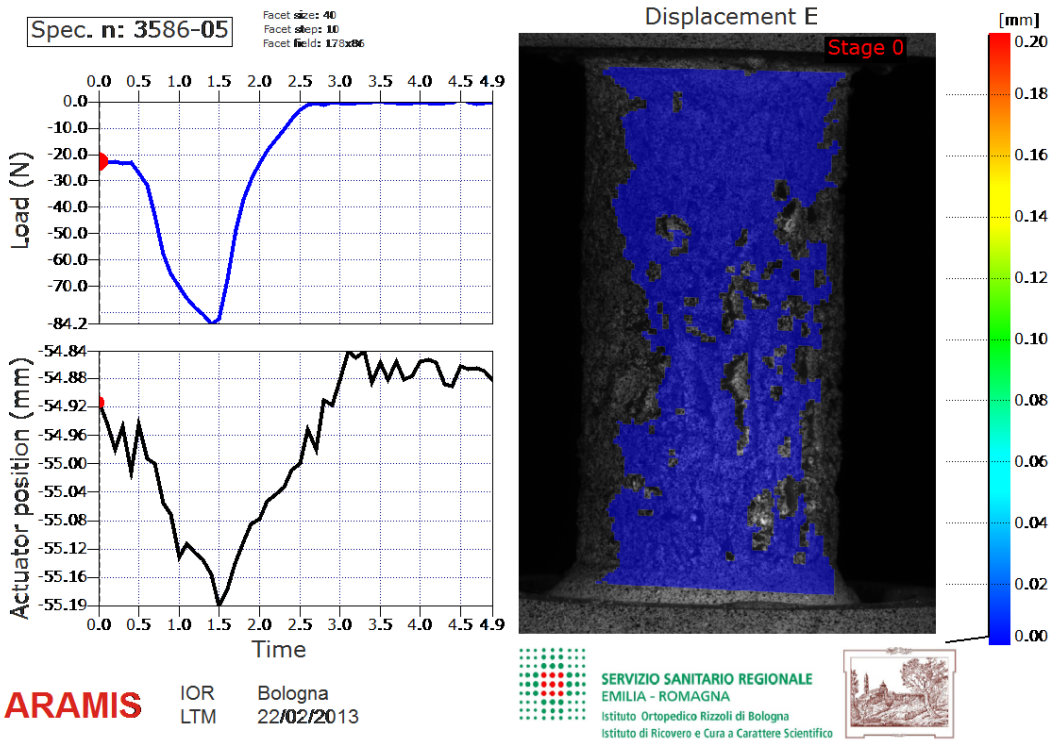

Figure 6.5: DIC report at frame 0: the acquisition of frame 0 represents the reference state for the DIC measurement. However, displacements must be detected at two frames belonging to the linear stage of the load-displacement curve. Selected frames for the calculation of frame displacements: 0.6 and 0.8.

modeling results:

1. The components of displacement (measured with the DIC and obtained from FEM modeling, respectively) were compared at a fixed height of the specimen. To do this, two reference levels[5] were chosen. The coordinates identifying all points of the undeformed mesh from DIC acquisition

[5]Levels were chosen far from the specimen's ends to avoid the influence of end-artifacts and in conformity with the heights at which the extensometer's knives are generally fastened.

at the considered heights were detected on the 3D micro-FEM model of the specimen through a Octave[6] algorithm. Spherical regions of nodes of the FEM models[7] were selected around the points of interest, with a radius of 0.02 mm, this value corresponding to 5 voxel sizes. Mean values were calculated for each selected region and for the three displacement's components, considering model nodes belonging to the spherical region. Results were normalized over the obtained range of displacements.

2. At the same time the visualization of Octave-converted VTK[18] files codifying the displacements registered by the DIC system, and described by the model, respectively, allowed the global qualitative comparison of the displacements.

6.2.4 Preliminary Results

Criticalities

1. The registration process had to deal with a positioning problem. This consisted in the lack of compliance of the reference systems of the two STL files. It can be supposed that this was introduced by the software used for the assembling of the two micro-CT stacks (see section 5.0.7). As a result of this bug, the complete reconstructed STL was not isomorph with respect to the reconstructed model, showing a scale factor on the 3 coordinates and inversion of the coordinates y and z. The registration was solved with the inversion of the STL file coordinates.

2. A second difficulty was found, regarding the registration's results. The location found for DIC's acquisition on the 3D model (see figure 6.6) shows locals penetrations of the acquired surface inside the reconstructed volume. The issue could be explained through the modification of the trabecular surface introduced by the pattern. Adhering on inter-trabecular

[6]Octave is freely available under the terms of the GNU GPL.
[7]the model is previously reduced to the only peripheral region.

vacuums, the applied paint caused the deviation between the geometry detected by the DIC and the micro-FEM model structure. As a result, the best-fitting procedure applied by the ARAMIS 5M software (for which we can not estimate the level of reliability) caused an error in the surface location.

3. A global comparison of displacements is shown in figure 6.9. Here, the presence of holes in the DIC's STL causes the partial lack of information on the local displacement measure. Secondly, the displacement field is monitored with large scale difference between the micro-FEM model and the DIC acquisition.

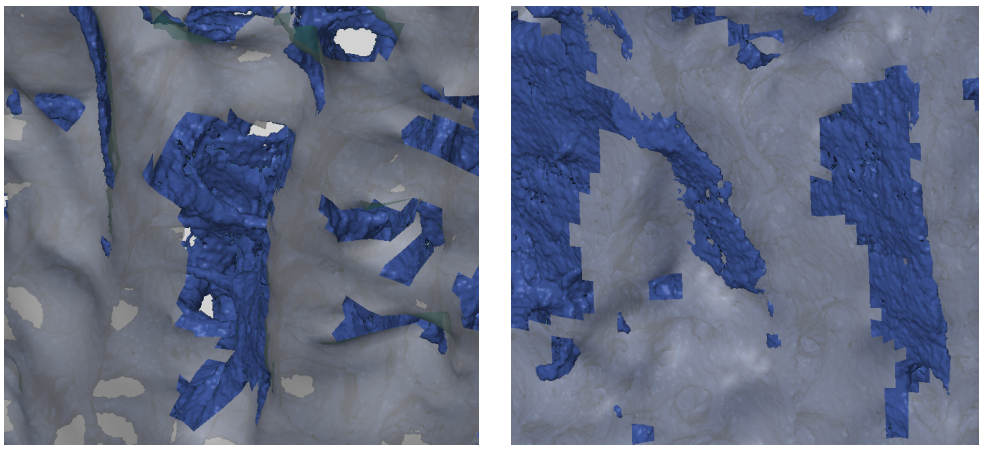

Figure 6.6: DIC acquisition registration procedure: representation of details concerning the adherence of the best-fit surface on the 3D model: local difficulties presented by the best-fitting algorithm can be noted.

Findings

1. The postprocessing output for the detection of displacements (from micro-FEM results) on the specimen's surface at two reference heights is showed in figure 6.7.

2. As a consequence of the registration difficulties, the minimum distance for the detection of points on the 3D model had to be increased until

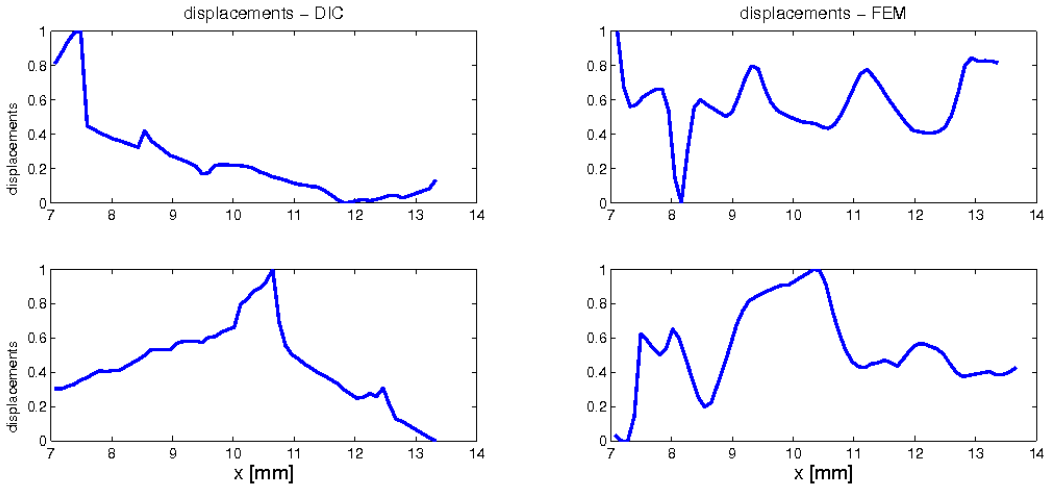

Figure 6.7: DIC (LEFT) and micro-FEM (RIGHT): comparison of displacements at extensometer's reference levels. BOTTOM: level 1; TOP: level 2). Results were normalized over the obtained range of displacements.

1 mm. In figure 6.8 the lack of adherence between DIC acquisition and reconstructed model can be observed.

3. A representation of the global pattern of displacements is shown in figure 6.9. Here, the presence of holes in the DIC's STL causes the partial lack of information on measured local displacement.

6.3 Discussion

In chapter 5, the relevance of information regarding local characteristics of the displacement field exhibited by the trabecular structure has been cleared. It has been supposed too how the presence of extensometer's knives, interfering with the response of singular trabeculaes, could cause the substantial deviation of the physical reality of mechanical tests from the discretization of micro-FEM models. An imaging based technique, able to realize the detection of the displacement field of trabecular structure at the surface of the specimen with no contact with the bone specimen, could represent a powerful tool for

the investigation of the tissue properties of cancellous bone from micro-FEM back calculation.
On one side, it has been assessed[5] how the application of a stochastic pattern for the DIC acquisition does not influence the mechanical response of cancellous bone. On the other, it has been shown here (see figure 6.7), how the modification of the trabecular surface introduced by the pattern, together with registration problems, cause the lack of matching between acquisition coordinates and reconstructed model.
Displacement's comparison at reference levels (figure 6.7) shows an agreement in the localization of the global peak of deformation for both heights. However, the DIC acquisition seem to be insensitive to local variations. A problem of spatial spacing could be the reason for this lack of information in the DIC's measurements. Acquisitions should be performed at a smaller facet size to accurately detect the behavior of single trabeculaes.

At a global scale, the preliminary comparison of DIC experimental measurements with the displacement field obtained through micro-FEM modeling, gives insufficient information for the interpretation of results. In this contest, the time spacing of DIC's measurement should be reduced[8] for the obtainment of more data characterizing the linear stage of mechanical tests.
In addition, the statistic sample (results were analyzed for only one specimen) is insufficient for a conclusion on the accordance between displacement fields.

6.3.1 Future developments

The application of rigid markers on the trabecular surface could be considered instead of the application of a stochastic pattern. This solution would allow the correct representation of trabecular surface by the DIC. On the other side this would cause the loss of local information on displacement. Further research of an answer to these experimental difficulties should be conduced.
At the same time, the development of a reliable procedure for the registration

[8] only three frames corresponding to the linear stage of the loading-displacement curve were acquired

of DIC's acquisition, together with the generation of an home-made optimal best-fitting algorithm suitable for unconnected surfaces, represent some of the mandatory future developments for the DIC-based experimental process.

In conclusion, it is pointed out here, how the experimental characterization with the DIC technique of the displacement field at the surface of cancellous bone specimens, would represent the base for the validation of our micro-FEM modeling approach for the characterization of tissue elastic properties of cancellous bone.

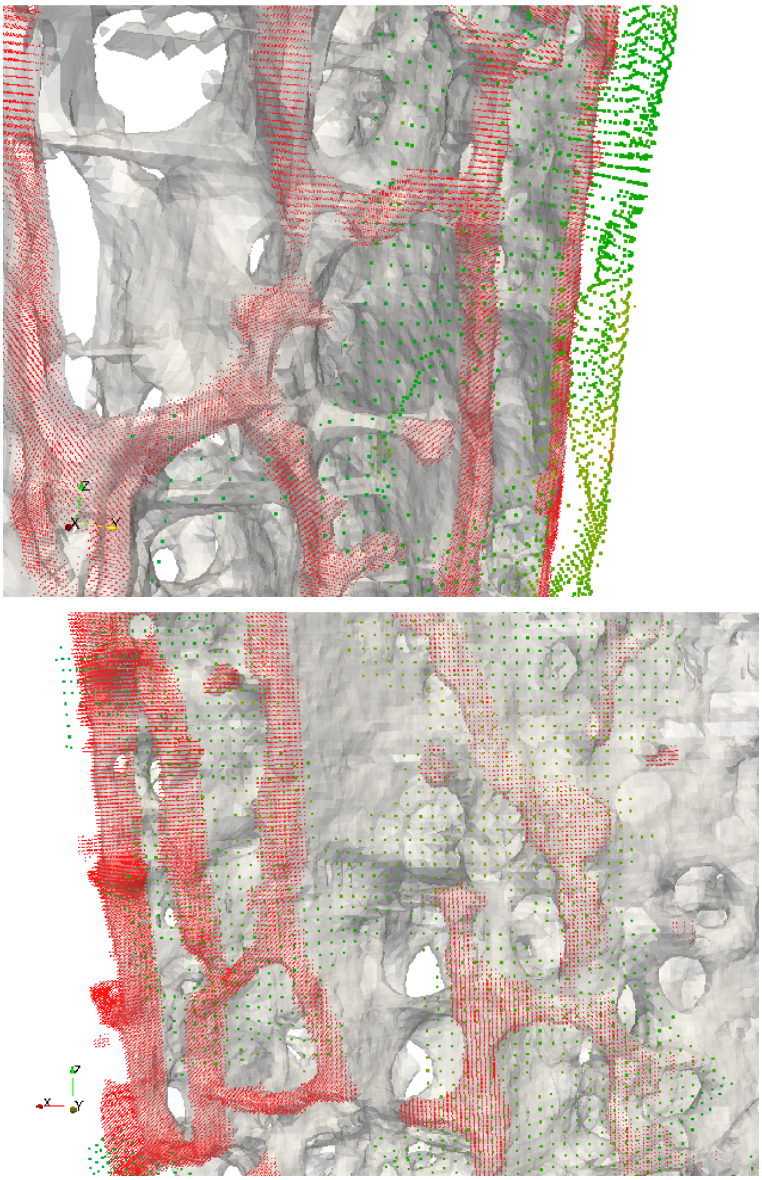

Figure 6.8: DIC and micro-FEM: The reconstructed micro-FEM model is represented in grey. The group of peripheral nodes of the FEM model selected for the post-processing procedure is plotted in red points. Green points identify the surface of DIC acquisition. TOP: a shift between the surface of DIC acquisition and micro-FEM model's structure is evident. This can be attributed to an error in the registration of the reference system for the ARAMIS®digital camera system. BOTTOM: the application of a pattern with water paint causes the filling of inter-trabecular cavities.

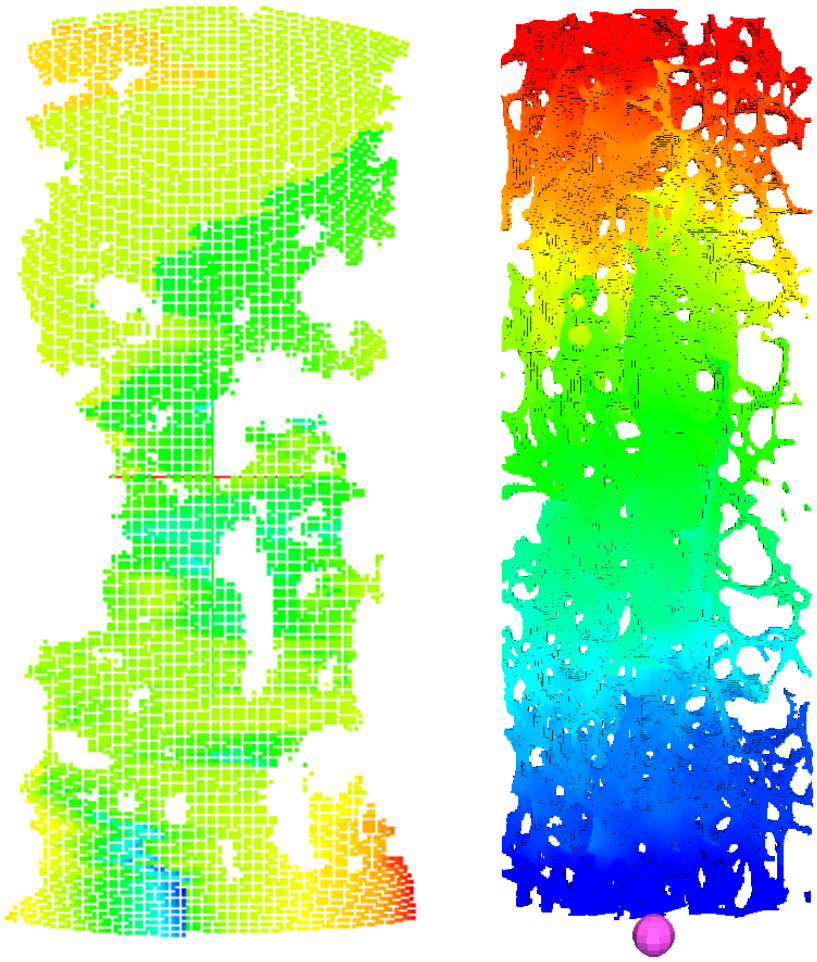

Figure 6.9: Global comparison of displacement from DIC measurements (LEFT) and micro-FEM results (RIGHT) among the specimen's z-axis. Visualization of global similarity in the displacement pattern is interfered by the presence of local peaks in the DIC acquisition.

Conclusions

The accurate prediction of bone fracture risk has clinical relevance in osteoporosis treatment as well as in the approach to bone reconstruction operations. One of the factors which determine the accuracy in fracture risk predictions, is the characterization of the mechanical properties of bone tissue. In the context of the research conduced at Rizzoli Orthopedic Institute (IOR), the validation of a micro-FEM based procedure for the experimental determination of cancellous bone elastic properties would represent a significant achievement for the estimation of fracture risk through subject-specific FEM models of bone.
In this work, the finite element modeling procedure in use at IOR for the estimation of the tissue properties of cancellous bone has been examined. The reliability of the newly developed ParFE-based micro-FEM modeling procedure has been assessed in the first part of this work. Predictions of tissue modulus obtained with our strategy are in agree with the results reported in literature and with those of a previous analysis conduced with the use of the Ansys solver. Large variations in modulus predictions occur only for a limited number of specimens and could be attributed to the uncertainty affecting experimental results or to deficiencies in the problem's characterization. A sensitivity study confirmed how the voxel size of 39 microns adopted for our models does not produce substantial deviation from the tissue modulus estimations obtained at scanner's resolution (19.5 microns voxel size available at IOR). In addition, a sensitivity test on the effects of a threshold variation on the prediction of cancellous tissue modulus, suggested how micro-FEM modeling could represent the basis for the characterization of the uncertainty which is introduced in our predictions by the error inherent with the determination of the threshold level [29].
However, the uncertainty related with an experimental approach which had

not been designed to support the numerical FEM analysis, have led to the development of an upgraded layout for mechanical tests, accounting for the best agreement between micro-FEM models and the physics of the experiment. Even though discrepancies emerged from preliminary tests, concerning the effects of experimental side-artifacts on local displacement's detection, all tissue modulus predictions obtained after the implementation of the new layout are in good agreement with last values reported in literature [1]. Even if the tested sample did not represent a statistical basis, the observation of low inter-specimen variability suggests how we could proceed through the validation process of the micro-FEM modeling procedure developed at IOR. Finally, it can be hypothesized how a validation tool could derive from the use of DIC for the measure of surface displacement's fields independently from micro-FEM models.

Ringraziamenti

Desidero ringraziare il mio relatore Prof. Ing. Luca Cristofolini e tutto il personale del Laboratorio di Tecnologia Medica dello IOR. In particolare, meritano una menzione Chiara Fersini, Giacomo Lionello e Luigi Falco, per il valido aiuto che mi hanno fornito durante questi mesi.
Grazie a Fulvia Taddei, Enrico Schileo e Massimiliano Baleani, per alimentare e condividere, all'interno dell'LTM, un approccio emotivo alla ricerca di alto livello.
Ringrazio poi Maria e mio fratello Lorenzo per l'aiuto datomi in questi ultimi giorni, oltre a mia Madre Emanuela e Claudio per il loro costante appoggio.
Infine, le riflessioni contenute in queste pagine sono il frutto di molti pomeriggi passati a discutere con il mio correlatore Martino Pani.
È a lui che dedico questo lavoro, unitamente al più profondo riconoscimento.

Bibliography

[1] Harun H Bayraktar and Tony M Keaveny. Mechanisms of uniformity of yield strains for trabecular bone. *Journal of biomechanics*, 37(11):1671–8, November 2004.

[2] Harun H. Bayraktar, Elise F. Morgan, Glen L. Niebur, Grayson E. Morris, Eric K. Wong, and Tony M. Keaveny. Comparison of the elastic and yield properties of human femoral trabecular and cortical bone tissue. *Journal of Biomechanics*, 37(1):27–35, January 2004.

[3] Grant Bevill, Senthil K Eswaran, Farhad Farahmand, and Tony M Keaveny. The influence of boundary conditions and loading mode on high-resolution finite element-computed trabecular tissue properties. *Bone*, 44(4):573–8, April 2009.

[4] Stephen C. Cowin. *Bone mechanics handbook (second edition): Stephen C. Cowin (Ed.); CRC Press, Boca Raton, FL, 2001, hardback ISBN 0-8493-9117-2*, volume 36. 2001.

[5] Luigi Falco. Caratterizzazione meccanica di tessuto osseo trabecolare: sviluppo di un protocollo sperimentale finalizzato alla validazione di un modello numerico. Master's thesis, Alma Mater Studiorum - University of Bologna, 2013.

[6] Seymour Geisser. *Predictive Inference*. Chapman and Hall, New York, NY, 1993.

[7] T Hara, E Tanck, J Homminga, and R Huiskes. The influence of micro-computed tomography threshold variations on the assessment of structural and mechanical trabecular bone properties. *Bone*, 31(1):107–109, 2002.

[8] T P Harrigan, M Jasty, R W Mann, and W H Harris. Limitations of the continuum assumption in cancellous bone. *Journal of Biomechanics*, 21(4):269–275, 1988.

[9] Jasper Homminga, Barbara R Mccreadie, Harrie Weinans, and Rik Huiskes. The dependence of the elastic properties of osteoporotic cancellous bone on volume fraction and fabric. *Journal of biomechanics*, 36(10):1461–7, October 2003.

[10] F J Hou, S M Lang, S J Hoshaw, D A Reimann, and D P Fyhrie. Human vertebral body apparent and hard tissue stiffness. *Journal of biomechanics*, 31(11):1009–15, November 1998.

[11] M. Jaasma, Harun H. Bayraktar, Glen L. Niebur, and Tony M. Keaveny. Biomechanical effects of intraspecimen variations in tissue modulus for trabecular bone. *Journal of Biomechanics*, 35(2):237–246, February 2002.

[12] C. Jacobs, B. R. Davisa, C. J. Riegera, J. J. Francis, M. Saad, and Fyhrie D. P. The impact of boundary conditions and mesh size on the accuracy of cancellous bone tissue modulus determination using large-scale finite-element modeling. *Journal of Biomechanics*, 32(11):1159–1164, November 1999.

[13] J Kabel, A Odgaard, B van Rietbergen, and R Huiskes. Connectivity and the elastic properties of cancellous bone. *Bone*, 24(2):115–20, February 1999.

[14] W A Kalender, D Felsenberg, H K Genant, M Fischer, J Dequeker, and J Reeve. The European Spine Phantom–a tool for standardization and quality control in spinal bone mineral measurements by DXA and QCT. *European Journal of Radiology*, 20(2):83–92, 1995.

[15] T M Keaveny, T P Pinilla, R P Crawford, D L Kopperdahl, and a Lou. Systematic and random errors in compression testing of trabecular bone. *Journal of orthopaedic research : official publication of the Orthopaedic Research Society*, 15(1):101–10, January 1997.

[16] T S Keller. Predicting the compressive mechanical behavior of bone. *Journal of Biomechanics*, 27(9):1159–1168, 1994.

[17] Chi Hyun Kim, Henry Zhang, George Mikhail, Dietrich Von Stechow, Ralph Müller, Han Sung Kim, and X Edward Guo. Effects of thresholding techniques on microCT-based finite element models of trabecular bone. *Journal of Biomechanical Engineering*, 129(4):481–486, 2007.

[18] Kitware. *VTK file formats for VTK Version 4.2*. Kitware www.kitware.com. Taken from The VTK Users Guide.

[19] A Ladd and John H. Kinney. Numerical errors and uncertainties in finite-element modeling of trabecular bone. *Journal of Biomechanics*, 31(10):941–945, October 1998.

[20] W B Lievers, A C Petryshyn, A S Poljsak, S D Waldman, and A K Pilkey. Specimen diameter and "side artifacts" in cancellous bone evaluated using end-constrained elastic tension. *Bone*, 47(2):371–7, August 2010.

[21] F Linde and I Hvid. The effect of constraint on the mechanical behaviour of trabecular bone specimens. *Journal of Biomechanics*, 22(5):485–490, 1989.

[22] F Linde, I Hvid, and F Madsen. The effect of specimen geometry on the mechanical behaviour of trabecular bone specimens. *Journal of Biomechanics*, 25(4):359–368, 1992.

[23] Giacomo Lionello. Messa a punto del metodo di correlazione di immagini per applicazioni biomediche. Master's thesis, Alma Mater Studiorum - University of Bologna, 2011.

[24] Uche Mennel and Marzio Sala. *Overview of ParFE: A Scalable Finite Element Solver for Bone Modeling*. Institute of Computational Science, ETH Zurich, 2006.

[25] G. L. Niebur, J. C. Yuen, A. C. Hsia, and T. M. Keaveny. Convergence Behavior of High-Resolution Finite Element Models of Trabecular Bone. *Journal of Biomechanical Engineering*, 121(6):629–635, December 1999.

[26] Glen L Niebur, Michael J Feldstein, Jonathan C Yuen, Tony J Chen, and Tony M Keaveny. High-resolution finite element models with tissue strength asymmetry accurately predict failure of trabecular bone. *Journal of Biomechanics*, 33(12):1575–1583, December 2000.

[27] Caroline Ohman, Massimiliano Baleani, Egon Perilli, Enrico Dall'Ara, Simone Tassani, Fabio Baruffaldi, and Marco Viceconti. Mechanical testing of cancellous bone from the femoral head: experimental errors due to off-axis measurements. *Journal of biomechanics*, 40(11):2426–33, January 2007.

[28] E Perilli, M Baleani, C Ohman, R Fognani, F Baruffaldi, and M Viceconti. Dependence of mechanical compressive strength on local variations in microarchitecture in cancellous bone of proximal human femur. *Journal of biomechanics*, 41(2):438–46, January 2008.

[29] E Perilli, F Baruffaldi, M Visentin, B Bordini, F Traina, a Cappello, and M Viceconti. MicroCT examination of human bone specimens: effects of polymethylmethacrylate embedding on structural parameters. *Journal of microscopy*, 225(Pt 2):192–200, February 2007.

[30] W Pistoia, B van Rietbergen, A Laib, and P Rüegsegger. High-resolution three-dimensional-pQCT images can be an adequate basis for in-vivo microFE analysis of bone. *Journal of biomechanical engineering*, 123(2):176–83, April 2001.

[31] Jeff Schneider and Andrew W. Moore. *A Locally Weighted Learning Tutorial using Vizier 1.0*.

[32] Hubert W. Schreier, Joachim R. Braasch, and Michael A. Sutton. Systematic errors in digital image correlation caused by intensity interpolation. *Optical Engineering*, 39(11):2915–2921, 2000.

[33] C H Turner, J Rho, Y Takano, T Y Tsui, and G M Pharr. The elastic properties of trabecular and cortical bone tissues are similar: results from two microscopic measurement techniques. *Journal of Biomechanics*, 32(4):437–441, 1999.

[34] D Ulrich, T Hildebrand, B Van Rietbergen, R Müller, and P Rüegsegger. The quality of trabecular bone evaluated with micro-computed tomography, FEA and mechanical testing. *Studies in health technology and informatics*, 40:97–112, January 1997.

[35] Kerem Un, Grant Bevill, and Tony M Keaveny. The effects of side-artifacts on the elastic modulus of trabecular bone. *Journal of biomechanics*, 39(11):1955–63, January 2006.

[36] B van Rietbergen. Micro-FE analyses of bone: state of the art. *Advances in experimental medicine and biology*, 496:21–30, January 2001.

[37] B van Rietbergen, S Majumdar, W Pistoia, D C Newitt, M Kothari, A Laib, and P Rüegsegger. Assessment of cancellous bone mechanical properties from micro-FE models based on micro-CT, pQCT and MR images. *Technology and health care : official journal of the European Society for Engineering and Medicine*, 6(5-6):413–20, December 1998.

[38] B van Rietbergen, H Weinans, R Huiskes, and A Odgaard. A new method to determine trabecular bone elastic properties and loading using micromechanical finite-element models. *Journal of Biomechanics*, 28(1):69–81, January 1995.

[39] E Verhulp, B van Rietbergen, and R Huiskes. Comparison of micro-level and continuum-level voxel models of the proximal femur. *Journal of biomechanics*, 39(16):2951–7, January 2006.

[40] E Verhulp, B van Rietbergen, R Müller, and R Huiskes. Indirect determination of trabecular bone effective tissue failure properties using micro-finite element simulations. *Journal of biomechanics*, 41(7):1479–85, January 2008.

[41] Eelco Verhulp. *Analyses of Trabecular Bone Failure*. PhD thesis, Universitetitsdrukkerij TU Eindhoven, Eindhoven, Netherlands, 2006.

[42] Nicolas Vilayphiou, Stephanie Boutroy, Elisabeth Sornay-Rendu, Bert Van Rietbergen, Francoise Munoz, Pierre D Delmas, and Roland Chapurlat. Finite element analysis performed on radius and tibia HR-pQCT

images and fragility fractures at all sites in postmenopausal women. *Bone*, 46(4):1030–1037, 2010.

[43] Yener N Yeni, Gregory T Christopherson, X Neil Dong, Do-Gyoon Kim, and David P Fyhrie. Effect of microcomputed tomography voxel size on the finite element model accuracy for human cancellous bone. *Journal of biomechanical engineering*, 127(1):1–8, February 2005.

[44] D. Zaccheo, L. Cattaneo, and C. E. Grossi. *Anatomia Microscopica degli Organi dell'Uomo 1.* UTET Torino, 1973.

[45] P Zioupos and J D Currey. Changes in the stiffness, strength, and toughness of human cortical bone with age. *Bone*, 22(1):57–66, 1998.

[46] P K Zysset, X E Guo, C E Hoffler, K E Moore, and S A Goldstein. Elastic modulus and hardness of cortical and trabecular bone lamellae measured by nanoindentation in the human femur. *J Biomech*, 32:1005–1012, 1999.